

**UNIVERSITÀ DEGLI STUDI DI NAPOLI “FEDERICO II”**

Dipartimento di Ingegneria Chimica, dei Materiali  
e della Produzione Industriale



**Tesi di Dottorato in Ingegneria dei Materiali e delle  
Strutture  
(XXVIII CICLO)**

***Chemical modifications of polysaccharides to realize  
versatile Oil Core – Polyelectrolyte Shell  
nanocapsules via Layer-by-Layer***

**Vincenzo Calcagno**

Marzo 2013 – Marzo 2016

***Chemical modifications of polysaccharides to realize  
versatile Oil Core – Polyelectrolyte Shell  
nanocapsules via Layer-by-Layer***

A THESIS SUBMITTED IN PARTIAL FULFILMENT OF  
THE REQUIREMENT FOR THE DEGREE OF  
DOCTOR OF PHILOSOPHY  
IN MATERIALS AND STRUCTURES ENGINEERING  
(XXVII CYCLE)

**AUTHOR**

Vincenzo Calcagno

**ADVISOR**

Prof. Dr. Paolo A. Netti

**TUTOR**

Dr. Raffaele Vecchione

**COORDINATOR**

Prof. Dr. Giuseppe Mensietieri

# Abstract

In the last decades, nanomedicine – the application of nanotechnology to medicine – has opened up an entirely new horizon of possibilities and applications, in particular for drug delivery and diagnostic. Indeed, a wide range of nanocarrier have been designed and realized. However, more recently researcher focused on the development of “multifunctional” platforms, i.e. nano-vectors able to simultaneously or sequentially perform several functionalities – enzymatic catalysis, controlled degradation, controlled drug release and sensing.

In this context polyelectrolyte multilayer (PEM) capsules fabricated via the Layer-by-Layer (LbL) technique have emerged as very attractive tool for the assembly of multifunctional carrier systems, because of its ideal features like simplicity, versatility, and nanoscale control.

The final aim of this research activity concerns the realization of completely biocompatible and biodegradable nanocarriers with diverse functionalities and purposes. The greater ambition, in particular, is the realization of nanometric sized drug vehicles entirely derived from natural materials but holding the features needed for the drug delivery. Starting from an inner oil-core carrier – with tunable sizes ranging from 80 to 200 nm, built up with natural materials like soybean oil and egg lecithin and

## Abstract

able to encapsulate hydrophobic drugs or contrasting agents - oil-core polyelectrolytes-shells nanocarriers have been realized. As for the liquid core, natural materials have been selected for the realization of the shell, and, in particular, polysaccharides. More in detail, polysaccharides used as coating have been opportunely modified in order to add desired functionalities to the final nano-vectors. As matter of the fact, it was demonstrated how the thiolation of the nanocapsules' surfaces, together with the appropriate choice of the materials, sizes and formulation, can positively effect on the oral delivery of an unstable nutraceutical, i.e. curcumin. Moreover, the modification of natural polyelectrolytes with thiol and olefin moieties allowed to covalently cross link the layers by applying a photo activated reaction, thiol-ene 'click' reaction: it was demonstrated that such strategy bring out to a final nano-system with enhanced biostability. Lastly, an *in situ* modification of heparin with an aminosilane allowed to apply a modified Stöber sol-gel method for the realization of a high versatile multilayered nanocarrier system featuring a hybrid polymer/silica-shell.

All the designed and realized nanocapsules did not show any cytotoxic effect, so resulting completely biocompatible and, therefore, of interest for the nanomedicine fields.

# Table of contents

## **Chapter 1** **1**

---

### **State of art**

1.1 Nanomedicine and drug delivery	3
1.2 LbL technique applied to nanomedicine	9
1.3 Polysaccharides-based polyelectrolyte multilayers	15
1.4 Oil-core polyelectrolyte nanocarriers	24
1.5 Aim of research and thesis outline	32
1.6 References	36

## **Chapter 2** **39**

---

### **Curcumin bioavailability from oil in water nano-emulsions: *in vitro* and *in vivo* study on the dimensional, compositional and interactional dependence**

2.1 Introduction	42
2.2 Results and discussions	45
2.3 Conclusions	70
2.4 Materials and Methods	72
2.5 Supplementary Section	88
2.6 References	104

## **Chapter 3** **108**

---

### **Biostability Enhancement of Oil Core - Polysaccharide Multilayer Shell via Photoinitiator Free Thiol-ene 'Click' Reaction**

3.1 Introduction	111
3.2 Results and discussions	114
3.3 Conclusions	130

3.4 Materials and Methods	131
3.5 Supplementary Section	141
3.6 References	148

**Chapter 4** **151**

---

**Multilayered silica-biopolymer nanocapsules with hydrophobic core and hydrophilic tunable shell thickness**

4.1 Introduction	154
4.2 Results and discussions	158
4.3 Conclusions	182
4.4 Materials and Methods	183
4.5 Supplementary Section	197
4.6 References	202

**Chapter 5** **205**

---

**Conclusion**

# Chapter 1

## State of art

Ho sempre tenuto in poco conto la cultura intesa come cosa che fa crescere agli occhi degli altri e alla loro considerazione.

La cultura non deve meravigliare che chi l'apprende, e mai gli altri.

Alda Merini – Poetess

For all things I have the strength through the one who gives me power.

Philippians 4:13 – Apostle Paul

For a man may work hard, guided by wisdom and knowledge and skill, but he must hand over his portion to a man who did not work for it. This too is futility and a great tragedy.

Ecclesiastes 2:21 – King Solomon

## 1.1 Nanomedicine and drug delivery

In his famous lecture “There’s plenty of room at the bottom” (Caltech, 1959), Nobel Prize Richard Feynman outlined the potential that the harnessing of nanoscopic materials could yields.<sup>1</sup> What make nanomaterials ‘special’ is that they have identical composition but exhibit properties completely different from their bulk moduli. This peculiarity was already exploited several centuries ago. For example, the Lycurgus Cup (**Figure 1.1**) is a late Roman (IV century A.D., British Museum) cut glass vessel. This vessel is a clear example of both the extraordinary fabrication method and of the exceptional workmanship involved. Moreover, this glass shows non unusual optical effects. Indeed, the glass is dichroic; in direct light it resembles a jade with an opaque green-yellow tone, but when light shine through the glass (transmitted light) it turn to a translucent ruby colour. After several investigations, scientists linked the dichroism to the presence of minute amounts of gold and silver in the glass. However, simply adding traces of gold and silver to glass would not produce these unique optical properties. The critical factor is the formation of minute submicroscopic crystals or colloids of the metals.<sup>2</sup>



**Figure 1.1.** The Lycurgus Cup in reflected (left) and transmitted (right) light. Colloidal systems can give rise to light scattering phenomena that result in dichroic effects. It was suggested that both the gold and silver contributed to the colour, the gold component being mainly responsible for the reddish transmission and the silver for the greenish reflection. [1958, 1202.1, Department of Prehistory and Europe, The British Museum, h:16.5 cm, d:13.2 cm. Images reprint with the permission of The British Museum Website]

Despite this and other ‘ancient’ examples of applied nanomaterials, nanotechnology has attracted wide interest as a new field of technology only starting from Feynman concepts. Results obtained during the years, before unthinkable, are well summarized by the words of Richard E. Smalley (Nobel Prize in Chemistry in 1996): *‘we’ve got to learn how to build machines, materials, and devices with the ultimate finesse that life has always used: atom by atom, on the same nanometer scale as the machinery in living cells’*.<sup>3</sup> [Presentation to the University of Dallas - Board of Councilors, December 7, 1995].

Nowadays nanotechnologies found applications in several fields as medicine, biotechnology, green technology, energy, industry, agriculture, food, art.<sup>a</sup> Since most of the application are centred on improving human health and diagnosing the human status, nanotechnology has given rise to a completely new field known as nanomedicine.

Nanomedicine can be defined as the application of nanotechnology to medicine.<sup>4</sup> Such field has opened up an entirely new horizon of possibilities and applications. For example, nanotechnologies applied to the physiological system has provided the possibility to study biological processes on a more intimate level and, consequently, to enhance their understanding. More importantly, nanomedicine has the aim to overcome the limitations related to the conventional medicine, for both diagnostic and therapy. In particular, the main limitations concern the poor safety and efficacy of the conventional therapies. Many therapeutic agents are not successful because of their limited ability to reach selectively the target tissue. For example, in cancer chemotherapy, cytostatic drugs damage both malignant and normal cells alike. Thus, a drug delivery strategy that selectively targets the malignant tumor would be the ideal solution.

---

<sup>a</sup> An innovative and promising subsection of nanotechnology derives from Carbon-based Nanomaterials. Such materials are finding application in medicine, composite materials, microelectronics, solar cells, electronic components, energy, optical, mechanical, etc.

Drug Delivery Systems (DDSs) are conceived to improve the pharmacological and therapeutic properties of drugs administered in vivo, designing carriers that can act as drug reservoirs. Drug carrier system should allow for the controlled release of drugs at the desired sites, thus positively altering both the pharmacokinetics and biodistribution of the drugs.<sup>5</sup> More in details, an ideal DDS should be able to reach selectively the target tissue, thus reducing the drug toxicity.

To this aim, DDS should result firstly stable and with a longer blood half-life to have enough time for the accumulation in the target tissue. Biostability is related to the material used, the degradation time and the body clearance.

The clearance is the result of the interaction with serum protein.<sup>6</sup> These proteins instantaneously bind onto the nanoparticle surface and dictate the long-term fate, metabolism, clearance, and immune response<sup>7</sup>, because they are able to “tag” the DDS for removal by the mononuclear phagocyte system (MPS) inside the liver and spleen. This process is known as opsonisation because a foreign organism or particle is covered with opsonins proteins and becomes visible to phagocytic cells. Moreover, it is followed by the phagocytosis, which is the engulfing and eventual destruction or removal of foreign materials from the bloodstream.<sup>8</sup> For this reason, an ideal DDS should be able to avoid the attachment of opsonins

proteins. The most usual way to keep drug carriers in the blood as long as is possible, is to “mask” them by modifying (grafting) their surface with water-soluble polymers with a well-solvated and flexible main chain, such as polyethylene glycol (PEG). The surface-grafted “protective” polymers effectively prevent, i.e. slow down, the opsonization of drugs and drug carriers and their clearance.<sup>9, 10</sup> Secondly, the DDSs should have an ideal size. Dimensions started to be considered important when Matsumura and Maeda<sup>11</sup> described the mechanism, called Enhanced Permeability and Retention (EPR) effect (**Figure 1.2**), of successful delivery of carriers to certain tissues.

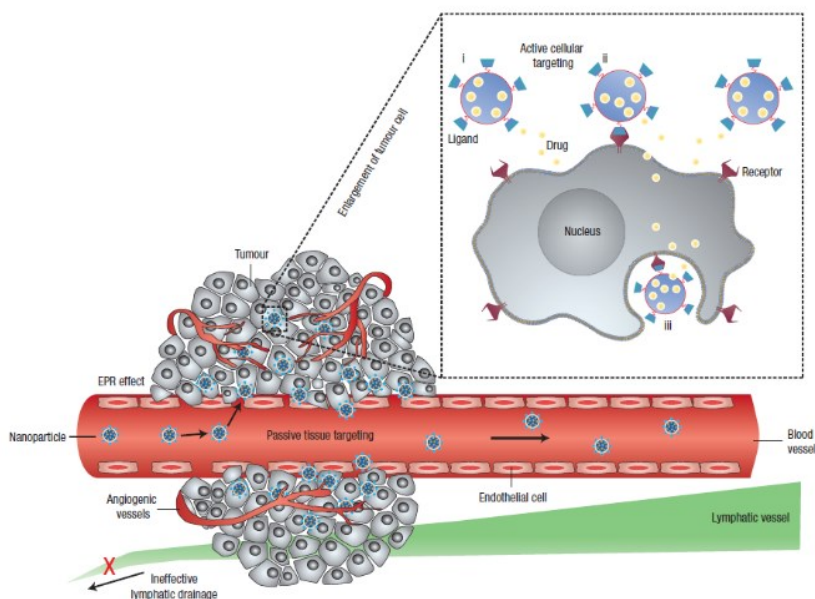


**Figure 1.2.** Schematic representation of passive and active targeting. Passive tissue targeting is achieved by extravasation of nanoparticles through increased permeability of the tumour vasculature and ineffective lymphatic drainage (EPR effect). Active cellular targeting (inset) can be achieved by functionalizing the surface of nanoparticles with ligands that promote cell-specific recognition and binding. Reprinted with permission from *Nat. Nanotechnol.*<sup>12</sup>

Their investigations showed that most solid tumors have blood vessels with defective architecture and usually produce extensive amounts of various vascular permeability factors. Consequently, most solid tumors exhibit enhanced vascular permeability, which will ensure a sufficient supply of nutrients and oxygen to tumor tissues for rapid growth. The EPR effect considers this unique anatomical and physiological nature of tumor blood vessels that facilitates transport and accumulation of macromolecules into tumor tissues. In contrast, this EPR effect-driven drug delivery does not occur in normal tissues.<sup>13</sup> As a result, in tumor tissues, large molecules and even relatively certain particles below 500 nm in size, preferably below 200 nm, can leave the vascular bed and accumulate inside the interstitial space.<sup>12, 14, b</sup>

Such spontaneous accumulation is called “passive” targeting, because a physical property such as the size, is used to help the DDS to reach its target, i.e. the tumour tissue. Passive targeting differs from the active one, where the DDS is opportunely modified to interact actively with tissues or cells to deliver its drug selectively (**Figure 1.2**, inset). Different biomolecules<sup>15</sup> (antibodies, aptamers, peptide or small molecules) have

---

<sup>b</sup> For this reason, DDSs scaled down to nano-scale are also called DDnSs or NDDSs, namely Drug Delivery nano Systems.

been used to recognize the tumour and to help nanocarriers to enter the cancer cell.<sup>16</sup>

Lastly, an ideal DDS should be designed in order to possess peculiar characteristics, namely to maximize the therapeutic activity while minimizing the toxic side effects of drugs. To this purpose the choice of materials and the design of the DDS are crucial. Many properties can be tailored for specific applications: solubility, biodistribution, biocompatibility, biodegradability, drug release, drug encapsulation and shape.<sup>17</sup> Below in this chapter it will be discussed about the possibility of using natural materials, appropriately chosen and modified, in order to design DDSs for specific applications.

## **1.2 LbL technique applied to nanomedicine**

Multilayer thin films have garnered intense scientific interest due to their potential application in diverse fields such as catalysis, optics, energy, membranes, and biomedicine. Layer-by-layer (LbL) assembly is a prevalent method for coating substrates with functional thin films.<sup>18</sup> Early studies on multilayer assembly date back to fifty years ago.<sup>19,20</sup> However, it is only in the last two decades that it has witnessed considerable growth. In particular, in 1990s Decher's group developed a "simple approach that would yield nanoarchitecture films with good positioning of individual

layers, but whose fabrication would be largely independent on the nature, size, and topology of the substrate”.<sup>21</sup> This process, known as layer-by-layer, is extremely simple (**Figure 1.3**).

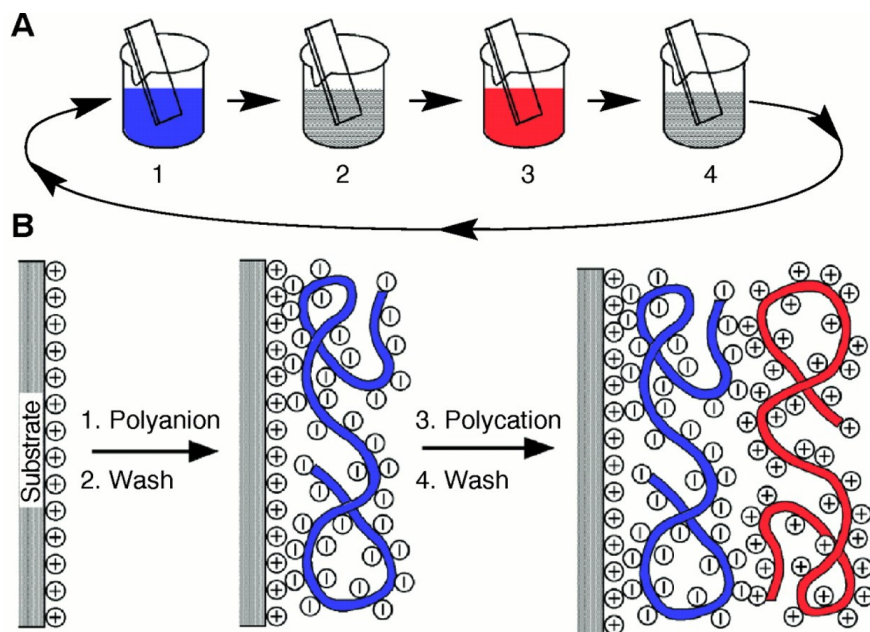


**Figure 1.3.** (A) Schematic of the film deposition process using slides and beakers. Steps 1 and 3 represent the adsorption of a polyanion and polycation, respectively, and steps 2 and 4 are washing steps. The four steps are the basic build-up sequence for the simplest film architecture, (A/B) $n$ . The construction of more complex film architectures requires only additional beakers and a different deposition sequence. (B) Simplified molecular picture of the first two adsorption steps, depicting film deposition starting with a positively charged substrate. Counterions are omitted for clarity. Polyion conformation and layer interpenetration are an idealization of the surface charge reversal with each adsorption step. [From G. Decher, *Science* 277, 1232 (1997). Reprinted with permission from AAAS]

It is a cyclical process in which a charged material is adsorbed onto a substrate, and after washing, an oppositely charged material is adsorbed on top of the first layer. This constitutes a single bilayer with a thickness

generally on the order of nanometers, and the deposition process can then be repeated until a multilayer film of desired thickness has been assembled.

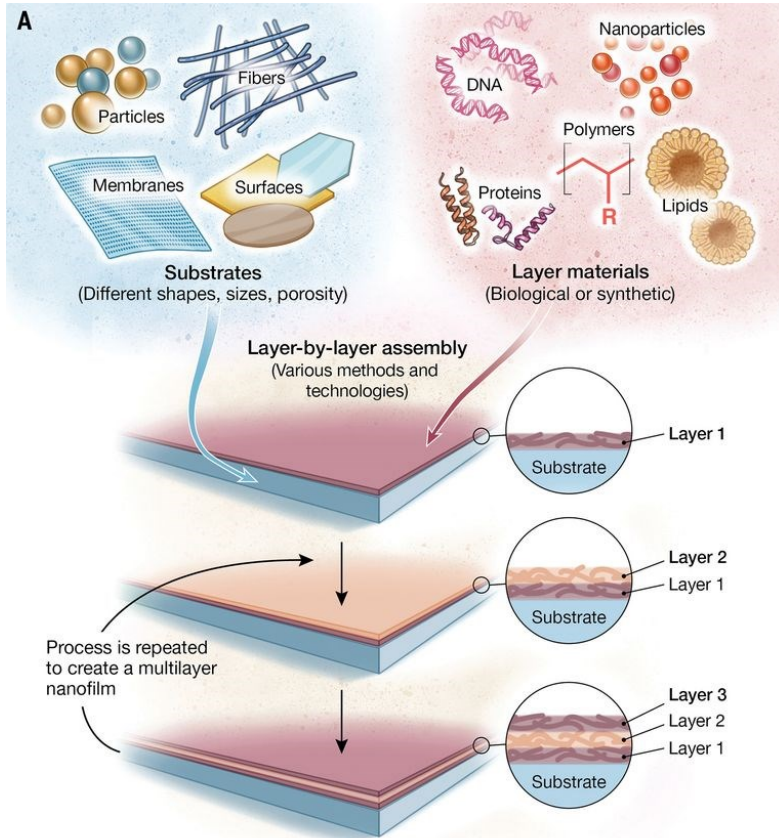


**Figure 1.4.** Versatility of layer-by-layer assembly. Schematic overview of LbL assembly [Illustration credit: Alison E. Burke and Cassio Lynn; from Richardson *et al.*, *Science*, 348, 6233 (2015). Reprinted with permission from AAAS]

In addition to the simplicity, the potential of this method consists in the possibility of controlling the film thickness at the nanometric scale. Moreover, it would be possible to build up infinite coatings on diverse substrates (e.g., flat surfaces, porous membranes, particles), simply changing the nature of the layers deposited. Indeed, although electrostatic

interactions remain widely used in films formation, other molecular interactions (e.g., covalent, hydrogen-bonding, host-guest) are now well established for LbL assembly with diverse materials (e.g., polymers, proteins, lipids, nucleic acids, nanoparticles, suprastructures) used as film constituents (**Figure 1.4**).<sup>18, 22</sup>

From first Decher's works, LbL was largely used thanks to the possibility to vary the substrate, the layers' materials, the LbL assembly technologies and methods. The simplicity, versatility, and the control at nanometer scale, provided by LbL assembly make it one of the most used technologies of coating in a diverse range of fields, including optics, energy, catalysis, separations, and nanomedicine (**Figure 1.5**).

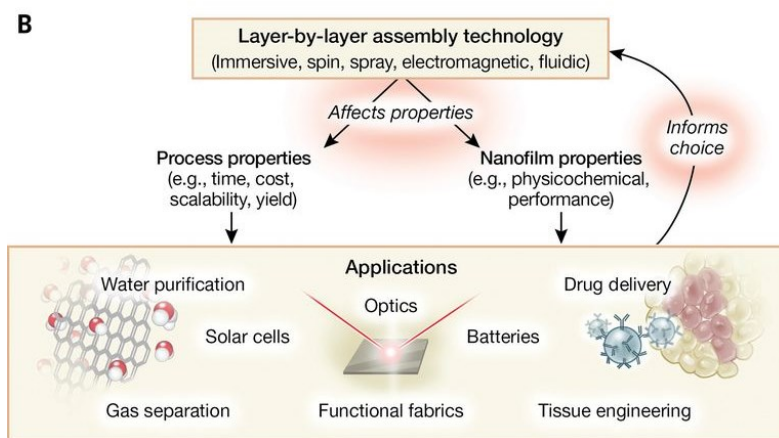


**Figure 1.5.** Versatility of layer-by-layer assembly. Overview showing that the assembly technology influences film and process properties, as well as application areas. [Illustration credit: Alison E. Burke and Cassio Lynn; from Richardson *et al.*, *Science*, 348, 6233 (2015). Reprinted with permission from AAAS]

In particular, LbL technique resulted to be very attractive for the realization of DDSs with the ideal features discussed above. Indeed, the facile construction on colloidal substrates (template) of multilayer architectures with nanometer precision allows to realize devices with multiple properties. For example, by varying the size of the template it is theoretically possible to obtain capsules with different sizes, ranging from micrometer or sub micrometer to nanometer scales.<sup>23</sup> Moreover, different functionalities can be simultaneously engineered in the same carrier by loading several types of components into the lumen or within the shell of the carrier. Their external surface can be functionalized to partially control their biodistribution (PEGylation<sup>24</sup> and active targeting<sup>25</sup>). Therefore, capsules with well-controlled size and shape, finely tuned shell thickness and variable shell compositions can be obtained by using LbL technique. Despite the potentiality of the LbL technique, some limitations must be taken into account. First of all, the process is very time consuming. The deposition of a film consisting of dozens of bilayers takes more than 10 h using a robotic dipping apparatus.<sup>26</sup> The most common technology for immersive assembly on particulate substrates is performed by adding polymer solution to dispersed dense particulate substrates, pelleting the particles with centrifugation, removing the supernatant, washing multiple times with a similar pelleting process, and then repeating the steps for

multilayer growth.<sup>27, 28</sup> This is generally time-consuming and labour-intensive due to the centrifugation steps, and particles dense and large enough to be pelleted are required. The time-consuming multistep assembly procedure, along with the aggregation of particles from repeated centrifugation steps and the difficulty to automate the procedures, has limited its industrial applications. To overcome these limits different approaches have recently been proposed. For example, the use of spray-assisted LbL-assembly, both for planar films as well as for the construction of polymeric particles, has emerged as a possible strategy to reduce the deposition times per layer from tens of minutes to a few seconds.<sup>23</sup> Another promising approach was recently proposed by Caruso et al.<sup>29</sup> who described the simple one-step assembly of metal–polyphenol (Fe(III)–TA) capsules with biologically tunable physicochemical properties.<sup>c</sup>

The limitations of LbL here reported can be overcome through the development of a facile and versatile strategy for particle engineering. This is, in fact, the only way to realize DDSs with desirable features together with an economical attraction.

---

<sup>c</sup> The method exploits a coordination complex of natural polyphenol tannic acid and Fe(III) ions. The assembly process results to be easy, low cost and scalable and the capsules obtained are pH responsiveness.

## 1.3 Polysaccharides-based polyelectrolyte multilayers

Polysaccharides are natural polymers that belong to the family of the carbohydrates and play fundamental roles in many biological contexts. Their structure is made of sugar rings linked by glycosidic bonds and various side functions. These highly abundant molecules are from various origins including algal origin (e.g. alginate and carrageenan), plant origin (e.g. cellulose, pectin and guar gum), microbial origin (e.g. dextran and xanthan gum), and animal origin (e.g. chitosan, hyaluronan, chondroitin and heparin).<sup>30</sup>

Naturally occurring polysaccharides are diverse in their physicochemical properties. They possess multiple chemical structures (**Figure 1.6**) and the chemical composition greatly varies, as well as the molecular weight (Mw) and ionic nature. This versatility also contributes to a wide range of biological activities. From a pharmaceutical standpoint, polysaccharides possess many favourable characteristics such as low toxicity, biocompatibility, stability, low cost, hydrophilic nature and availability of reactive sites for chemical modification.<sup>31</sup>

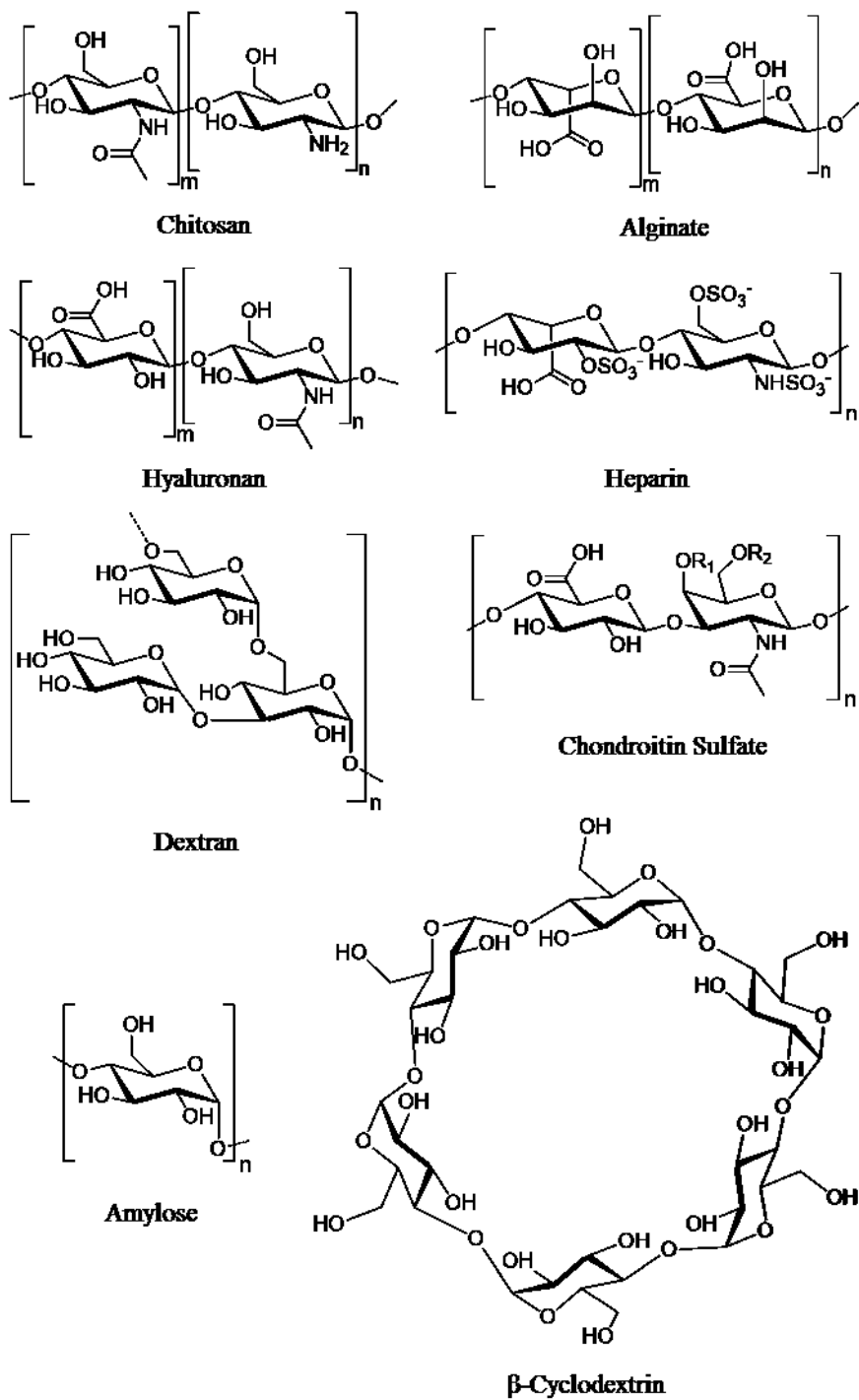


**Figure 1.6.** Chemical structure of some natural occurring polysaccharides.

Two elements are of utmost importance in the chemistry of polysaccharides. Firstly, the glycosidic bonds can be the target of glycoside hydrolase enzymes and can thus be biodegraded relatively easily. Secondly, the side groups can directly affect the polysaccharide's charge density, hydration and chemical reactivity, and can also be responsible for the formation of secondary structures. When charges are present, polysaccharides behave like polyelectrolytes. The negative groups ( $\text{COO}^-$ ) with  $pK_a$  around 3–5 or sulfate groups ( $\text{SO}_3^-$ ) with a  $pK_a$  of around 0.5–1.5.<sup>32</sup> The positively charged groups are ammonium groups ( $\text{NH}_3^+$ ) with a  $pK_a$  of around 7–10.<sup>33, 34</sup>

In particular, the presence of negative and positive groups make these polymers suitable for LbL application.<sup>35</sup> Indeed, Polyelectrolyte Multilayer (PEM) films give rise to self-assembly *via* LbL, because of both interactions between the negative and positive groups and the entropic gain associated with these interactions.

In addition, the presence of carboxylic and ammonium groups makes these polymers suitable for chemical modifications. However, certain difficulties are encountered when working with polysaccharides. Chemical modification can be a real challenge because of the high hydration shell and poor solubility in organic solvents. Due to their lower solubility, pH and ionic strength  $I$  can only be varied to a lower extent than for their

synthetic counterparts. The advantages and limitations of using polysaccharides are summarized in **Table 1.1**, as reported by Crouzier et al.<sup>35</sup>

**Table 1.1.** Comparison between the advantages and disadvantages of synthetic polyelectrolytes and polysaccharides used for the build-up of multilayer films in the context of biomedical and biomaterials research (as reported by Crouzier et al.<sup>35</sup>)

	Synthetic polyelectrolytes	Polysaccharides
Advantages	<ul style="list-style-type: none"> <li>• Large choice of chemistry, structures and charge densities</li> <li>• Flexibility</li> <li>• Large working range of pH and ionic strength</li> <li>• Easy chemical modification</li> <li>• Abundant and usually cheap</li> <li>• Available with highly controlled quality</li> </ul>	<ul style="list-style-type: none"> <li>• Natural polyelectrolytes (biomimetism)</li> <li>• Interesting structural properties: interaction with water, self-assembly, hydrogel formation</li> <li>• Functional properties: specific cell receptor, interaction with bioactive molecules, present in the pericellular coat</li> <li>• Biodegradability and biocompatibility (for most of them)</li> </ul>
Limitations	<ul style="list-style-type: none"> <li>• Most often non-biodegradable</li> <li>• Potentially harmful degradation products</li> <li>• No particular bioactivity</li> </ul>	<ul style="list-style-type: none"> <li>• Limited availability with well-defined properties (purity, polydispersity)</li> <li>• Chemical modification can be particularly difficult due to the poor reactivity of the group, low charge density and poor solubility in solvents</li> <li>• Limited pH and ionic strength working range due to solubility issues</li> </ul>

These peculiar properties of polysaccharides explain the reason of their use as biomaterial. Moreover, they are naturally degraded by different

kinds of enzymes present *in vivo* giving polysaccharides a great advantage over synthetic polyelectrolytes.<sup>35, 36</sup> These superior advantages for biomedical applications as compared to synthetic polyelectrolytes explain why they have been increasingly employed as film constituents since the early 2000s.

The properties of two common polysaccharides used in this research project (i.e. chitosan and heparin) are detailed below in the next paragraph.

### ***Chitosan and glycol chitosan***

Chitosan (CT) is a linear polysaccharide composed of  $\beta$ -(1,4)-linked D-glucosamine and N-acetyl-D-glucosamine (**Figure 1.7**). Even though the discovery of chitosan dates from the 19th century, it has only been over the last three decades that this polymer has received attention as a material for biomedical and drug delivery applications. The accumulated information about the physicochemical and biological properties of chitosan led to the recognition of this polymer as a promising material for drug delivery and, more specifically, for the delivery of delicate macromolecules.<sup>37</sup> CT is obtained by deacetylation from chitin, a highly abundant polysaccharide, which is the main component of the crustaceans and insects exoskeleton, and certain fungi.<sup>38</sup> Due to the limited solubility of chitin in aqueous solutions, chitosan is more suitable for industrial applications.<sup>39</sup> Whereas chitin is a polymer of N-acetyl-D-glucosamine

units, chitosan is less easily defined in terms of its exact chemical composition. It usually refers to a family of polymers that are characterized by the number of sugar units per polymer molecule (n+m), which defines the molecular weight, and the degree of deacetylation (DD, **Figure 1.7**).

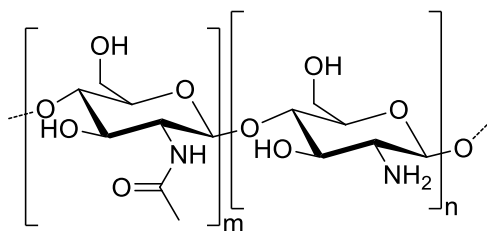


**Figure 1.7.** Chemical structure of chitosan. CT is a linear polysaccharide composed of  $\beta$ -(1,4)-linked D-glucosamine (n) and N-acetyl-D-glucosamine (m). The relative abundance of the acetylated or deacetylated forms can be expressed in percentage as Degree of Acetylation (DA) or Degree of Deacetylation (DD). The amine group of D-glucosamine results to be positively charged in acidic media making chitosan a polycation.

The degree of deacetylation (DD) affects the  $pKa$ <sup>34</sup> and, consequently, the solubility of chitosan in aqueous solutions, making the polymer soluble in acidic solutions and insoluble in neutral or in weak alkaline solutions.<sup>40</sup>

The intriguing properties of CT have been known for many years and the polymer has been used in the fields of agriculture, industry and medicine.<sup>38, 41</sup> In particular, the pharmaceutical and biomedical applications of CT probably offer the greatest promise.<sup>37, 41</sup> CT lacks irritant or allergic effects and is biocompatible with both healthy and infected human skin.<sup>42</sup> When chitosan was administered orally in mice, the LD50 was found to be in excess of 16 g/kg, which is higher than that of

sucrose.<sup>38</sup> CT is approved for dietary applications in several country and it has been approved by the FDA for use in wound dressings.<sup>43</sup>

Due to its protonable amine groups, CT has a polycationic nature and, therefore is able to form PEM films. Actually, the choice of a polycationic polysaccharide is very limited. In fact, only chitosan is currently available and used in PEM films.<sup>35</sup> Thanks to its numerous interesting properties, above mentioned, chitosan is probably by far the most widely used polysaccharide in LbL film.<sup>44</sup> Its positive charge also facilitates adherence to mucosal surfaces, which are mostly negatively charged.<sup>37</sup> In addition, the amine groups can be also used for chemical modifications. As reported in **Table 1.1**, however, the main problems concerning chemical modification of the amine group are (i) the difficulty to perform any modification with a limited pH working range and (ii) the reduced solubility of the modified chitosan in water due to the loss of free amine groups. Several attempts were made to improve the water solubility of CT, but most of them also reduce the fraction of free amine groups. On the other hand, a different modification of chitosan was proposed to obtain a polymer with improved water solubility but with no reduction of free amine groups. Glycol chitosan (GC) owes its water solubility to the incorporation of the hydrophilic glycol group (**Figure 1.8**), introduced by

reacting chitin with ethylene oxide followed by its deacetylation.<sup>45, d</sup> For these reasons, GC could represent a valid alternative to CT for the realization of PEM films, in particular when modified polymers are required.

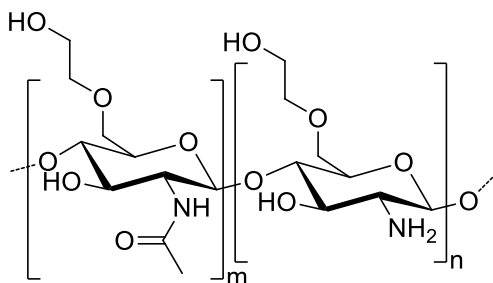


**Figure 1.8.** Chemical structure of glycol chitosan. GC is a modified chitosan with a glycol linked to the hydroxyl in position 6 of the sugar ring.

### *Heparin*

Heparin is a sulfated polysaccharide belonging to the family of glycosaminoglycans (GAG). Like most of the GAGs, heparin is a linear polysaccharide constituted by alternating disaccharide sequences of a uronic acid and an aminosugar. The uronic acid residues of heparin are L-iduronic acid (IdoA) and D-glucuronic acid (GlcA), and its only aminosugar is D-glucosamine (GlcN). GlcN is prevalently N-sulfated in heparin and N-acetylated in minor sequences. Both the uronic acid

<sup>d</sup> Knight et al. characterized GC and proposed a different structure with mono- and di-substitution of amine groups, so resulting partially N-glycolated.

(especially IdoA) and the aminosugar bear O-sulfate groups (**Figure 1.9**).<sup>46</sup>

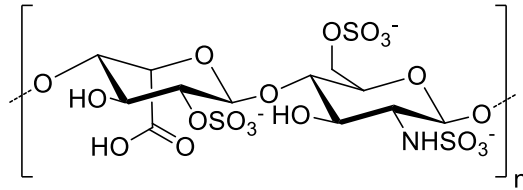


**Figure 1.9.** Chemical structure of the most abundant disaccharide sequence of heparin (IdoASO<sub>3</sub><sup>-</sup> - GlcNSO<sub>3</sub><sup>-</sup>).

Due to high content of sulfate and carboxyl groups, heparin has the highest negative charge density of any known biological molecule.<sup>47</sup> Thus, in contrast with CT and its low density charge and limited pH working range, heparin is a strong polyelectrolyte with an higher solubility in a wide pH range. This features reflect on the possibility to easier modify the polymer, in particular, exploiting its carboxylic groups. The Mw of heparin varies between 5 to 40 kDa and it is extracted mainly from mucosal tissues of porcine and bovine.<sup>46</sup> Clinically, heparin has been used as an anticoagulant since the 1930s.<sup>46</sup> Beyond its anticoagulant activity, heparin has been shown to have antiviral activity, regulate angiogenesis and inhibit complement activation.<sup>48</sup>

The high negative charge density makes heparin suitable for PEM. Indeed, as strong polyelectrolyte, its negative charge is almost independent on the pH (in particular, because of the sulfate groups).<sup>35</sup> For example, Boddohi

et al.<sup>49</sup> studied PEM assembly of heparin and chitosan as a function of pH and ionic strength, showing how these parameters effect on the interaction of the two polyelectrolytes and on the thickness of the resulting PEMs.

## 1.4 Oil-core polyelectrolyte nanocarriers

As previously mentioned, LbL technique has been widely explored to realize micro- and nanocapsules with different functions and properties. LbL technique is very versatile, in fact different materials can be used for the realization of the layer; in addition, different templates with cores of different size and nature can be chosen.<sup>18</sup> In the case of a typical PEM carriers (with micrometric or sub micrometric size) a solid core is used as a “sacrificial” template and a hollow shell is obtained by dissolution. Then the hollow shell can be refilled with the desired composition by changing pH, salt or temperature, factors that influence shell permeability.<sup>23, 50</sup> Alternatively, loading of active components can be accomplished before formation of the cores (e.g. by co-precipitation with core materials) or by adsorption onto pre-formed templates (**Figure 1.10**). Solid organic (latexes) or inorganic (e.g. CaCO<sub>3</sub>) microparticles have mostly been used as cores for formation of capsules with active ingredients.<sup>51</sup>

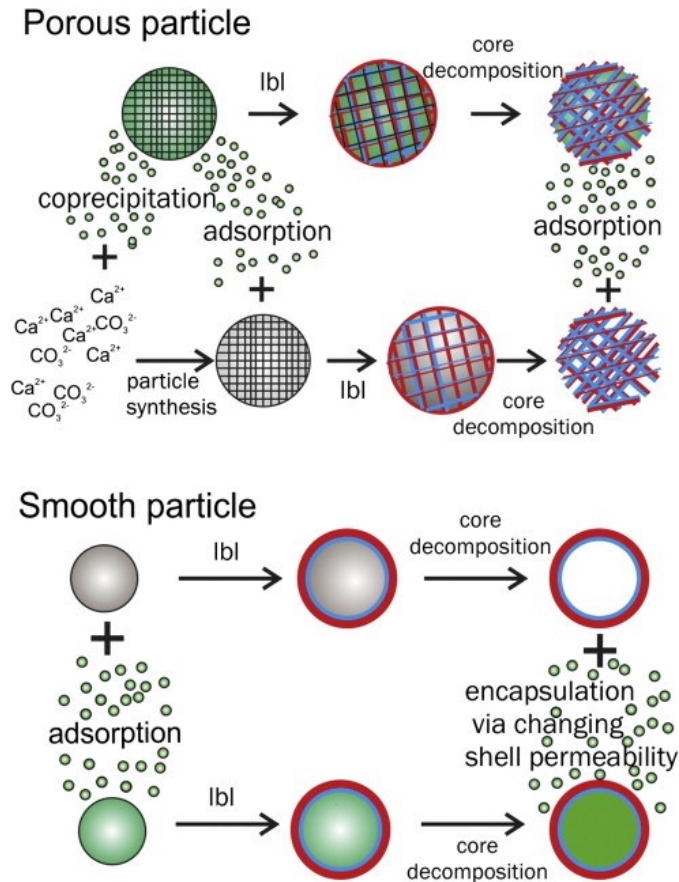


**Figure 1.10.** Schematic of loading based on smooth and porous particles, using the layer-by-layer (LbL) technique for capsule shell formation, followed by decomposition of the core material. [Reprinted from Parakhonskiy et al.<sup>51</sup>]

The principle disadvantages of the method of sacrificial core are (i) some traces of the destroyed core that might be trapped in the capsules, (ii) the disruption of the shell structure in consequence to the core dissolution and (iii) a low efficiency of loading of the active substance into the hollow shells.<sup>52, 53</sup> In addition, it must be taken into account that many therapeutic substances are lipophilic and these strategy could result unsuccessful.<sup>54</sup>

In the past decades a large effort has been devoted to the development of functionalized nanoscale oil-core carriers (e.g., micro- and nanoemulsions, colloidosome particles, polymeric nanoparticles and nanocapsules) that selectively deliver biologically active compounds to diseased sites such as malignant cancers (**Figure 1.11**).<sup>55, 56</sup> Indeed, the development of novel types of micro- and nanocontainers is constantly one of the main topics in the scientific research and in the last few years the major progress in the synthesis and application of various methods of template mediated synthesis of drug vehicles has been achieved.<sup>57, 58</sup>

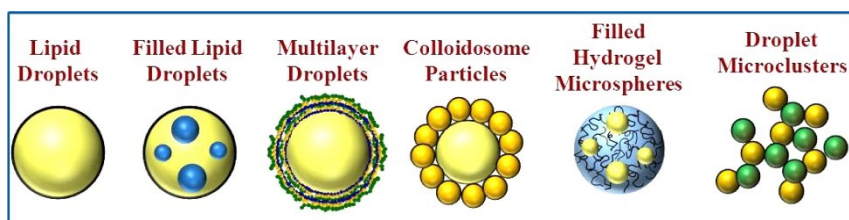


**Figure 1.11.** Examples of structured emulsions that can be created by structural design principles using emulsion droplets as a building block

The key functions of the these nanocarriers are:

- successfully encapsulation of hydrophobic drugs in order to target cells;
- to improve drug efficacy and provide for its better intracellular penetration;
- to serve as shields to protect a hydrophobic therapeutic or diagnostic cargo (e.g., photosensitizers and other NIR dyes,

cytostatics, quantum dots, magnetic nanoparticles, PET or MRI contrasts) from degradation and various toxic interactions with the biological environment.<sup>54, 57, 58</sup>

For all the reasons discussed above, an alternative method of encapsulation of hydrophobic active ingredients was proposed, namely the LbL coating on emulsion and microemulsion droplets.<sup>52, 53, 59, 60</sup> However, the process of liquid core enclosure is more challenging since the application of the rinsing step between deposition of both polycation and polyanion layer is usually not straight forward. Excess of polymer, used for the layer formation, may induce polymer depletion flocculation. Moreover, at the next adsorption step polyanion/polycation complexes would be formed, and it would be difficult to separate them from capsules suspension.<sup>18, 54</sup> A number of strategies<sup>54</sup> have been applied to produce stable multilayer systems without droplet aggregation during the rinsing:

- Centrifugation method. Any excess non-adsorbed polyelectrolyte molecules are then removed by centrifuging the suspension, collecting the particles, and resuspending them in a rinsing solution. The main problem with this method is the possible coalescence of emulsion droplets during centrifugation. In addition, the centrifugation of micro- and nanoemulsions is problematic due to small size and/or low density difference.

- Filtration method. The excess of polyelectrolyte molecules in the continuous phase is removed by membrane filtration of the suspension. A filter is used such that only polyelectrolyte molecules pass through it – not the emulsion drops. By applying an external pressure, the aqueous phase containing the excess polyelectrolyte is forced to pass through the filter. At the same time, a rinsing solution is added to the colloidal suspension to keep the overall volume of the system constant. After the rinsing step, the suspension is mixed with the solution of polyelectrolyte of an opposite charge. Filtration of nanoemulsions requires usage of ultrafiltration cells with membranes with the cut-off of 50–100 nm; therefore, high pressure needs to be applied with the substantial risk of membrane fouling. As an alternative, dialysis can be used, but long time and large amount of rinsing solutions are required.
- Saturation method. In that method the rinsing step is omitted since it is possible to add just enough polyelectrolyte to completely coat all of the particles present in the system, so that there is a few amount of free polyelectrolyte remaining in the aqueous phase. For every system the right amount, namely the “saturation concentration”, has to be determined empirically. The saturation method can be conveniently used for micro- or nanoemulsions

without any limitations. Unfortunately, it leads to a systematic dilution of the emulsions at every adsorption step. This method, used for the realization of the DDSs presented in this work, is better displayed in the following paragraph.

### ***2.1.1. Saturation method for oil-core polyelectrolyte multilayer***

The main problem with using the LBL technique to prepare multilayer emulsions is the tendency for droplet to aggregate during the preparation. To minimize or avoid droplet aggregation it is important to carefully control solution composition and preparation conditions:<sup>61</sup> (i) there should be sufficient polyelectrolyte present to saturate all of the droplet surfaces; (ii) the polyelectrolyte molecules should adsorb to the droplet surfaces more rapidly than when droplet–droplet collisions occur; (iii) there should not be too much polyelectrolyte present to promote depletion flocculation; (iv) the repulsive interactions between the coated droplets should be strong enough to prevent droplet aggregation.

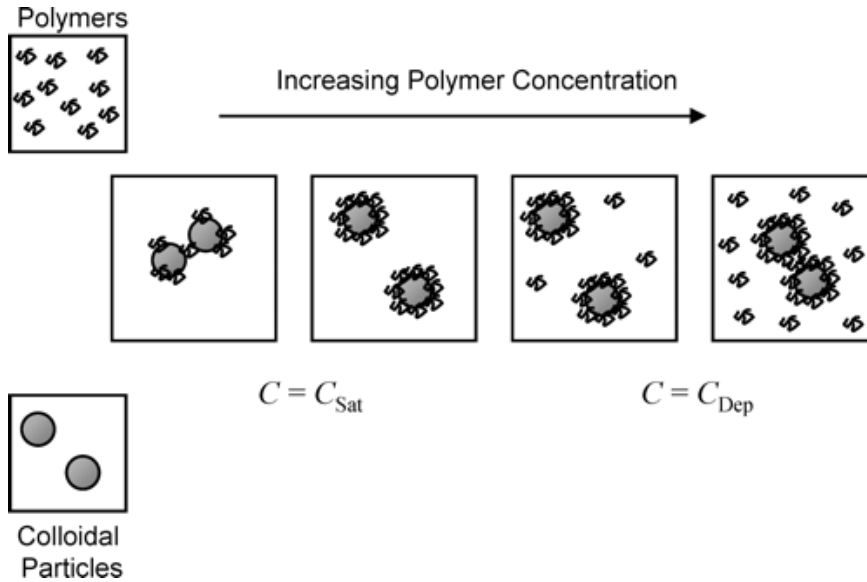


**Figure 1.12.** Schematic diagram of the different events occurring when an electrically charged polyelectrolyte is added to a colloidal dispersion containing oppositely charged spherical particles.

**Figure 1.12** shows a schematization of the model proposed by Mc Clements<sup>61</sup> in which is well summarized the different events occurring when an electrically charged polyelectrolyte is added to a colloidal dispersion containing oppositely charged spherical particles. Particles, in fact, are stable to droplet aggregation when their surfaces are completely saturated with polyelectrolyte ( $C_{sat}$ ) and there is no free polyelectrolyte present in the continuous phase. On the contrary, when the polyelectrolyte concentration is insufficient to completely saturate the particle surfaces, bridging flocculation occurs. On the other side, when the concentration of free polyelectrolyte exceeds another critical value ( $C_{Dep}$ ) depletion flocculation occurs because the attractive depletion forces are strong

enough to overcome the various repulsive forces. Finally, when the concentration is intermediate between saturation and depletion, i.e. when there is free polyelectrolyte in the continuous phase but it is not enough to promote depletion flocculation, the system results to be stable. However, it is more desirable that no free polyelectrolyte is present because polyanion/polycation complexes would be formed at the next adsorption step.

These considerations highlight the importance of determine the saturation concentration  $C_{\text{sat}}$  for each layer deposited around the particle. To obtain empirically this value, the most convenient method contemplates the measurements of the change in  $\zeta$  (zeta) potential along with the change in the mean particle diameter when a polyelectrolyte is added to an emulsion containing oppositely charged droplets. The optimal addition of polyelectrolyte can be determined as corresponding to the point just before reaching the plateau of the dependence of zeta potential on the amount of polyelectrolyte (**Figure 1.13**).<sup>54, 61</sup>

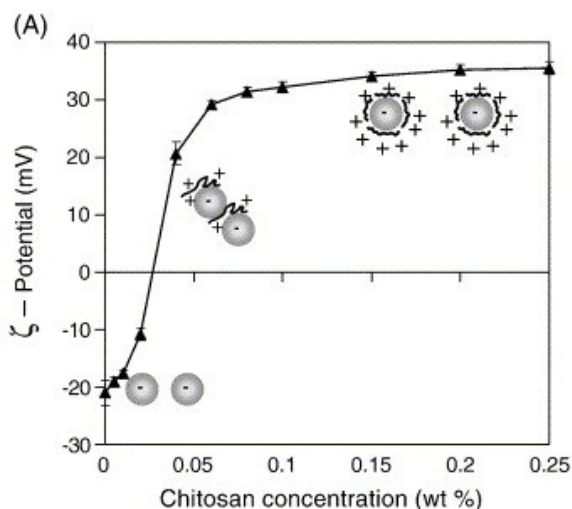


**Figure 1.13.** Change in electrical charge ( $\zeta$ -potential) as cationic chitosan is added to the anionic emulsion. [Reprinted from McClements<sup>61</sup>]

More recently, Vecchione et al. proposed alternative methods to determine the saturation concentration, based on spectrofluorimetry<sup>62</sup> or isothermal titration calorimetry (ITC).<sup>63</sup> In particular, the ITC-based method allows not only to perform a complete physicochemical characterization of the system, but also to detect two separate binding events, instead of just one saturation event.

## 1.5 Aim of research and thesis outline

LbL technique represents a very attractive tool for the realization of DDSs with ideal features like simplicity, versatility, and nanoscale control. The final aim of this research activity concerns the realization of completely biocompatible and biodegradable nanocarriers with diverse functionalities and purposes. The greater ambition, in particular, is the realization of

nanometric sized drug vehicles entirely derived from natural materials but holding the features needed for the drug delivery. My research group started few years ago to realize systems with these facets. Starting from natural materials like soybean oil and egg lecithin as surfactant they were realized nanoscaled oil-core carriers in which hydrophobic drugs or contrasting agents have been successful encapsulated.<sup>62</sup> The O/W nanoemulsions proposed by Vecchione et al. possess relevant characteristics. Thanks to the use of a high pressure homogenizer the O/W emulsion obtained has a tunable size ranging from 80 to 200 nm (depending on the pressure applied and the surfactant used) with an excellent size distribution (PDI below 0.1).<sup>62</sup> The so realized nanoemulsion has been used as liquid core for the realization of oil-core polyelectrolytes-shells nanocarriers. As for the liquid core, natural materials have been selected also for the realization of the shell, and, in particular, polysaccharides and polyaminoacids.<sup>62, 63</sup>

Starting from these conditions this research project has focused on the modifications of the polysaccharides used as coating in order to add desired functionalities to the final nano-vectors. In **Chapter 2** a nanoemulsion loaded with curcumin and coated with a modified chitosan (with thiol moieties) is presented as an oral delivery nanocarrier (**Figure 1.14**, on the left). *In vitro* tests tried to clarify the routes of the nanosystem

and, in particular, how it interacts and passes the intestinal barrier. *In vivo* tests, instead, showed how the size and the amount of thiols on the surface effect on the drug assimilation and anti-inflammatory activity.

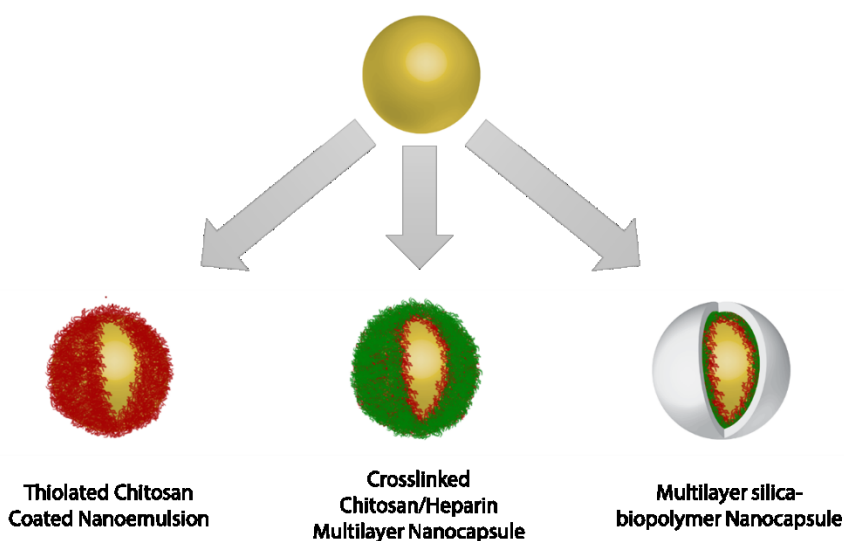


**Figure 1.14.** Schematic summary of the nano-systems proposed in the current thesis. Starting from an oil in water nanoemulsion, three different systems are proposed. For each system modification of biopolymers used (chitosan and heparin) was needed in order to add functionalities and obtain versatility.

In **Chapter 3** a multilayer system with modified glycol chitosan and heparin is proposed (**Figure 1.14**, in the center). The glycol chitosan is modified with a thiol moiety, whereas heparin is modified with an allylic moiety. The polymer modifications allowed to apply a photo activated reaction – thiol-ene ‘click’ reaction – to covalently cross link the layers. The system submitted to cross-linkage result to be more stable than the unmodified one, even if changes in pH and ionic strength occur. It then could represent a proof of concept for the realization of LbL nanocapsules

with enhanced biostability. In **Chapter 4** a multi-shell nanocarrier system featuring a hybrid polymer/silica-shell is proposed and realized (**Figure 1.14**, on the right). In detail, a bilayer composed of chitosan and heparin has been deposited on an oil core and an *in situ* modification of heparin with an aminosilane (APTS) allowed the realization of an outer silica shell, using a modified Stöber sol-gel method.<sup>64</sup> The final system resulted to be highly versatile: the possibility to tune the shell thickness determines its mechanical properties; the possibility to load the oil core with lipophilic drugs or contrast agents together with the possibility to further functionalize the polymeric shell allow for the use of the system for drug delivery or diagnostic; the possibility to modify the external surface and to coat it with PEG allows to improve the half-life and to add targeting functionalities. Final conclusions and future perspectives are synthetically presented and discussed in **Chapter 5**. The reader will appreciate how the current thesis have been presented in order of complexity of the final system but also how the realization of each system results to be relatively simple and, in consequence, potentially scalable for industrial applications.

## 1.6 References

1. R. P. Feynman, *Engineering and science*, 1960, **23**, 22-36.
2. I. Freestone, N. Meeks, M. Sax and C. Higgitt, *Gold Bulletin*, 2007, **40**, 270-277.
3. R. E. Smalley, 2001.
4. Y. Ge, S. Li, S. Wang and R. Moore, *Nanomedicine: Principles and Perspectives*, Springer, 2014.
5. A. Kumar, H. M. Mansour, A. Friedman and E. R. Blough, *Nanomedicine in drug delivery*, CRC Press, 2013.
6. T. Cedervall, I. Lynch, S. Lindman, T. Berggård, E. Thulin, H. Nilsson, K. A. Dawson and S. Linse, *Proceedings of the National Academy of Sciences*, 2007, **104**, 2050-2055.
7. I. Lynch and K. A. Dawson, *Nano Today*, 2008, **3**, 40-47.
8. D. E. Owens and N. A. Peppas, *International journal of pharmaceutics*, 2006, **307**, 93-102.
9. A. L. Klibanov, K. Maruyama, V. P. Torchilin and L. Huang, *FEBS letters*, 1990, **268**, 235-237.
10. V. P. Torchilin and V. S. Trubetskoy, *Advanced drug delivery reviews*, 1995, **16**, 141-155.
11. Y. Matsumura and H. Maeda, *Cancer research*, 1986, **46**, 6387-6392.
12. D. Peer, J. M. Karp, S. Hong, O. C. Farokhzad, R. Margalit and R. Langer, *Nature nanotechnology*, 2007, **2**, 751-760.
13. J. Fang, H. Nakamura and H. Maeda, *Advanced drug delivery reviews*, 2011, **63**, 136-151.
14. V. Torchilin, *Advanced drug delivery reviews*, 2011, **63**, 131-135.
15. F. Alexis, E. Pridgen, L. K. Molnar and O. C. Farokhzad, *Molecular pharmaceutics*, 2008, **5**, 505-515.
16. V. P. Torchilin, in *Drug delivery*, Springer, 2010, pp. 3-53.
17. L. Y. Qiu and Y. H. Bae, *Pharmaceutical research*, 2006, **23**, 1-30.
18. J. J. Richardson, M. Björnmalm and F. Caruso, *Science*, 2015, **348**, aaa2491.
19. J. Kirkland, *Analytical Chemistry*, 1965, **37**, 1458-1461.
20. R. Iler, *Journal of Colloid and Interface Science*, 1966, **21**, 569-594.
21. G. Decher, *Science*, 1997, **277**, 1232-1237.
22. X. Zhang, H. Chen and H. Zhang, *Chemical Communications*, 2007, DOI: 10.1039/B615590A, 1395-1405.

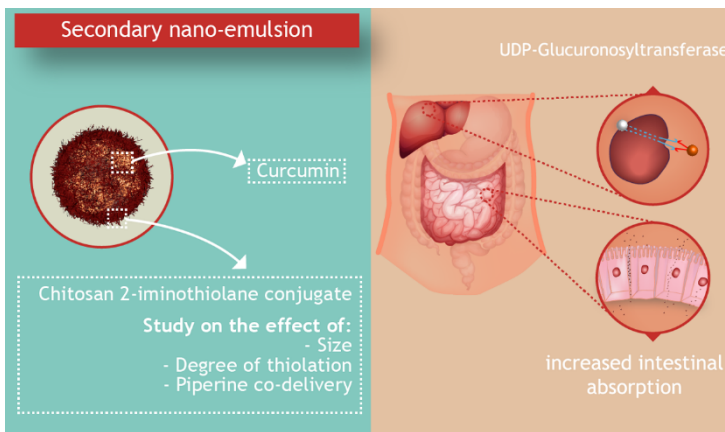
23. L. L. del Mercato, M. M. Ferraro, F. Baldassarre, S. Mancarella, V. Greco, R. Rinaldi and S. Leporatti, *Advances in colloid and interface science*, 2014, **207**, 139-154.
24. U. Wattendorf, O. Kreft, M. Textor, G. B. Sukhorukov and H. P. Merkle, *Biomacromolecules*, 2007, **9**, 100-108.
25. M. M. Kamphuis, A. P. Johnston, G. K. Such, H. H. Dam, R. A. Evans, A. M. Scott, E. C. Nice, J. K. Heath and F. Caruso, *Journal of the American Chemical Society*, 2010, **132**, 15881-15883.
26. S. Koker, R. Rycke and B. G. áDe Geest, *Soft Matter*, 2014, **10**, 804-807.
27. F. Caruso, R. A. Caruso and H. Möhwald, *Science*, 1998, **282**, 1111-1114.
28. E. Donath, G. B. Sukhorukov, F. Caruso, S. A. Davis and H. Möhwald, *Angewandte Chemie International Edition*, 1998, **37**, 2201-2205.
29. H. Ejima, J. J. Richardson, K. Liang, J. P. Best, M. P. van Koeverden, G. K. Such, J. Cui and F. Caruso, *Science*, 2013, **341**, 154-157.
30. V. Sinha and R. Kumria, *International journal of pharmaceutics*, 2001, **224**, 19-38.
31. S. Mizrahy and D. Peer, *Chemical Society Reviews*, 2012, **41**, 2623-2640.
32. H. Wang, D. Loganathan and R. J. Linhardt, *Biochem. J*, 1991, **278**, 689-695.
33. J. Kyte, *Structure in protein chemistry*, Garland Science, 2006.
34. Q. Z. Wang, X. G. Chen, N. Liu, S. X. Wang, C. S. Liu, X. H. Meng and C. G. Liu, *Carbohydrate polymers*, 2006, **65**, 194-201.
35. T. Crouzier, T. Boudou and C. Picart, *Current Opinion in Colloid & Interface Science*, 2010, **15**, 417-426.
36. C. Picart, A. Schneider, O. Etienne, J. Mutterer, P. Schaaf, C. Egles, N. Jessel and J.-C. Voegel, *Advanced Functional Materials*, 2005, **15**, 1771-1780.
37. K. Janes, P. Calvo and M. Alonso, *Advanced drug delivery reviews*, 2001, **47**, 83-97.
38. V. Dodane and V. D. Vilivalam, *Pharmaceutical Science & Technology Today*, 1998, **1**, 246-253.
39. S. Mima, M. Miya, R. Iwamoto and S. Yoshikawa, *Journal of Applied Polymer Science*, 1983, **28**, 1909-1917.
40. R. Muzzarelli and C. Muzzarelli, in *Polysaccharides I*, Springer, 2005, pp. 151-209.
41. M. Rinaudo, *Progress in polymer science*, 2006, **31**, 603-632.

42. R. A. Muzzarelli, C. Jeuniaux and G. W. Gooday, 1986.
43. T. Kean and M. Thanou, *Advanced Drug Delivery Reviews*, 2010, **62**, 3-11.
44. E. Yilmaz, in *Biomaterials*, Springer, 2004, pp. 59-68.
45. D. K. Knight, S. N. Shapka and B. G. Amsden, *Journal of Biomedical Materials Research Part A*, 2007, **83**, 787-798.
46. H. G. Garg, R. J. Linhardt and C. A. Hales, *Chemistry and biology of heparin and heparan sulfate*, Elsevier, 2011.
47. R. J. Linhardt, *Journal of medicinal chemistry*, 2003, **46**, 2551-2564.
48. R. J. Linhardt, S. A. Ampofo, J. Fareed, D. Hoppensteadt, J. Folkman and J. B. Mulliken, *Biochemistry*, 1992, **31**, 12441-12445.
49. S. Boddohi, C. E. Killingsworth and M. J. Kipper, *Biomacromolecules*, 2008, **9**, 2021-2028.
50. A. A. Antipov and G. B. Sukhorukov, *Advances in Colloid and Interface Science*, 2004, **111**, 49-61.
51. B. V. Parakhonskiy, A. M. Yashchenok, M. Konrad and A. G. Skirtach, *Advances in colloid and interface science*, 2014, **207**, 253-264.
52. S. Sivakumar, V. Bansal, C. Cortez, S. F. Chong, A. N. Zelikin and F. Caruso, *Advanced Materials*, 2009, **21**, 1820-1824.
53. D. Grigoriev, T. Bukreeva, H. Möhwald and D. Shchukin, *Langmuir*, 2008, **24**, 999-1004.
54. K. Szczepanowicz, U. Bazylińska, J. Pietkiewicz, L. Szyk-Warszyńska, K. A. Wilk and P. Warszyński, *Advances in colloid and interface science*, 2014.
55. J.-z. Ma, Y.-h. Liu, Y. Bao, J.-l. Liu and J. Zhang, *Advances in colloid and interface science*, 2013, **197**, 118-131.
56. A. Kowalczyk, R. Trzcinska, B. Trzebicka, A. H. Müller, A. Dworak and C. B. Tsvetanov, *Progress in Polymer Science*, 2014, **39**, 43-86.
57. J. Nicolas, S. Mura, D. Brambilla, N. Mackiewicz and P. Couvreur, *Chemical Society Reviews*, 2013, **42**, 1147-1235.
58. S. D. Steichen, M. Caldorera-Moore and N. A. Peppas, *European Journal of Pharmaceutical Sciences*, 2013, **48**, 416-427.
59. K. Szczepanowicz, D. Dronka-Góra, G. Para and P. Warszyński, *Journal of microencapsulation*, 2010, **27**, 198-204.
60. K. Szczepanowicz, H. Hoel, L. Szyk-Warszyńska, E. Bielanska, A. Bouzga, G. Gaudernack, C. Simon and P. Warszyński, *Langmuir*, 2010, **26**, 12592-12597.

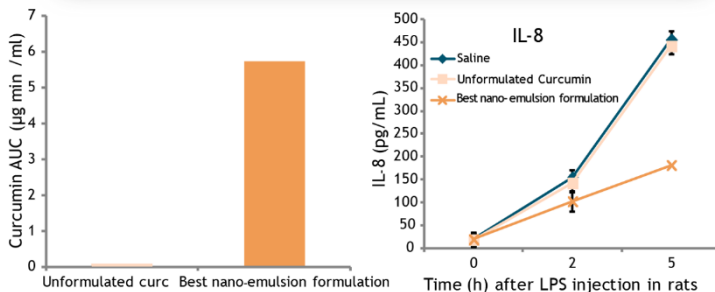
61. D. J. McClements, *Langmuir*, 2005, **21**, 9777-9785.
62. R. Vecchione, U. Ciotola, A. Sagliano, P. Bianchini, A. Diaspro and P. Netti, *Nanoscale*, 2014, **6**, 9300-9307.
63. I. Fotticchia, T. Fotticchia, C. A. Mattia, P. A. Netti, R. Vecchione and C. Giancola, *Langmuir*, 2014, **30**, 14427-14433.
64. W. Stöber, A. Fink and E. Bohn, *Journal of colloid and interface science*, 1968, **26**, 62-69.

# Chapter 2

## Curcumin bioavailability from oil in water nano-emulsions: *in vitro* and *in vivo* study on the dimensional, compositional and interactional dependence<sup>1</sup>



Case of 110 nm; piperine co-delivery; maximum thiolation



<sup>1</sup> This work has been submitted for publication to Journal of Controlled Release: R. Vecchione, V. Quagliariello, D. Calabria, V. Calcagno, E. De Luca, R. V. Iaffaioli, P. A. Netti. "Curcumin bioavailability from oil in water nano-emulsions: *in vitro* and *in vivo* study on the dimensional, compositional and interactional dependence". The Supplementary Section is not included in the submitted publication.

**Abstract.** Although nanocarriers can enhance the bioavailability of free curcumin in the blood, a systematic study on the parameters that affect such enhancement is still missing. In this work we focused the attention on a nanocarrier represented by an oil in water nano-emulsion coated with a thiol modified chitosan and carried out a comprehensive study on the effects that parameters such as size, co-delivery of piperine and degree of chitosan modification can exert on curcumin bioavailability and quantified their impact. We obtained an unprecedented pharmacokinetic profile of curcumin with the best formulation, represented by a combination of a small nano-emulsion size (110 nm), co-delivery of curcumin and piperine (weight ratio 100:1) and a high degree of chitosan thiolation (around 15%). Then, we assessed its anti-inflammatory properties after oral administration in rats at low doses ( $\leq 0.1$  times the volume administered in the pharmacokinetic study) compatible with a possible transfer to humans. Furthermore, the proposed food grade nano-emulsions loaded with curcumin did not show any cytotoxic effect on normal fibroblasts, while they were able to promote death in colon cancer cells in agreement with the common knowledge of the selective action of curcumin.

## 2.1 Introduction

Curcumin, a bioactive compound isolated from the rhizome of the *Curcuma longa* plant, has a long history of use in traditional Chinese and Indian medicine. An interesting example concerns the common use of curcumin powder for the treatment of cough and related respiratory diseases<sup>1</sup> and as an antidysenteric.<sup>2</sup> Moreover, in the past, it was also used to treat dental diseases, digestive disorders such as dyspepsia and acidity, indigestion, flatulence, ulcers and many inflammatory conditions in different body regions.<sup>3</sup> From a chemical point of view, curcumin is a diferuloyl methane molecule [1,7-bis (4-hydroxy-3-methoxyphenyl)-1,6-heptadiene-3,5-dione] containing two ferulic acid residues joined by a methylene bridge. Curcumin acts as a ROS scavenger, increases antioxidant glutathione levels by induction of glutamate cysteine ligase, and acts as an anti-inflammatory agent through the inhibition of NF- $\kappa$ B signaling.<sup>4</sup> It acts through the inhibition of I- $\kappa$ B phosphorylation and thus prevents I- $\kappa$ B degradation by the proteasomes. Despite its numerous applications, the most relevant issues concerning the pharmacokinetics of curcumin are: molecular instability, poor solubility in water, rapid conjugation in the liver with biliary excretion and poor enteral absorption.<sup>5</sup> To increase its bioavailability, several approaches have been tried:

phospholipid complexes (phytosomes), which increased the area under the blood concentration-time curve (AUC) of curcumin after oral administration in rats by 5 times;<sup>6</sup> association with cyclodextrin, with a ten-fold increase in curcumin AUC;<sup>7</sup> BCM-95 extract, whose bioavailability in rats was 7.8 times higher than unformulated curcumin;<sup>8</sup> mixing of curcumin with an essential oil obtained from standardized turmeric where AUC was 7–8 times higher than unformulated curcumin.<sup>9</sup> Another interesting approach to improve the biodistribution of curcumin is based on its combination with piperine, the alkaloid responsible for the pungency of black pepper and long pepper; it inhibits the glucuronidation processes by the enzyme UDP-glucuronosyltransferase (with  $K_i$  of 70  $\mu\text{M}$ ) in the liver and small intestine, as demonstrated by the administration of unformulated curcumin and piperine.<sup>10, 11</sup> It is also known that oil in water nano-emulsions can enhance bioavailability, as well as provide an anti-inflammatory action as a response to the free curcumin in the blood.<sup>12</sup> The best performing nano-emulsion produced so far has provided no more than a ten-fold increase in the AUC compared to unformulated curcumin in mice.<sup>13</sup> The best performing systems have been up to now based on the use of colloidal curcumin nanoparticles, named 'theracurmin' that showed AUC after oral administration 40-fold higher than that of curcumin powder in rats.<sup>14</sup> Motivated by the very interesting properties of curcumin, in our

study we proposed an easily tunable nanocarrier in order not only to find out optimal conditions to further enhance curcumin bioavailability, but also to better understand the impact of different nanocarrier parameters to address the design of more and more performing nanocarriers. In particular, we developed and tested biologically, *in vitro* and *in vivo*, a new nanometric formulation of curcumin combined with the alkaloid piperine, both loaded in oil in water nano-emulsions stabilized by a layer of chitosan chosen for its resistance to the gastro tract and adhesive properties towards the intestinal lumen.<sup>15</sup> Due to the enhanced adhesive properties of the chitosan derivative possessing thiol moieties,<sup>16</sup> we optimized the degree of functionalization of chitosan with 2-iminothiolane and tested the system at different degrees of functionalization to quantify its impact. Emulsion size is another important parameter to investigate; although most of the studies report bioavailability improvement with a reduction in nanocarrier size,<sup>17</sup><sup>18</sup> there is evidence that -in some cases- size plays a minor role.<sup>19</sup> In this context, we analyzed the effects of size on the bioavailability of free curcumin by using a first emulsion with a 110 nm diameter and a second almost double in size. In combination with the pharmacokinetic study we also carried out a biodistribution analysis and evaluated the cytotoxic effect of the curcumin loaded nano-emulsion on normal fibroblasts and on colon cancer cells to assess curcumin activity upon encapsulation in our

nanocarrier. Finally, to assess the efficacy of the proposed nanotool, as a functional test, we tested the anti-inflammatory properties of the best formulation on lipopolysaccharide (LPS) treated rats in comparison with a traditional lipid formulation based on curcumin phosphatidylcholine complexation at different volume doses, including volumes compatible with a possible transfer to humans.

## 2.2 Results and discussions

### *Nano-emulsions analysis*

Particle size of curcumin loaded nano-emulsions was characterized by DLS. Smaller nano-emulsions coated with pristine chitosan exhibited a size of ~110 nm in diameter and a PDI of ~0.09, as depicted in **Figure 2.1F**. However, the use of chitosan 2-iminothiolane conjugate as a coating did not significantly affect the final size and PDI even at the highest degree of modification (size ~110 nm and PDI ~0.1). Then, to study the effects of size on bioavailability, the formulation with a lower amount of lecithin surfactant was also measured by DLS showing a *circa* double final size (size ~230 nm and PDI ~0.06). In this work pristine chitosan was modified with FITC and as an example the smaller nano-emulsion containing curcumin was coated with such FITC labeled chitosan to be visualized in

fluorescence. In particular, this nano-emulsion was characterized by using a STED microscope (high resolution < 100 nm), since the expected size was around 110 nm. This size measured by DLS was confirmed by STED analysis, as illustrated in **Figure 2.1A-E**, where confocal and STED acquisition are compared. Real size given by the STED image indicates that most of the nano-droplets are about 110 nm large, proving the narrow distribution feature of our secondary nano-emulsions. Statistical analysis confirmed size and monodispersity provided by DLS. In addition, as shown in a previous work<sup>20, 21</sup> the process utilized to produce such chitosan coated nano-emulsions allows stability to last longer than 1 year. This characterization demonstrates -as already shown by DLS- the capability to dimensionally control our nanocarriers so that all the results can be associated to a specific size. The degrees of functionalization measured by applying the Ellman's test were 7.2% for the chitosan 2-iminothiolane conjugate at the medium degree of modification (CT-IT-m), 15.1 % for the highest degree of modification (CT-IT-h) in the case of deposition on the larger nano-emulsion size and -finally- 13.6% for the highest degree of modification in the case of deposition on the smaller nano-emulsion.

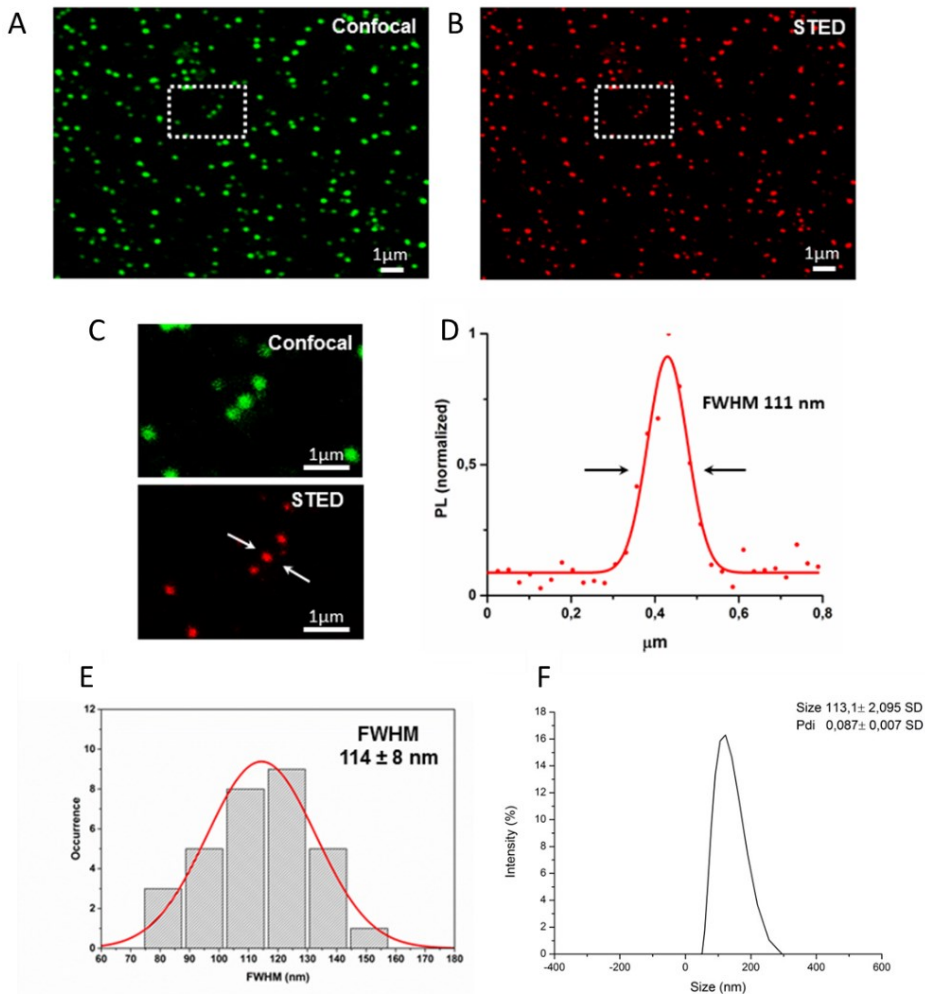


**Figure 2.1.** Analysis of chitosan coated nano-emulsions loaded with curcumin: (A) Confocal and (B) STED imaging; (C) Enlargements of the areas boxed in A and B; (D) Gaussian fit of the intensity point measured on the STED image. The white arrows show the point where the line profile was measured; (E) Statistical analysis of the FWHM obtained with the Gaussian fit of 30 individual emitting spots; (F) DLS measurement.

Changes in the structure upon functionalization can be evidenced also by NMR spectra, presented in **Figure 2.2**. Compared to the spectrum of pristine chitosan (in the bottom of the image), it is possible to observe the appearance of new peaks, in particular at 1.76 ppm, 2.30 ppm and 2.42

ppm, associated with the methylene groups of the thio-butyl-amidine (at the top right corner of the figure).

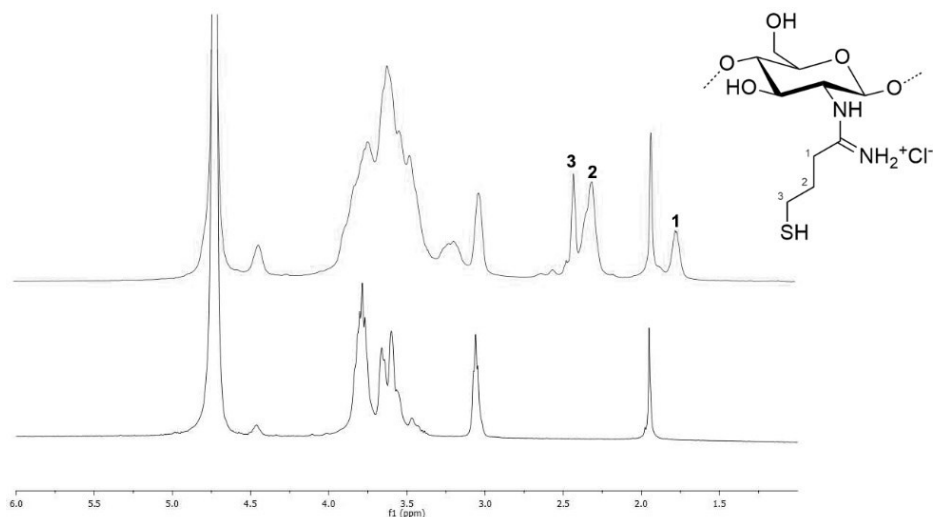


**Figure 2.2.** 1D  $^1\text{H}$  NMR spectra of pristine chitosan (bottom line) and chitosan 2-iminothiolane conjugate (top line). New signals associated with the methylene groups of the thio-butyl-amidine appear after the functionalization, in particular at 1.76 ppm, 2.30 ppm and 2.42 ppm.

### *Cell cytotoxicity*

We tested the biosafety of the nano-emulsions and the capability of our nano-emulsion to maintain curcumin activity by carrying out cytotoxicity tests on the different formulations loaded and non-loaded with curcumin and/or piperine always at 1/100 w/w ratio with curcumin. First of all, cell viability results demonstrated, in 3T3 (**Figure 2.3A**) and HT29 (**Figure 2.3B**) cell lines, the non-toxicity of the different formulations alone indicating the biosafety of the tested carriers.

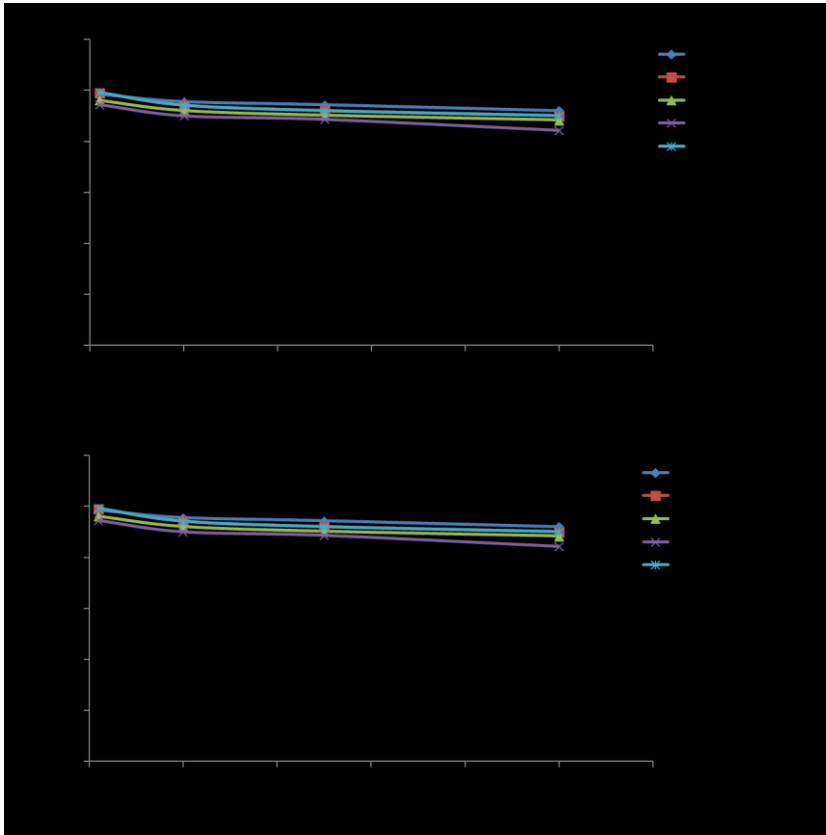


**Figure 2.3.** Viability of 3T3 (A) and HT29 (B) cells after 24 h of exposure at 37 °C as a function of nano-emulsion (mg oil/ml) without curcumin. \* $p < 0.01$ ; \*\* $p < 0.05$ ; n.s.: not significant

As regards formulated curcumin, against fibroblasts, nano-emulsions loading curcumin alone and in combination to piperine (weight ratio 100:1) did not show a significant toxicity up to 100  $\mu\text{g/ml}$  of corresponding curcumin concentration for incubation times up to 24 h (**Figure 2.4**).

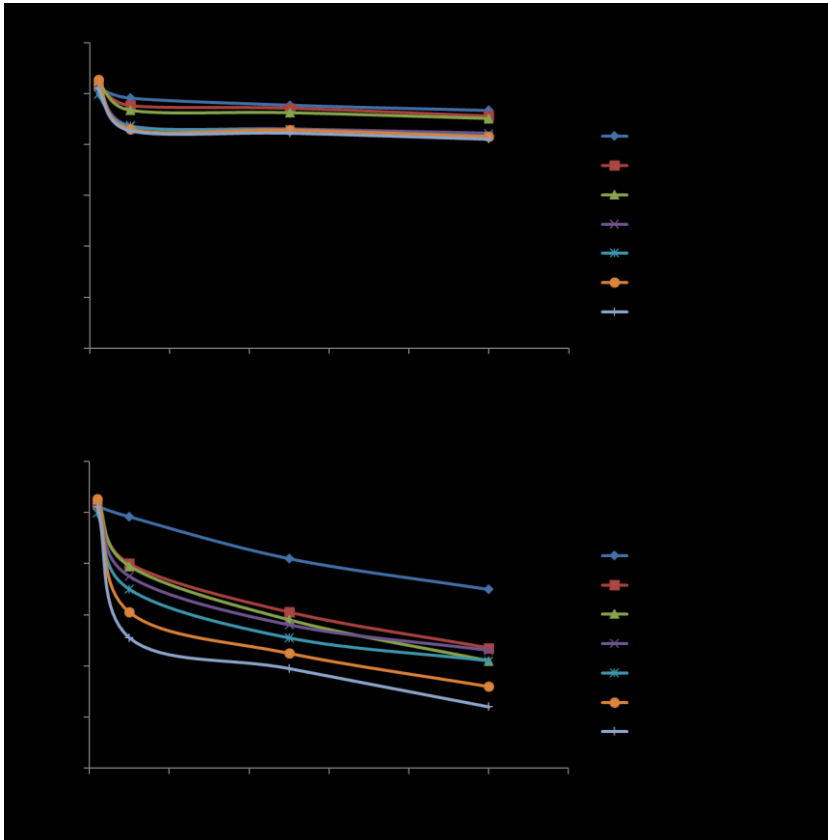


**Figure 2.4.** Viability of 3T3 (A) and HT29 (B) cells after 24 h of exposure at 37 °C as a function of nano-emulsion (mg oil/ml) and curcumin ( $\mu\text{g/ml}$ ) concentration. \* $p < 0.01$ ; \*\* $p < 0.05$ ; n.s: not significant.

Similarly, unformulated piperine and nano-emulsions loaded with piperine (Figure 2.5) showed no significant cytotoxicity against both cell lines.

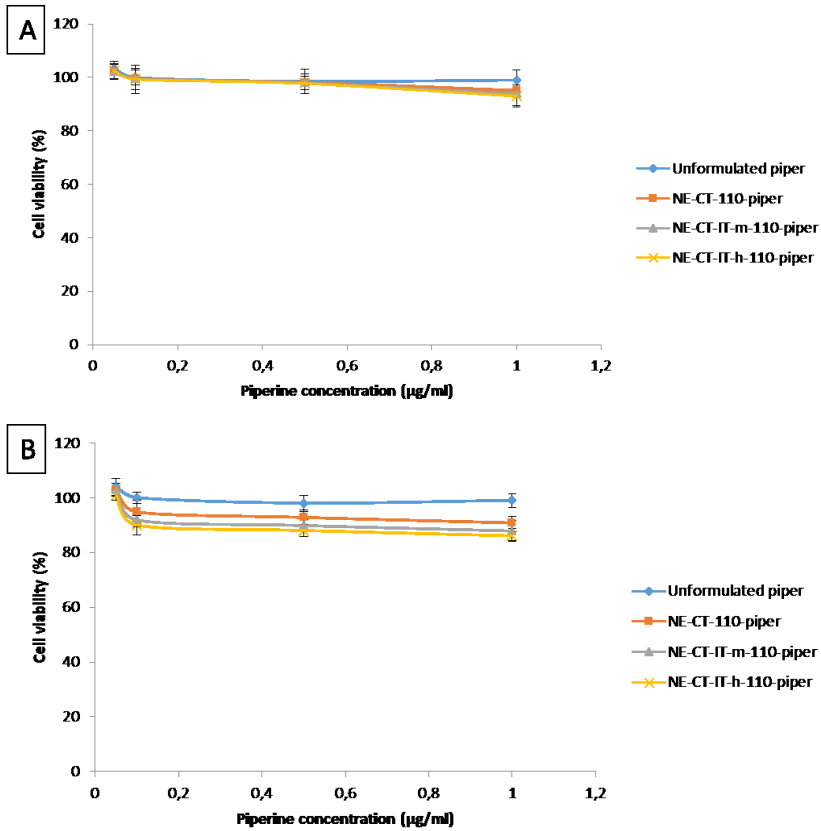


**Figure 2.5.** Viability of 3T3 (A) and HT29 (B) cells after 24 h of exposure at 37°C as a function of piperine ( $\mu\text{g/ml}$ ) concentration.

In contrast, formulated curcumin showed high toxicity in the colon cancer cells (HT29 cell line, **Figure 2.6B**) after 24 h of contact compared to unformulated curcumin (**Figure 2.4B**). In addition, NE-CT-110-curc showed a lower level of toxicity compared to NE-CT-IT-h-110-curc ( $p < 0.05$ ).

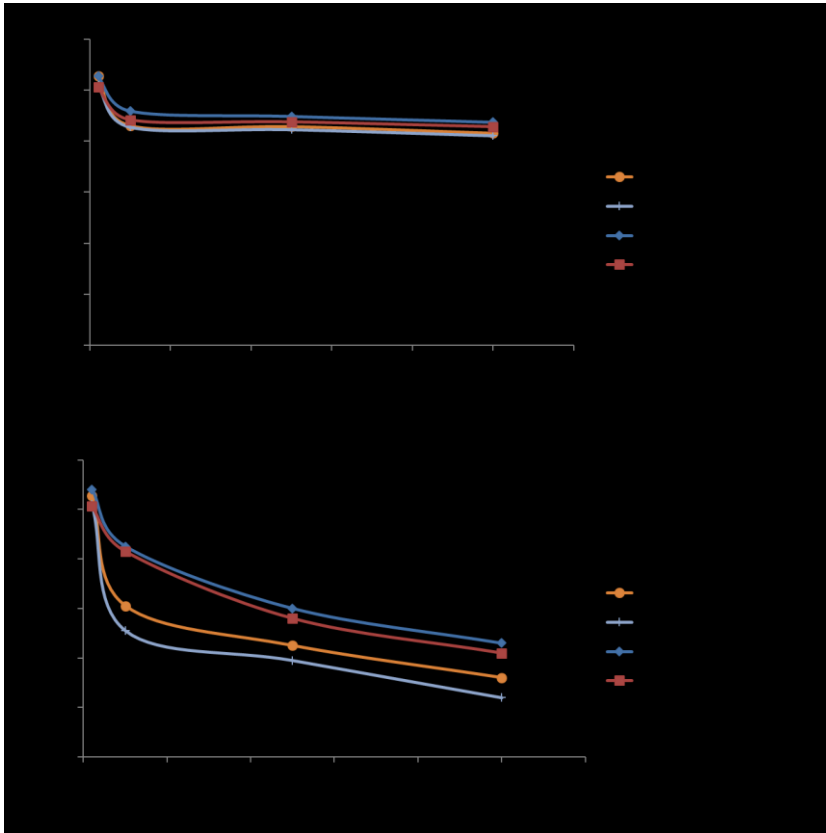


**Figure 2.6.** Viability of 3T3 (A) and HT29 (B) cells after 24 h of exposure at 37 °C as a function of nano-emulsion (mg oil/ml) and curcumin ( $\mu\text{g/ml}$ ) concentration. \* $p < 0.01$ ; \*\* $p < 0.05$ ; n.s: not significant.

This effect can be explained considering the higher cytoadhesive properties of thiolated polymers due to more interactions with the cellular membrane.<sup>22, 23</sup> According to this concept an IC<sub>50</sub> at 65 and at 25  $\mu\text{g/ml}$ , respectively, for NE-CT-IT-m-110-curc and NE-CT-IT-h-110-curc, was observed, indicating a concentration-dependent interaction between the thiol groups on chitosan and the cell membrane. Administration of curcumin and piperine in combination led to a higher level of cytotoxicity, that is statistically significant only when comparing NE-CT-IT-h-110-curc

and NE-CT-IT-h-110-curc-piper( $p < 0.05$ ), as depicted always in; this behavior suggests a possible adjuvant action of piperine in the anti-proliferative molecular mechanism of curcumin against human colon cancer cells (**Figure 2.4B** and **Figure 2.6B**). On the basis of these results, the best cytotoxic formulation was the NE-CT-IT-h-110-curc-piper, exhibiting an IC<sub>50</sub> value at 24 h of 15  $\mu\text{g/ml}$  of curcumin, which was significantly lower than curcumin concentrations needed to reach IC<sub>50</sub> by the other formulations (in the case of unformulated curcumin IC<sub>50</sub> was not reached at all). Interestingly, comparing results on both cell lines, we observed selective toxicity of curcumin against human colon cancer cells in agreement with recent literature sources reporting selective anticancer properties of this molecule alone,<sup>24</sup> or in combination with conventional anticancer drugs.<sup>25-27</sup> These results prove that the selective action property of curcumin is maintained when encapsulated in our nano-emulsions.

### ***Cancer cell imaging and internalization studies***

Following FITC emission, a cell uptake study was carried out. For this analysis we used the 110 nm curcumin nano-emulsion coated with FITC-labelled chitosan, NE-FITC-CT-110-curc at a correspondent curcumin volume concentration of 1  $\mu\text{g/ml}$ . The graph presented in **Figure 2.7** corresponds to the amount of internalized nano-emulsions (expressed as

$\mu\text{g}$  of chitosan /mg of proteins), plus cell surface-bound nano-emulsions. NE-FITC-CT-110-curc were taken up very rapidly by HT29 cell line, with a value of 150  $\mu\text{g}$  of corresponding chitosan per mg cell protein reached after as early as 4 h of incubation; other literature reports confirm the rapidity of cellular uptake due to electrostatic interactions between the cellular membrane and the positively charged chitosan <sup>28</sup>.

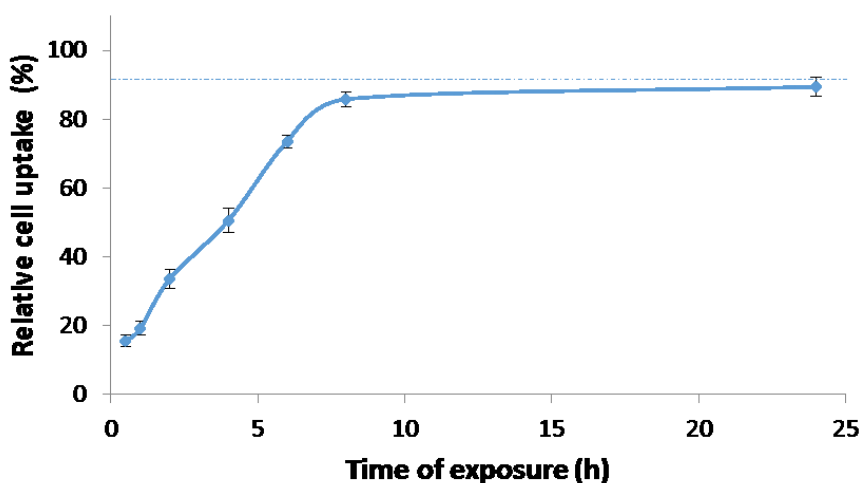


**Figure 2.7.** Overall cellular uptake quantification of NE-FITC-CT-110-curc at a corresponding curcumin concentration of 1  $\mu\text{g}/\text{ml}$  internalized in colon cancer cells (HT29 cell line) as a function of time.

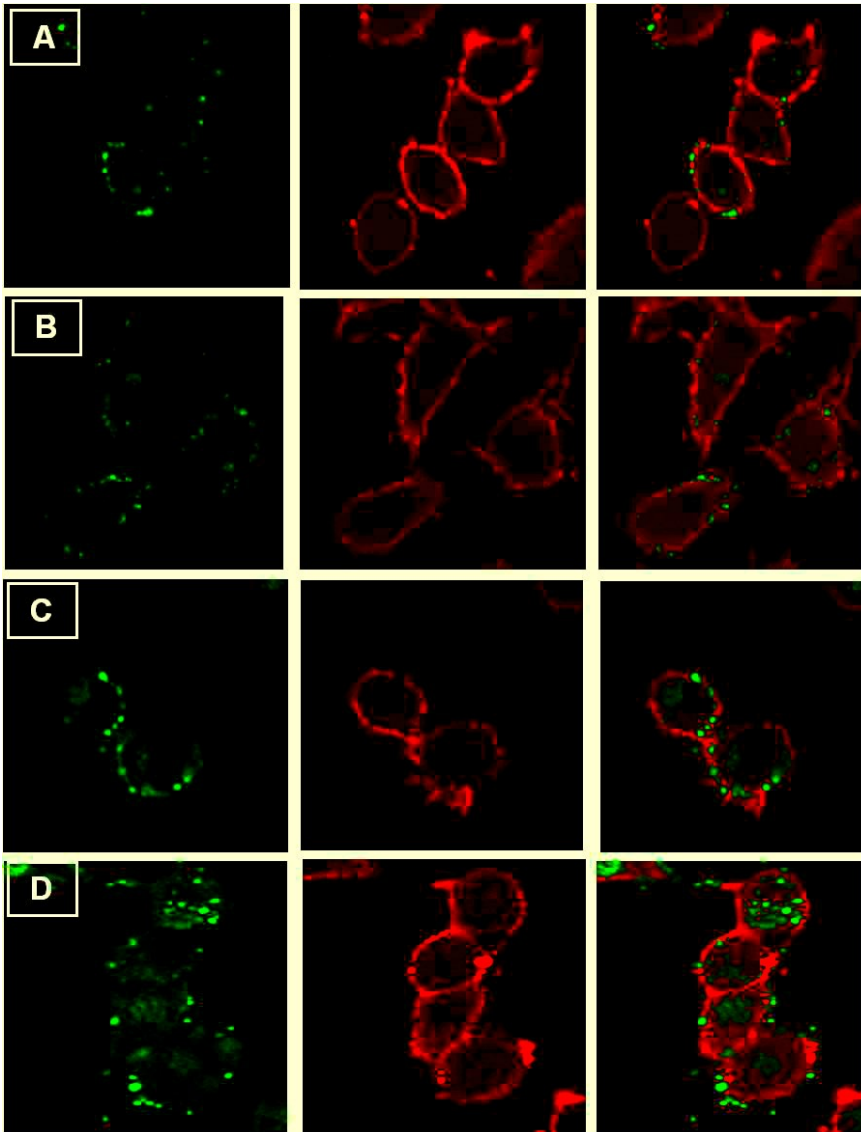


**Figure 2.8.** Confocal Laser Scanning Microscope images of colon cancer cells (HT29 cell line) after 0.5 (A), 2 (B), 4 (C) and 24 h (D) of contact with NE-FITC-CT-110-curc at a corresponding curcumin concentration of 1  $\mu\text{g}/\text{ml}$ ; the green punctuated fluorescence corresponds to uptaken nano-emulsion, which clearly moves from a peripheral to a central (perinuclear) localization during the incubation time. Green signal: FITC; Red signal: Concanavalin A Tetramethylrhodamine Conjugate. Scale bar: 50  $\mu\text{m}$ .

Confocal images show that NE-FITC-CT-110-curc (green in **Figure 2.8**) was visibly associated to peripheral intracellular compartments at early

time points (0.5-4 h, **Figure 2.8A-C**), whereas a more central localization was recorded after 24 h (**Figure 2.8D**). These results demonstrate the nano-emulsion uptake ability and the time dependent internalization in human colon cancer cells with a tendency to accumulate in the perinuclear regions of the cells after 24 h, which is generally advantageous for drugs that intercalate with DNA -such as curcumin.

### ***Pharmacokinetic studies***

Pharmacokinetic data related to 8 mg/kg doses are reported in **Table 2.1** and **Figure 2.9**. They include data related to absolute curcumin AUC, curcumin C<sub>max</sub>, curcumin AUC ratio with its two main metabolites and relative curcumin bioavailability (%). As shown, compared to unformulated curcumin, orally administered nano-emulsions loaded with curcumin always determined an increase in both maximum concentration (C<sub>max</sub>) and AUC of the curcumin and its two metabolites, glucuronidated and sulphated; thus, formulated curcumin led to a greater intestinal drug adsorption capacity than unformulated curcumin, with a consequent increase in its metabolized forms.

**Table 2.1.** Calculated nanomolar plasma peak levels (Cmax), time of peak levels (Tmax), AUC expressed as  $\mu\text{g min/ml}$  and relative bioavailability (%).

Formulations (8 mg/kg of curcumin)	Parameters	Curcumin	Curcumin glucuronide	Curcumin sulphate
Unformulated cure	Cmax (nM)	0.12 ± 0.04	4.5 ± 0.25	0.21 ± 0.18
	Tmax (min)	30	30	60
	AUC ( $\mu\text{g min/ml}$ )	0.09 ± 0.03	3.7 ± 0.1	0.34 ± 0.11
	Relative bioavailability (%)	1		
NE cure	Cmax (nM)	0.28 ± 0.19	68.7 ± 5.4	0.48 ± 0.25
	Tmax (min)	15	30	60
	AUC ( $\mu\text{g min/ml}$ )	0.27 ± 0.07	71.4 ± 8.6	0.38 ± 0.08
	Relative bioavailability (%)	3 ± 0.1		
NE-CT-110-cure	Cmax (nM)	0.69 ± 0.47	112.5 ± 2.5	0.84 ± 0.56
	Tmax (min)	15	30	60
	AUC ( $\mu\text{g min/ml}$ )	0.52 ± 0.13	121.8 ± 7.3	0.93 ± 0.17
	Relative bioavailability (%)	5.7 ± 0.8		
NE-CT-110-cure-piper	Cmax (nM)	1.05 ± 0.32	88.7 ± 1.8	0.9 ± 0.33
	Tmax (min)	15	30	60
	AUC ( $\mu\text{g min/ml}$ )	0.83 ± 0.18	81.1 ± 4.3	0.98 ± 0.12
	Relative bioavailability (%)	9.2 ± 1.5		
NE-CT-IT-m-110-cure	Cmax (nM)	1.69 ± 0.5	201.5 ± 2.4	0.82 ± 0.2
	Tmax (min)	15	30	60
	AUC ( $\mu\text{g min/ml}$ )	1.86 ± 0.21	211.8 ± 13.3	1.21 ± 0.3
	Relative bioavailability (%)	9.5 ± 1.1		
NE-CT-IT-m-110-cure-piper	Cmax (nM)	2.78 ± 0.31	101.8 ± 3.1	0.98 ± 0.83
	Tmax (min)	15	30	60
	AUC ( $\mu\text{g min/ml}$ )	1.98 ± 0.34	118.3 ± 15.6	0.63 ± 0.3
	Relative bioavailability (%)	22 ± 2.8		
NE-CT-IT-h-110-cure	Cmax (nM)	2.07 ± 0.21	341.1 ± 1.7	1.14 ± 0.4
	Tmax (min)	15	30	60
	AUC ( $\mu\text{g min/ml}$ )	2.99 ± 0.55	316.2 ± 18.3	2.09 ± 0.22
	Relative bioavailability (%)	33.2 ± 2.7		
NE-CT-IT-h-110-cure-piper	Cmax (nM)	3.98 ± 0.13	153.4 ± 2.6	1.28 ± 0.61
	Tmax (min)	15	30	60
	AUC ( $\mu\text{g min/ml}$ )	5.73 ± 0.61	156.7 ± 17.2	1.47 ± 0.13
	Relative bioavailability (%)	64 ± 4.3		
NE-CT-IT-h-220-cure	Cmax (nM)	1.07 ± 0.18	172.1 ± 2.3	0.96 ± 0.9
	Tmax (min)	15	30	60
	AUC ( $\mu\text{g min/ml}$ )	1.19 ± 0.15	216.4 ± 11.2	2.09 ± 0.3
	Relative bioavailability (%)	13.2 ± 1.2		
NE-CT-IT-h-220-cure-piper	Cmax (nM)	2.18 ± 0.23	1.07 ± 1.9	0.88 ± 0.31
	Tmax (min)	15	30	60
	AUC ( $\mu\text{g min/ml}$ )	2.11 ± 0.18	102.7 ± 16.2	0.97 ± 0.12
	Relative bioavailability (%)	23.4 ± 1.9		
Phosphatidylcholine based formulation of cure	Cmax (nM)	0.61 ± 0.21	121.4 ± 5.2	0.93 ± 0.46
	Tmax (min)	15	30	60
	AUC ( $\mu\text{g min/ml}$ )	0.85 ± 0.18	163.8 ± 17.3	0.66 ± 0.13
	Relative bioavailability (%)	9.4 ± 0.5		
Phosphatidylcholine based formulation of cure-piper	Cmax (nM)	1.06 ± 0.42	82.8 ± 4.3	0.91 ± 0.49
	Tmax (min)	15	30	60
	AUC ( $\mu\text{g min/ml}$ )	1.44 ± 0.22	89.9 ± 11.8	0.59 ± 0.1
	Relative bioavailability (%)	16 ± 1.3		

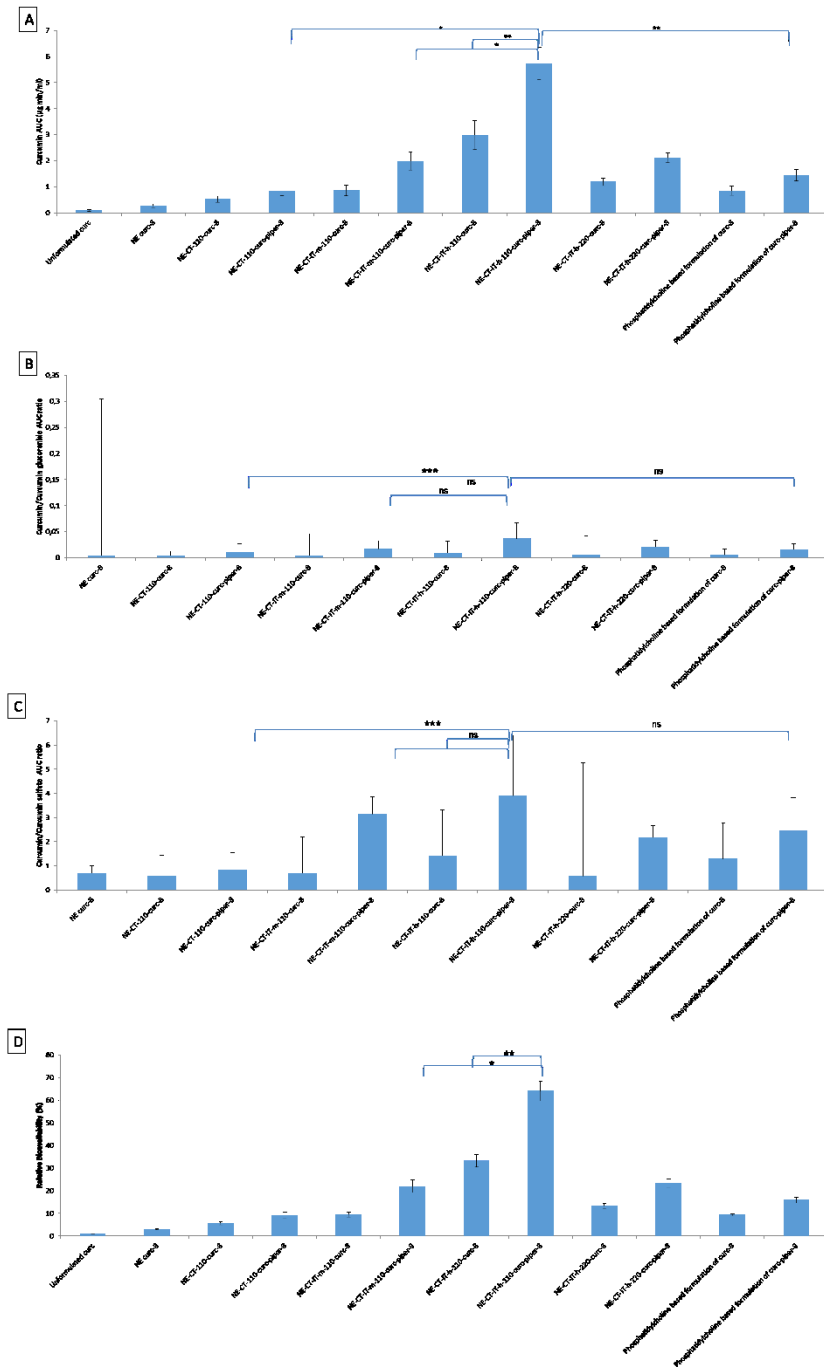


**Figure 2.9.** Curcumin AUC (A) AUC ratio between curcumin and curcumin glucuronide and sulphate (B, C) and relative bioavailability (%) comparison (D) between unformulated curcumin and nano-emulsions at 8 mg/kg orally administered in rats. \*p<0.01; \*\*p<0.001; \*\*\*p<0.05; ns: not significant.

For example, the relative bioavailability of NE-CT-IT-h-110-curc-piper-8 was 64 times higher than that of Unformulated curc-8. In relation to the different nano-emulsion parameters, the presence of thiols on chitosan 2-iminothiolane conjugate demonstrated a central role in increasing curcumin AUC after oral administration in rats; the beneficial effects of piperine co-delivery, are also evident as well as the role of the size, whose scaling was fundamental to strongly gain in curcumin AUC.

In particular, all the results summarized in **Table 2.1** and **Figure 2.9** confirm the essential role of piperine in the pharmacokinetic profile of curcumin, in agreement with previous works related to the co-administration of unformulated curcumin and piperine.<sup>11, 29</sup> In fact, as reported in **Figure 2.9**, which describes the ratios of metabolites (glucuronide, C and sulphate, E) to parent curcumin AUCs, the presence of piperine determined beneficial changes in curcumin metabolism with the various treatments.

In addition, with respect to the effect of chitosan modification, as reported in **Table 2.1** and **Figure 2.9**, focusing on the cases of piperine co-delivery, oral administration of NE-CT-110-curc-piper-8, NE-CT-IT-m-110-curc-piper-8 and NE-CT-IT-h-110-curc-piper-8, compared to Unformulated curc-8, increased AUC of curcumin 9.2, 22 and 63.6 times, respectively. These data indicate the important role of the degree of chitosan

modification with 2-iminothiolane in the phenomena of uptake and intestinal absorption after oral administration in rats.

Finally, from **Table 2.1** and **Figure 2.9** it is also possible to make a comparison in terms of size. Specifically, NE-CT-IT-h-220-curc-piper-8 increased curcumin AUC 23.4 times compared to Unformulated curc-8 but, very interestingly curcumin AUC value was drastically lower than curcumin AUC provided by NE-CT-IT-h-110-curc-piper-8 ( $2.11 \pm 0.18$  vs.  $5.73 \pm 0.61$ ;  $p < 0.001$ ), indicating the essential role of size of the nano-emulsion in the phenomena of uptake and intestinal absorption after oral administration in rats.

For completeness, we also performed a comparison with a more traditional lipid formulation based on a curcumin phosphatidylcholine complexation under the same conditions of dilution; our best nano-emulsion showed a significant improvement in curcumin bioavailability, as reported in **Table 2.1** and **Figure 2.9A**. For example, NE-CT-IT-h-110-curc-piper increased curcumin AUC 4 times compared to curcumin-piperine phosphatidylcholine complexation ( $5.73 \pm 0.61$  vs.  $1.44 \pm 0.22$ ) in a statistically significant manner ( $p < 0.001$ )

In conclusion, on the basis of these pharmacokinetic data, co-administering curcumin and piperine in stabilized lipid 110 nm nano-emulsions and coated with chitosan 2-iminothiolane conjugate at the

highest degree of modification, we achieved, compared to other pharmacokinetic studies after oral administration in rats, a 6-fold increase in curcumin AUC compared to the most recent nano-emulsion systems,<sup>13</sup> and a 1.6-fold increase compared to the best performing system so far reported.<sup>14</sup>

Very interestingly, from an applicative point of view, even administering 0.8, 0.4 or 0.2 mg/kg of corresponding curcumin concentration of CT-IT-h-110-curc-piper, we continued to see detectable amount of curcumin and its metabolites as shown in **Table 2.2** and **Figure 2.10** and the difference between concentrations was always statistically significant.

**Table 2.2.** Calculated nanomolar plasma peak levels ( $C_{max}$ ), time of peak levels ( $T_{max}$ ) and Area Under Curve (AUC) expressed as  $\mu\text{g min/ml}$  for NE-CT-IT-h-110-curc-piper at 0.8, 0.4 and 0.2 mg/kg of corresponding curcumin concentration.

Formulations	Parameters	Curcumin	Curcumin glucoronide	Curcumin sulphate
NE-CT-IT-h-110-curc-piper (8 mg/kg of curcumin)	$C_{max}$ (nM)	3.98 ± 0.13	153.4 ± 2.6	1.28 ± 0.61
	$T_{max}$ (min)	15	30	60
	AUC ( $\mu\text{g min/ml}$ )	5.73 ± 0.61	156.7 ± 17.2	1.47 ± 0.13
NE-CT-IT-h-110-curc-piper (0.8 mg/kg of curcumin)	$C_{max}$ (nM)	0.65 ± 0.09	24.8 ± 1.2	0.21 ± 0.1
	$T_{max}$ (min)	15	30	60
	AUC ( $\mu\text{g min/ml}$ )	0.85 ± 0.12	25.7 ± 2.8	0.26 ± 0.02
NE-CT-IT-h-110-curc-piper (0.4 mg/kg of curcumin)	$C_{max}$ (nM)	0.36 ± 0.07	13.6 ± 0.9	0.13 ± 0.2
	$T_{max}$ (min)	15	30	60
	AUC ( $\mu\text{g min/ml}$ )	0.51 ± 0.11	14.2 ± 1.5	0.14 ± 0.03
NE-CT-IT-h-110-curc-piper (0.2 mg/kg of curcumin)	$C_{max}$ (nM)	0.2 ± 0.06	7.2 ± 0.5	0.09 ± 0.05
	$T_{max}$ (min)	15	30	60
	AUC ( $\mu\text{g min/ml}$ )	0.22 ± 0.05	6.8 ± 0.9	0.09 ± 0.01

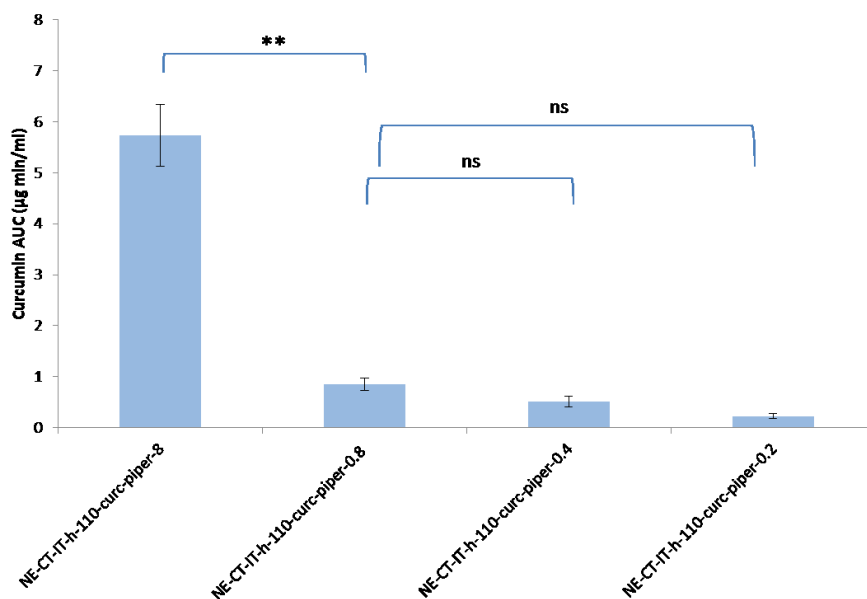


**Figure 2.10.** Curcumin AUC comparison between unformulated curcumin and nano-emulsions at 8, 0.8, 0.4, 0.2 mg/kg orally administered in rats. \* $p < 0.01$ ; \*\* $p < 0.001$ ; \*\*\* $p < 0.05$ ; ns: not significant.

### ***Biodistribution studies***

We evaluated the biodistribution of different fluorescent nano-emulsions, such as NE-FITC, NE-CT-110-FITC and NE-CT-IT-h-110-FITC, from the gastrointestinal tract to different organs within 2 h after a single oral administration in rats. Accumulation of nano-emulsions in different organs expressed as % of the injected dose is shown in **Figure 2.11**. All tested nano-emulsions induced a significant increase in fluorescence in at least one of the tested organs, as expected in the case of passage through the intestinal wall. In the stomach there was a time dependent decrease in fluorescence related to all formulations with a very low percentage of the

injected dose 2 h after oral administration; conversely, we observed a time dependent increase in fluorescence in the liver and spleen with higher levels of accumulation achieved 2 h after oral administration. The general high fluorescence intensity in liver can be justified by the presence of the reticuloendothelial system (RES); in fact, oral delivery along its path unavoidably encounters liver parenchyma where hepatocytes and liver macrophages (Kupffer cells) are able to recognize and metabolize nanocarriers like liposomes and/or macromolecules; the same happens at the spleen level.<sup>30</sup> In this context, the co-delivery of piperine was helpful since it could inhibit some enzymatic activities of curcumin useful for its bioavailability, as demonstrated in the pharmacokinetic study. Interestingly, in the small intestine (after 1 h of administration) and liver (after 2 h of administration) the percentage of the injected dose of NE-CT-IT-h-110-FITC was significantly higher than that of the NE-CT-110-FITC ( $p < 0.01$  for both organs) and NE-FITC ( $p < 0.005$ ,  $p < 0.01$  for small intestine and liver, respectively).

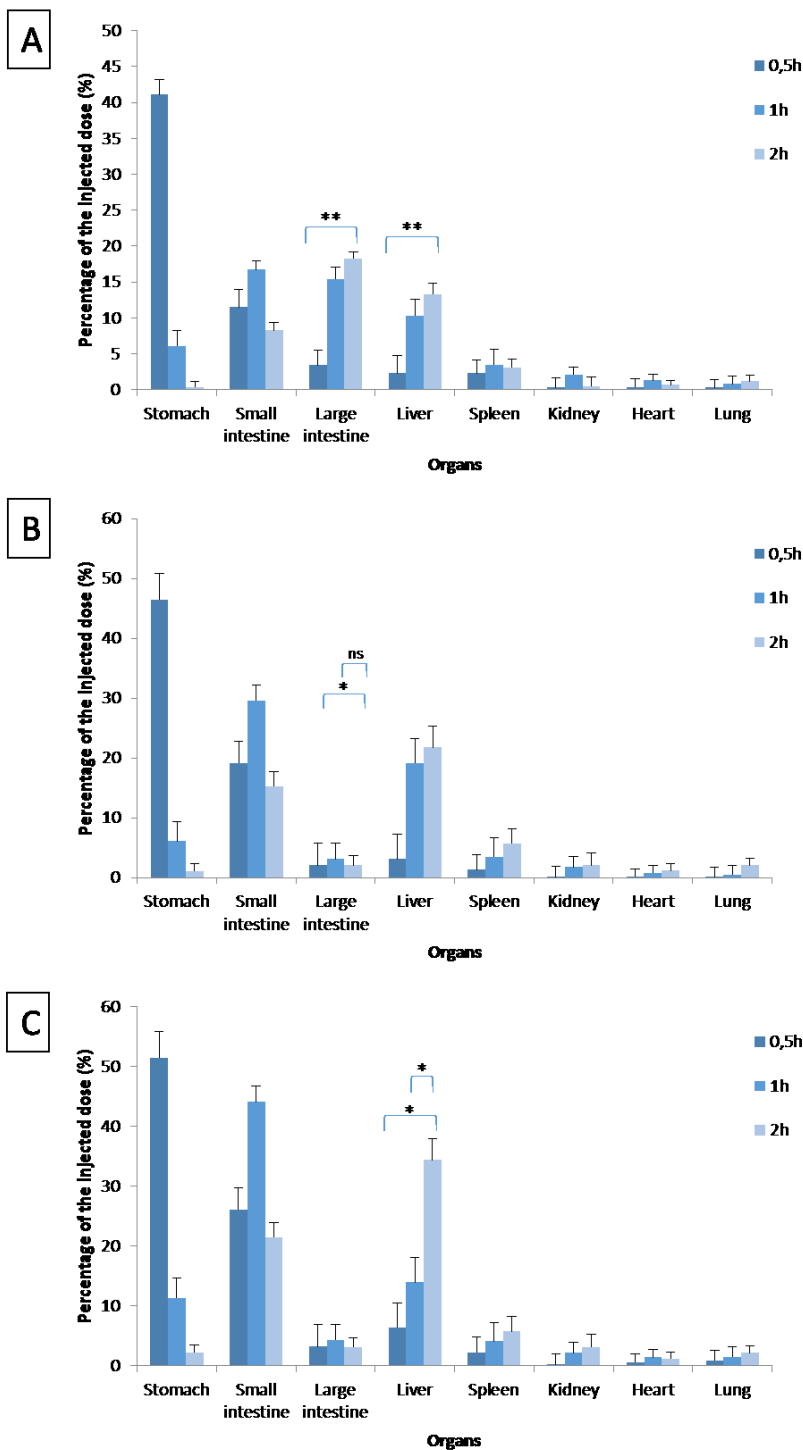


**Figure 2.11.** Biodistribution study in rats after a single oral administration of NE-FITC (A), NE-CT-110-FITC (B) and NE-CT-IT-h-110-FITC (C). \* $p < 0.001$ ; \*\* $p < 0.01$

Specifically, the percentage of the injected dose of NE-CT-IT-h-110-FITC was more than 3 times higher, at 1 h after administration, compared to NE-FITC and 1.5 times compared to NE-CT-110-FITC ( $p < 0.01$ ) in agreement with a supposed improved passage through the intestinal barrier deriving from the higher mucoadhesive ability of nano-emulsions determined by the presence of chitosan and especially of modified chitosan (**Figure 2.11A-C**).

Conversely, NE-FITC seemed to accumulate more in the large intestine compared to the others ( $p < 0.001$ ) indicating, probably, a worse mucoadhesive ability in the small intestine. Future experiments are under investigation for the use of  $^{14}\text{C}$ -labelled curcumin in order to follow more closely the destiny of the drug.

### *Anti-inflammatory effects in lipopolysaccharide-exposed rats*

Many cytokines and interleukins have been reported to act as anti or pro-inflammatory factors; it has been recently found that these are produced also by cancer cells, or by the tumor microenvironment, in order to develop their progression and survival.<sup>31, 32</sup> In this study, we focused our attention on four molecules, tumor necrosis factor ( $\text{TNF-}\alpha$ ), interleukin (IL)- $1\beta$ , IL-8 and IL-6.  $\text{TNF-}\alpha$  is an extremely potent autocrine and paracrine mediator of inflammation and several studies demonstrated its over expression in

cancer tissue and carcinoma cell lines.<sup>33</sup> IL-1  $\beta$  is another essential pro-inflammatory cytokine that plays a regulatory role in the growth of cancer cells also by autocrine mechanisms;<sup>34</sup> IL-8 is a pro-inflammatory cytokine with a key role in the initiation and amplification of acute inflammatory reactions<sup>35</sup> and regulation of tumor cell growth and metastasis of thyroid, colon and breast cancer. IL-6 is a cytokine whose hypersecretion by tumor microenvironment induces proliferation and a more aggressive phenotype, for example, in ER-positive breast cancer cells;<sup>36</sup> it is also well known that an increased IL-6 expression is related to an advanced stage of disease and decreased survival in colorectal cancer patients.<sup>37</sup>

On the basis of the emerging key role of cytokines in tumor growth and survival, a potential modulation of the plasma concentration of these cytokines also under pro-inflammatory conditions could be crucial. The above mentioned pro-inflammatory cytokines (TNF- $\alpha$ , IL-1 $\beta$ , IL-8 and IL-6) were produced in this study upon LPS injection *in vivo*. These cytokines were used, both in cellular and animal studies, as mediators of molecules present in the outer membranes of Gram-negative bacteria.<sup>38, 39</sup> As shown in **Figure 2.12**, interleukin plasma concentration increased exponentially by two (IL-1 $\beta$ , IL-8) and three (IL-6) orders over 5 h upon LPS injection in rats (point 0) with a mean value of  $356.6 \pm 11.1$ ,  $455.3 \pm 19.2$  and  $853.8$

$\pm 14.5$  pg/ml, respectively. Instead, TNF- $\alpha$  levels showed a sharp plasmatic increase by two orders over 2 h upon LPS administration with a successive plateau phase with a mean concentration of  $788.5 \pm 7.3$  pg/ml after 5 h. The increase in plasma concentration of the analysed interleukins is in agreement with literature,<sup>40</sup> and is mainly related to the TLR4 receptor stimulation by LPS with subsequent induction of cytokines and interleukin production.<sup>41</sup>

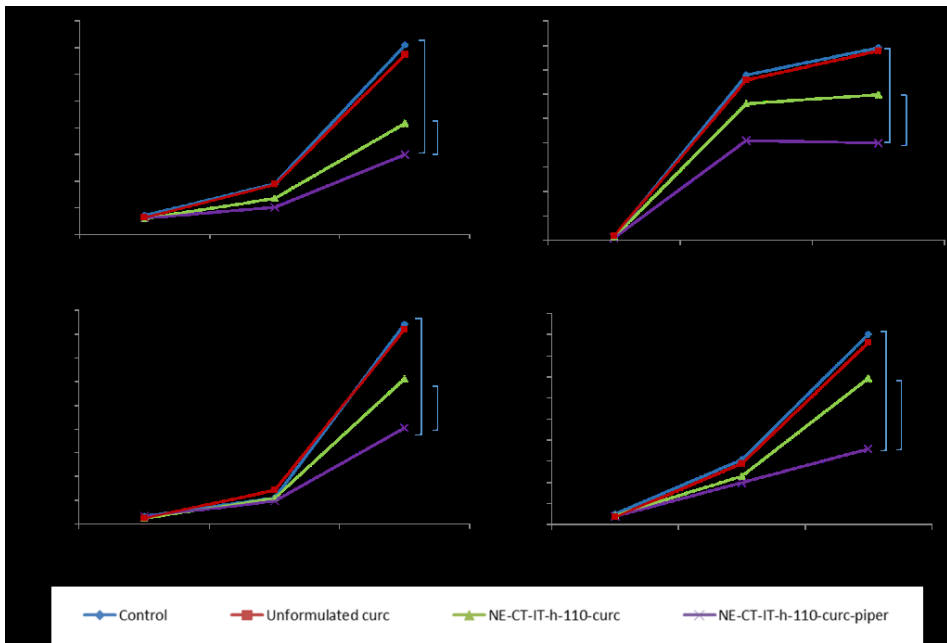


**Figure 2.12.** Effects of Unformulated curc-8, NE-CT-IT-h-110-curc-8 and NE-CT-IT-h-110-curc-piper-8 on plasma cytokine levels-time profiles in lipopolysaccharide-exposed rats. The levels of plasma cytokines were measured before and after 2 and 5 h the LPS intraperitoneal injection in rats pre-treated with normal saline solution (Control) and Unformulated curc at 0.8 mg/kg; NE-CT-IT-h-110-curc at the same curcumin dose of 0.8 mg/kg; NE-CT-IT-h-110-curc, at the same curcumin dose of 0.8 mg/kg and piperine 0.01 mg/kg. \*  $p < 0.001$ . \*\*  $p < 0.05$ .

Oral pre-administration of Unformulated curc-0.8 did not show any statistically significant changes in cytokine levels in plasma, demonstrating no significant anti-inflammatory activity (**Figure 2.12**). Conversely, oral pre-administration of NE-CT-IT-h-110-curc-0.8 reduced the magnitude of the increase in plasma IL-1 $\beta$ , IL-8, IL-6 and TNF- $\alpha$  levels; specifically, the treatment reduced approximately by 40% ( $213 \pm 9$  vs.  $356 \pm 11$ ) 25% ( $588 \pm 11$  vs.  $788 \pm 7$ ), 26% ( $632 \pm 22$  vs.  $853 \pm 14$ ) and 24% ( $346 \pm 25$  vs.  $455 \pm 19$ ) the production of IL-1 $\beta$ , TNF- $\alpha$ , IL-6, IL-8, respectively, compared to the control group ( $p < 0.005$ ), (**Figure 2.12**). In the presence of piperine co-delivery NE-CT-IT-h-110-curc-piper-0.8 reduced the magnitude of the increase in plasma IL-1 $\beta$ , IL-8, IL-6 and TNF- $\alpha$  levels in an even more significant manner indicating the adjuvant effect of the alkaloid piperine; specifically, it reduced approximately by 57% ( $153 \pm 13$  vs.  $356 \pm 11$ ), 48% ( $406 \pm 15$  vs.  $788 \pm 7$ ), 51% ( $416 \pm 18$  vs.  $853 \pm 14$ ) and 60% ( $181 \pm 15$  vs.  $455 \pm 19$ ) the production of IL-1 $\beta$ , TNF- $\alpha$ , IL-6, IL-8, respectively, compared to the control group ( $P < 0.001$ ) (**Figure 2.12**). These data indicate that even at a 1/10 dose ( $=0.75$  ml/kg), the best formulation coming from the pharmacokinetic study, NE-CT-IT-h-110-curc-piper, has an effective anti-inflammatory action when orally administered to LPS treated rats.

Moreover, we tested the anti-inflammatory effect of two lower doses, such as NE-CT-IT-H-110-curc-piper-0.4 and of NE-CT-IT-H-110-curc-piper-0.2. As it is possible to see from **Figure 2.13**, in both cases a relevant reduction of IL-1 $\beta$ , TNF- $\alpha$ , IL-6, IL-8, as compared to the control groups ( $P < 0.01$ ) was obtained.

Specifically, the first dose (0.4 mg/kg) reduced by approximately 37% ( $253 \pm 15$  vs.  $402 \pm 22$ ), 30% ( $582 \pm 23$  vs.  $821 \pm 31$ ), 32% ( $628 \pm 33$  vs.  $921 \pm 28$ ) and 39% ( $293 \pm 23$  vs.  $478 \pm 11$ ) the production of IL-1 $\beta$ , TNF- $\alpha$ , IL-6, IL-8, respectively, compared to the control group ( $P < 0.01$ ). The second dose (0.2 mg/kg) reduced by approximately 25% ( $301 \pm 14$  vs.  $402 \pm 22$ ), 14% ( $702 \pm 26$  vs.  $821 \pm 31$ ), 19% ( $745 \pm 27$  vs.  $921 \pm 28$ ) and 14% ( $407 \pm 17$  vs.  $478 \pm 11$ ) the production of IL-1 $\beta$ , TNF- $\alpha$ , IL-6, IL-8, respectively, compared to the control group ( $P < 0.01$ ).

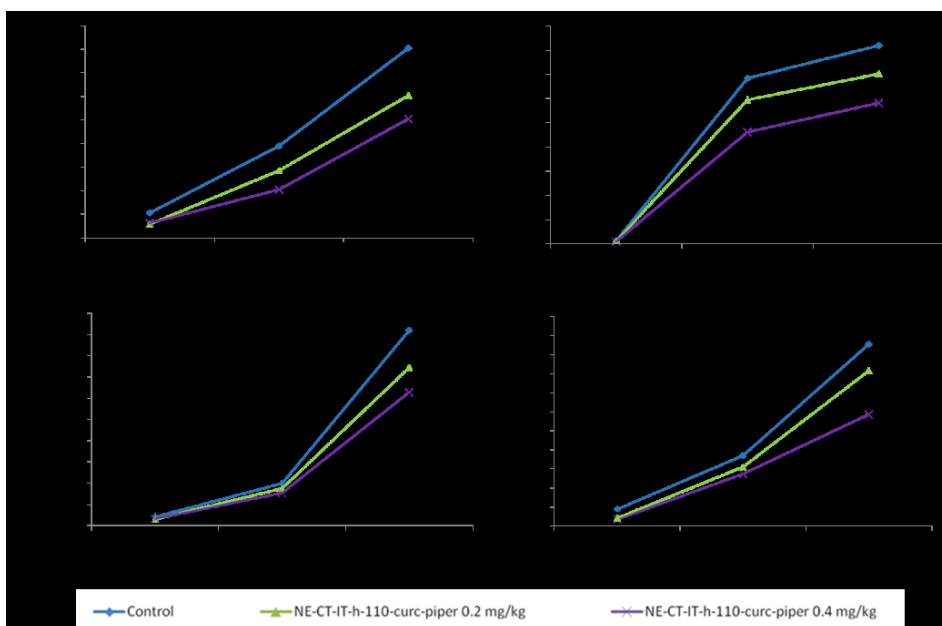


**Figure 2.13.** Concentration dependent anti-inflammatory effects of NE-CT-IT-h-110-curc-piper-0.8; NE-CT-IT-h-110-curc-piper-0.4 and NE-CT-IT-h-110-curc-piper-0.2 in lipopolysaccharide-exposed rats. The levels of plasma cytokines were measured just before and after 2 and 5 h from the LPS intraperitoneal injection. \* $p < 0.05$ ; \*\* $p < 0.01$ ; \*\*\* $p < 0.001$

## 2.3 Conclusions

The oral route remains the easiest way to effectively deliver natural substances, such as nutraceuticals. In this work we used a modular system to convey curcumin based on a food grade nano-emulsion; the system is capable of controlling the interface properties and therefore the interaction with the intestinal barrier by easy deposition of functionalized biopolymers. In particular, we studied curcumin bioavailability by using chitosan with different degrees of modification with 2-iminothiolane and the effects of the nano-emulsion size by comparing 110 nm and 230 nm

emulsions and the effects of piperine co-delivery, which has been already reported to enhance curcumin bioavailability. We obtained the highest degree of bioavailability in the case of the smaller nano-emulsion coated with the highest degree of chitosan modification with 2-iminothiolane and co-delivery of piperine. Apart from elucidating the roles played by the different parameters in a systematic way, we obtained a relative bioavailability of NE-CT-IT-h-110-curc-piper which was 64 times higher than unformulated curcumin, the highest ever reached. Then, we showed very high anti-inflammatory activities based on the reduction of IL-1 $\beta$ , TNF- $\alpha$ , IL-6 and IL-8 in LPS treated rats at 0.8 mg of curcumin per kg of rat (corresponding to 0.75 ml/kg of rat) and even significant at doses as low as 0.2 mg of curcumin per kg of rat (corresponding to 0.19 ml/kg of rat). In addition, we propose a modular system which may add complexity by exploiting its capability to further deposit layers and create multi-compartmentality and therefore multifunctionality. Given the anti-inflammatory and also chemopreventive power of curcumin, we have planned clinical trials in the care of the inflammatory bowel disease (IBD) and in chemoprevention of the colorectal cancer. In addition, based on the selective action of the curcumin against cancer cells as proved in literature, we demonstrated that this property is maintained when curcumin is encapsulated in our systems. Finally, studies of combinatory treatments of

chemotherapy drugs and curcumin, both orally administered, exploiting their pharmacological synergism and chemosensitization in different cancer types are currently under investigation.

## **2.4 Materials and Methods**

### ***Materials***

Oil in water nano-emulsions were obtained by using a formulation based on pharma grade products such as soy-bean oil and Lipoid E80 lecithin, both purchased from Lipoid and used without further purification. Millipore® Milli-Q water was used for the preparation of all emulsions and solutions. The emulsions were then coated with chitosan (CT, LMW 90-150 kDa, DD 84% determined via <sup>1</sup>H-NMR) also purchased from Sigma-Aldrich and purified before use.<sup>42</sup> For the in fluorescence analysis, chitosan was chemically labelled with Fluorescein 5(6)-isothiocyanate (FITC, m.w.=389.38 g/mol) purchased from Sigma Aldrich. 1,4-diazabicyclo[2.2.2]octane (dabco) (m.w.=112.17 g/mol), antifade, also purchased from Sigma Aldrich, was used to avoid the bleaching phenomenon of FITC. Optical dishes FD3510 (Fluorodish Cell Culture Dish - 35mm) with a cover glass bottom were used to allow STED observation of the samples. Curcumin (from *Curcuma longa* (Turmeric), powder, m.w.=368.38) and piperine (97%, m.w.=285.34) were both

purchased from Sigma-Aldrich and used with no further purification. 2-Iminoethiolane hydrochloride (2-IT), DL-Dithiothreitol (DTT), deuterium oxide (D<sub>2</sub>O), trifluoroacetic acid (TFA), 5,5'-dithiobis(2-nitrobenzoic acid) (DTNB, also known as Ellman's reagent) were also purchased from Sigma Aldrich while dialysis membranes (12-14 kDa MWCO) from Spectrum Laboratories, Inc. and used during the phases of functionalization and characterization of the chitosan. For cellular studies Dulbecco's Modified Eagle's Medium (DMEM) and McCoy's 5A medium were obtained from Sigma Aldrich, instead Fetal Bovine Serum (FBS), Penicillin/Streptomycin (10000 U/ml) and Glutamine were purchased from Invitrogen, Life Technologies. For pharmacokinetic and anti-inflammatory studies, Proteinase k and Lipopolysaccharide (LPS) were obtained from Sigma-Aldrich.

### *Synthesis of CT-IT*

Chitosan Low Molecular Weight (CT-LMW, 100 mg, 0.50 mmol) was dissolved in 10 ml of 0.1 M of acetic acid solution. After complete dissolution, pH was adjusted to 6 with NaOH. 2-iminoethiolane hydrochloride (2-IT, 40 mg, 0.30 mmol in one case and 20 mg, 0.15 mmol in the other case) were added and pH was further adjusted to 6.5 with NaOH and HCl. The reaction proceeded under magnetic stirring and at room temperature overnight. After reaction, DL-Dithiothreitol (DTT, 40

mg, 0.25 mmol) was added and left to react for 1 h. Then the pH was adjusted to 3.5 with HCl and the sample was dialyzed (dialysis tubing with 12-14 KDa Cut-Off) and freeze-dried for 48 h. Eight dialysis cycles were executed: 4 cycles with NaCl 1% w/v pH 3 water solution, and 4 cycles with pH 3 water solution. Samples were characterized with <sup>1</sup>H NMR spectroscopy and the amount of free thiols was evaluated with the Ellman's test.<sup>42, 43</sup>

### ***Synthesis of CT-FITC***

Chitosan Low Molecular Weight (CT-LMW, 100 mg, 0.50 mmol) was dissolved in 10 ml of 0.1 M of acetic acid solution. After complete dissolution, a solution of FITC (5.0 mg in 500  $\mu$ l of DMSO) was added dropwise. The reaction proceeded overnight at room temperature. Sample was then precipitated adjusting the pH to 10 with NaOH and the precipitate was collected by centrifuge (9000 rpm, 15 min). Sample was washed with water by means of several centrifugations, until negligible fluorescence was detected in the supernatant (using Perkin Elmer 2300 Enspire Plate Reader,  $\lambda_{ex}$  = 488 nm,  $\lambda_{em}$  = 510 nm). Finally, the purified product was freeze-dried for 48 h.

### ***Sample preparation and characterization***

The systems proposed in this work are mainly based on nano-emulsions coated with chitosan; however, other formulations were also used as a control. Two different sizes of nano-emulsions were prepared depending on the amount of surfactant, Lipoid E 80, dissolved in soy-bean oil and for each size we prepared two different carriers, one with curcumin and one with piperine. In particular, 5.8 g of surfactant in 24 ml of oil were used for the smaller emulsion and 1.44 g of surfactant in 24 ml of oil were used for the larger emulsions. For curcumin loaded nano-emulsions, 100 mg of curcumin were added to the 24 ml of oil phase while for piperine loaded nano-emulsions 400 mg of piperine were added to the 24 ml of oil phase. To promote dissolution, the oil phase containing surfactant and biomolecule (curcumin or piperine) was mixed by alternating a high speed blender (RZR 2102 control, Heidolph) at 60 °C and 500 r.p.m. to room temperature sonication with an immersion sonicator (Ultrasonic Processor VCX500 Sonic and Materials), according to a process protocol previously reported.<sup>20, 44</sup> Then, to obtain the pre-emulsion, the oil phase was added dropwise to 90 g of Milli-Q water and mixed using the immersion sonicator and controlling temperature in order to avoid overheating. The pre-emulsions were finally passed at 2000 bar through the high-pressure valve homogenizer (Microfluidics M110PS) according to the same previous protocol.<sup>20</sup> Primary emulsions were then coated with pristine

chitosan or chitosan 2-iminothiolane conjugate, exploiting their positive charge for the deposition around the oil droplets stabilized with lecithin, which is negative. Chitosan solutions were prepared in 0.1 M acetic acid Milli-Q water bringing the pH to 4 with a small addition of NaOH 6 M solution. The two phases were mixed 1:1 (v:v) quickly under vigorous stirring and kept under stirring for 15 min to allow uniform chitosan deposition, thus obtaining secondary emulsions. The final concentration of oil was 10% (wt.), whereas chitosan was 0.1% (wt.) to guarantee saturation of chitosan around emulsion.<sup>20,44</sup> The emulsions coated with chitosan were passed through a high-pressure valve homogenizer at 700 bar for 100 continuous steps, and re-processed after a few days in the same conditions on the same systems (at 700 bar for 100 continuous steps) having found benefit in terms of stability by double re-dispersion process, as previously reported.<sup>20</sup> Emulsions were measured in terms of size and Z-potential (Zetasizer zs nano series ZEN 3600, Malvern Instruments Ltd., Malvern, U.K.) by diluting them up to a droplet concentration of approximately 0.025% (wt.) using Milli-Q water in the case of primary emulsions and acetic acid solution (pH 4, 20 mM) in the case of secondary emulsions. The Z-potential analysis was carried out by setting 50 runs for each measurement, whereas default refractive index ratio (1.52) and 5 runs for each measurement (1 run lasting 100 s) were used in the calculations of

the particle size distribution. Secondary emulsions embedding curcumin and coated with FITC-labelled chitosan were also observed with a SP8-STED fluorescence optical microscope (Leica Microsystems, GmbH, Germany) using a 100X oil immersion objective (HCX PL APO 100x/1.40 OIL). Samples were excited at 488 nm, and the emitted fluorescence was collected between 500 and 550 nm. For image acquisitions in STED mode, a continuous doughnut-shaped STED laser emitting at 592 nm was used. Samples were diluted with a 20 mM acetic acid solution at pH 4 at the final oil concentration of 0.02% (wt.) and put in glass bottom FD3510 optical dishes. After 30 min of incubation the samples were washed out 3-times with a 5% (wt) dabco antifade solution and observed with a microscope. Images were acquired with a pixel size of 25 nm. The full width at half maximum (FWHM), as represented between arrows in the **Figure 2.1**, and the statistical analysis of the profiles were obtained using Origin 9.1.

As control systems -apart from pure curcumin and piperine- we also tested a phytosome formulation. Curcumin and curcumin-piperine phosphatidylcholine complexes were prepared as described in literature.<sup>45</sup> Briefly, the complex was prepared with curcumin and hydrogenated soy phosphatidyl choline (HSPC) at a molar ratio of 1:1. Weighed amount of curcumin and HSPC were put in a 100 ml round bottom flask and 20 ml of dichloromethane was added. The mixture was refluxed at a temperature

of maximum 60 °C for 2 h. The obtained solution was evaporated and 10 ml of n-hexane was added under continuous stirring. The curcumin–phospholipid complex was precipitated, subsequently filtered and dried under vacuum to remove traces of solvents. The same procedure was followed for the synthesis of the curcumin-piperine phosphatidylcholine complex.

All the tested samples are summarized with their acronyms in **Table 1**. To represent a particular amount in mg of curcumin per kg of rat, this value will be reported at the end of the identifying code, e.g. NE-CT-110-curc-8 to indicate a formulation based on the 110 nm nano-emulsion coated with chitosan and at a dose of 8 mg of curcumin per kg of rat (corresponding to 7.5 ml of 10 %wt emulsion) will be delivered. Lower doses indicated with 0.8, 0.4 and 0.2 are obtained by administering lower amounts of emulsion (0.75, 0.38 and 0.19 ml/kg, respectively). In the case of piperine co-delivery, piperine is always intended as 1/100 w/w as compared to curcumin amount.

### ***Cell culture***

Mouse fibroblast (NIH/3T3, ATCC® CRL-1658™) and colon cancer cell lines (HT29 ATCC®) were seeded (density 3000 cells/well) in 96-well plates, cultured in DMEM and McCoy's 5A medium, respectively, and

both with 2mM glutamine, 10% FBS 1% penicillin streptomycin (full medium) and incubated for 24 h under standard sterile conditions for cell cultures (5% CO<sub>2</sub>, 37°C).

### *Cell cytotoxicity experiments*

The cytotoxicity of the nano-emulsions was assessed on both NIH/3T3 and HT29 evaluating their mitochondrial dehydrogenase activity by means of a modified MTT [3-(4,5-dimethylazol-2-yl)-2,5-diphenyltetrazolium bromide] method according to the manufacturer's instructions (Dojindo Molecular Technologies Inc., Rockville, MD). Cells were seeded in 96-well plates at a density of 10000 cells per well in complete medium at 37 °C in a humidified 5% CO<sub>2</sub> atmosphere. After 24 h of appropriate growth, we tested viability of both cell lines incubated one day, under standard conditions, with all the systems. Curcumin concentration was tested from 2 up to 100 µg/ml in all the cases; the weight ratio between curcumin and piperine was fixed at 100/1 w/w. At the end of the incubation period, cells were washed three times with PBS at pH 7.4 and incubated with 100 µl of a MTT solution (0.5 mg/ml in cell culture medium) for 4 h at 37 °C. The absorbance measurements were acquired at a wavelength of 450 nm with the Tecan Infinite M200 plate-reader using I-control software. The relative cell viability (%) was calculated by the formula  $[A]_{\text{test}}/[A]_{\text{control}} \times 100$ ,

where “[A]test” is the absorbance of the test sample, and “[A]control” is the absorbance of the control cells incubated solely with culture medium. After evaluating cell cytotoxicity, the total protein content was measured by using the Micro BCA protein assay kit (Pierce). Briefly, cells were washed with ice-cold PBS, and incubated for 15 min in 150 µl cell lysis buffer (0.5% v/v Triton X-100 in PBS), to which 150 µl of Micro BCA protein assay kit reagent (prepared following the instructions of the manufacturer) were added. The absorbance at 562 nm was finally measured on a plate reader. The cytotoxicity measurements were then normalized by the amount of total protein content in each well.

***Cancer cell uptake studies: uptake quantification and cell-imaging by Confocal Laser Scanning Microscope***

For uptake quantification studies in colon cancer cells, after culturing HT29 cell line as previously described,  $5 \times 10^3$  cells/well were seeded in 24-well plate and allowed to grow for 24 h. The medium was then replaced with 500 µl of a solution composed by culture medium and the 110 nm nano-emulsion coated with FITC-labelled chitosan (NE-FITC-CT-110-cure), with an equivalent curcumin molar concentration of 2.71 µM (corresponding to 0.24 wt% of O/W emulsion) and incubating them for a time comprised between 0.5 and 8 h. Cells were then washed twice with

PBS (pH 7.4) and after specified time intervals the experiments were terminated by removing the supernatant, washing the cells three times with 10 mM PBS and lysing them with 0.1 ml of 0.5% Triton X-100 in 0.2 N NaOH. The membrane-bound and internalized nano-emulsions were quantified by analyzing the fluorescence of the cell lysate ( $\lambda_{\text{exc}} = 492 \text{ nm}$ ,  $\lambda_{\text{em}} = 528 \text{ nm}$ ), employing a calibration with a solution composed of the 110 nm nano-emulsion coated with FITC-labelled chitosan with a curcumin concentration ranging from 5  $\mu\text{M}$  (corresponding to 0.44 wt% of O/W emulsion) up to 0.1 nM (corresponding to 0.00009 wt% of O/W emulsion) dispersed in a cell lysate solution ( $10^6$  untreated cells dissolved in 1 ml of the Triton X-100/0.2 N NaOH solution).

For cell imaging studies in colon cancer cells, after culturing HT29 cell line as previously described and washing the cells with PBS twice (pH 7.4), the membrane was stained by using concanavalin A tetramethylrhodamine conjugate (Invitrogen, Life Technology) at a final concentration of 100  $\mu\text{g/ml}$ . Subsequently, cells were thoroughly rinsed three times with PBS and fixed with a 2.5% glutaraldehyde in PBS for 20 min. Then, cells were blocked with 1% BSA in PBS for 20 min and washed three times with PBS. Finally, they were observed Using a Confocal Microscope (C1 Nikon) equipped with an EZ-C1 Software for data acquisition and 60x oil immersion objective. The nanostructures were

imaged through excitation/emission of FITC at 492/528 nm while the cell membrane with excitation/emission at 555/580 nm.

### ***HPLC assay***

Analysis of samples was performed using an Agilent Infinity 1200. Separation was achieved with a C18 column (2.1 mm × 250 mm) kept at 35°C. The mobile phase consisted of two components: A: 10 mM ammonium acetate pH 4.5, B: acetonitrile. Initial conditions were 95% A progressing to 55% A at 20 min and 5% A at 33 min. The retention time was 4.6 min. The flow rate was 1.5 ml/min. Curcumin and conjugated metabolites were detected at 426 nm and reduced curcumin metabolites at 280 nm using a Varian 325 UV-vis detector. The precision of the procedure was determined by a repeatability method. Solutions of curcumin, curcumin glucuronide and curcumin sulfate containing 0.5 ng and 1000 ng/ml were injected into the system repeatedly five times. The percentage RSD (relative standard deviation) of injection repeatability and analysis repeatability for curcumin, curcumin glucuronide and curcumin sulfate was 0.897% and 0.915%, 0.902% and 0.892%, 0.882% and 0.903%, respectively. The results obtained confirm good precision of the method used for quantification of curcumin and curcumin metabolites in

rats. The linearity of the method used for curcumin, curcumin glucuronide and curcumin sulfate was checked at six concentration levels over the concentration range of 0.5-1000 ng/ml. For all equations obtained, the mean correlation coefficient ( $R^2$ ) was  $0.997 \pm 0.001$ . Limit of quantification for curcumin, curcumin glucuronide and curcumin sulfate was 0.13, 0.21 and 0.12 ng/ml for 100  $\mu$ l injection volume.

### *Pharmacokinetic studies*

Forty-five male Wistar albino rats (mean weight: 400 g) were purchased from Charles River (Calco, Italy) and kept under a 12 h light/dark cycle on standard lab chow. All animals were maintained within conditions specified in approved Institutional Animal Care and Use Committee protocols. The experiment protocol had been previously approved by the local ethics committee. After overnight fasting, animals were randomized in 15 groups (n=3) based on oral administration of all the samples previously listed in the table. For all the systems, the volume administered to the rats was 7.5 ml when using piperine, weight ratio between curcumin and piperine was 100/1 w/w, as from literature.<sup>46</sup> We chose to work with such high doses to allow the reading of free curcumin in the blood in all the systems including the less performing that is the unformulated curcumin.

For each formulation we took, in triplicate, 0.2 ml of blood from rat at each time point (15, 30, 60 and 120 min after oral administration) for a final volume of blood drawn of 0.8 ml, that is <1% of total blood volume (TBV) of a rat weighing 400 g (according to the Veterinary Recommendations for Multiple Blood Draws). Blood was collected by withdrawal via the tail vein into heparinised tubes, centrifuged at 7,000 g for 15 min and plasma was then decanted. Curcumin and curcumin metabolites (glucuronide and sulphate) were extracted from plasma by solid phase extraction; specifically, 0.2 ml of plasma were loaded onto a 0.2 cc Oasis HLB cartridge and washed with 0.2 ml of a solution of methanol: water: glacial acetic acid at 25:25:1 v/v ratio and eluted with 0.2 ml of methanol containing 2% (v/v) of glacial acetic acid. Eluent was evaporated to dryness at 45 °C under nitrogen, and the residue was re-suspended in a 75 µl of 50% v/v water/ acetonitrile solution. Studies of AUC 0-120 min of curcumin and curcumin metabolites were performed only up to 2 h guided by similar works in literature.<sup>47</sup> The relative oral bioavailability of curcumin was calculated according to the equation: Relative BA (%) = 100 x [(AUC<sub>formulation</sub> / dose<sub>formulation</sub>) / (AUC<sub>unformulated curcumin</sub> / dose<sub>unformulated curcumin</sub>)] as described in literature.

### ***Biodistribution studies***

Biodistribution study was performed according to literature;<sup>48</sup> briefly, thirty-six male Wistar albino rats (average weight: 400 g) also purchased from Charles River (Calco, Italy), were housed in temperature and humidity-controlled rooms and allowed free access to basal diet and water *ad lib* for 7 d before starting the experiment. Rats were randomly divided into 4 groups (n=3/group) depending on the different times of digestion after oral administration of fluorescent nano-emulsion (NE-110-FITC), fluorescent 110 nm nano-emulsion coated with chitosan (NE-CT-110-FITC) and fluorescent 110 nm nano-emulsion coated with chitosan 2-iminothiolane conjugate at a high degree of modification (NE-CT-IT-h-110-FITC): 0.5 h, 1 h, and 2 h. Loading of FITC in the nano-emulsions was obtained by mixing 4 ml of ethanol solution of FITC (0.75 mg/ml) to the soybean oil during the emulsion preparation and drying the ethanol from the mixture with a mild heating. The final concentration of FITC in the emulsion at 10% (w/v) of oil in water is 125 µg/ml. A single dose of 7.5 ml of FITC loaded nano-emulsions was administered through oral gavage. Rats in the control group received the same volume of vehicle solution (PBS) only. We selected a rather high dose to increase the likelihood of generating detectable amounts of the fluorescent nano-emulsion in tissues. After proper time of digestion, rats were sacrificed and

the harvested tissue samples (small intestine, large intestine, liver, spleen, stomach, heart, lung, kidney) were digested using an aqueous enzyme solution containing 1 g/l proteinase K (Sigma-Aldrich) in 50 mM  $\text{NH}_4\text{HCO}_3$  buffer (to maintain a constant pH value of 7.4 during enzymatic digestion) and 5 g/l SDS to improve activity of the enzyme.<sup>49</sup> Specifically, organs were carefully weighed and digested in digestion buffer at a weight ratio of 1:5. The samples were thoroughly vortexed and incubated at 37 °C under continuous stirring in a magnetic stirrer for 4 h. Fluorescence of the samples was measured using a Tecan Infinite M200 plate-reader with I-control software at excitation/emission wavelengths of 420/528 nm. The NE-CT-IT-h-110-FITC concentration was determined based on previously prepared standard calibration curves in each organ separately, obtained by spiking blank organ lysates (prepared as previously described) with serial dilutions of fluorescent nano-emulsions ranging from 0 to 50 mg/ml.<sup>50</sup>

### ***Anti-inflammatory effects in lipopolysaccharide-exposed rats***

Forty-two male Wistar albino rats (mean weight: 400 g) purchased from Charles River (Calco, Italy) were treated as in the biodistribution study before starting the experiment. Rats were randomly divided into 7 groups (n=6/group): control (normal saline); Unformulated curc, NE-CT-IT-h-110-curc-0.8, NE-CT-IT-h-110-curc-piper-0.8. In order to verify the

possible concentration dependent effects of the formulations, we subsequently tested the anti-inflammatory effects of: control (normal saline), NE-CT-IT-h-110-curc-piper-0.4, NE-CT-IT-h-110-curc-piper-0.2 Solutions were administered daily for 2 weeks by oral gavage and, after this period, a single intraperitoneal injection (IP) of LPS at 5 mg/kg was performed. Blood samples were taken just before (= time 0), and at two different times (2, 5 h) after LPS injection under ether anaesthesia- by withdrawal via the tail vein. This timing aimed to obtain the maximum production of pro-inflammatory cytokines after IP administration of LPS in rats, as observed in literature.<sup>39, 51</sup> Blood samples were collected in heparinised tubes and immediately centrifuged at 3000 rpm for 10 min at 4 °C in order to obtain plasma that was collected, frozen, and kept at -80° C until use for IL-1 $\beta$ , TNF- $\alpha$ , IL-6 and IL-8 analysis performed by enzyme-linked immunosorbent assay (ELISA) method using commercial kits (Bio-Rad Laboratories, Inc., Italy). Results are expressed as mean  $\pm$  S.D. Data were statistically analyzed using one-way ANOVA tests  $p < 0.05$  was considered to be significant.

## 2.5 Supplementary Section<sup>2</sup>

In this supplementary work an air liquid interface (ALI) of CaCo2 cells in Transwell was realized as an *in vitro* testing platform (**Figure 2.14**) to evaluate the potential of an oral nano-delivery system very similar to the system presented in the main work of this chapter – i.e. an oil-in-water nanoemulsion coated with a thiolated glycol chitosan (**Figure 2.15**).

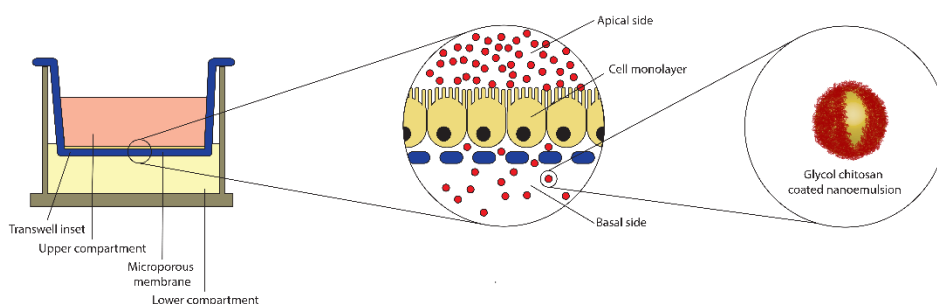


**Figure 2.14.** Schematic representation of air liquid interface of Caco-2 cells in Transwell system (on the left). In the central inset an enlarged view of the cell monolayer grown on the microporous membrane. On the left the oral nano-delivery system consisting of O/W nanoemulsion coated with a thiolated glycol chitosan.

Again, curcumin was chosen as model drug because of its lipophilic nature, its poor stability and its poor oral administration. The presented testing platform allowed a comprehensive understanding on the route of the nano-system carrying the curcumin, its interaction with the intestinal mucosa and the antioxidant effects on cells. Results demonstrated that the

---

<sup>2</sup> The work here illustrated has been realized with the precious collaboration of Dr. Angela Langella and our relative research groups. Result here presented will be part of a paper currently under preparation: A. Langella, V. Calcagno, V. de Gregorio, G. Imparato, F. Urciuolo, R. Vecchione, P. A. Netti. "Oral nano-delivery system for colon targeted drug delivery: *in vitro* study of curcumin biodistribution"

in Transwell model, able to promote the polarization of the intestinal epithelium, is suitable to mimic as closely as possible the *in vivo* conditions.

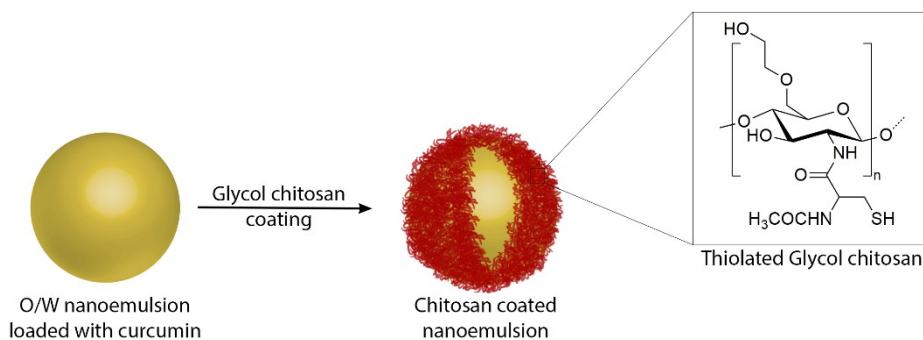


**Figure 2.15.** Schematic representation of the oral nano-delivery system proposed: an oil in water nanoemulsion loaded with the curcumin and coated with GC-NAC (glycol chitosan modified with N-acetyl-L-cysteine).

### ***Results and discussion***

*Nanoemulsion analysis.* Particle size of the starting nano-emulsion and of the nano-emulsion coated with glycol chitosan was characterized by DLS. Starting from a nano-emulsion loaded with curcumin (1 µg/ml of curcumin in 20 % (v/v) of O/W nano-emulsion) with a size of ~100 nm and a PDI of ~0.07, the coating with glycol chitosan did not significantly affect size and particle size distribution – size increases of few nanometer (~105 nm) and PDI value remains below ~0.08. It is noteworthy that these values of size and PDI were obtained with the simple deposition of the polymer under vigorous stirring. In contrast to what was required for nano-emulsion

coated with CT-IT, where the final system had a higher oil concentration (10% w/w) and larger volume were needed, here it was not necessary to perform a double re-dispersion process with the high pressure homogenizer – the final oil concentration is 2% (w/w) and only few milliliters are required for the tests. In addition to DLS analysis, confocal imaging of nano-emulsion coated with rhodamine B labelled chitosan (**Figure 2.16A**) and electron microscopy imaging of nanocapsules stained with OsO<sub>4</sub> vapors were performed (SEM micrograph in **Figure 2.16B** and TEM micrograph in **Figure 2.16C**), thus clearly confirming the good size distribution and dimensions.

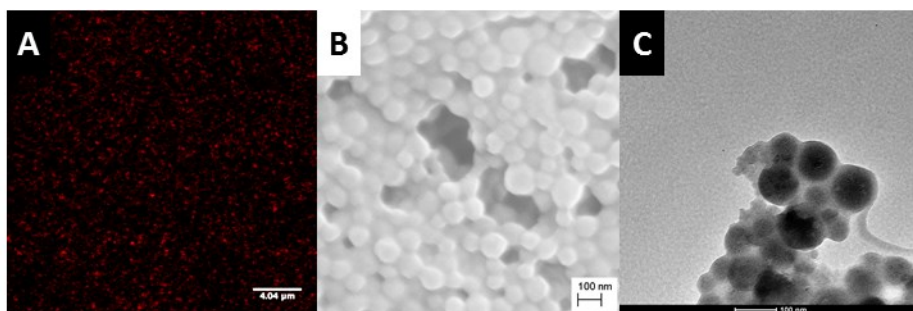


**Figure 2.16.** Imaging characterization of O/W nanoemulsion coated with GC-NAC: (A) confocal image of nanocapsules coated with rhodamine B labelled glycol chitosan; (B) SEM image and (C) TEM image of nanocapsules stained with OsO<sub>4</sub> vapors. Osmium staining strengthened the soft nanocapsules in order to avoid collapse due to the vacuum of electron microscopes.

The biopolymer used for the coating was previously modified with a thiolation agent, the N-acetyl-L-cysteine (NAC), through an amidation reaction with a water soluble carbodiimide as condensing agent (EDC,

ethyl-3-(3-dimethylaminoisopropyl)-carbodiimide) and 1-hydroxy-1,2,3-benzotriazole (HOBt) as additive.<sup>52</sup> Polymer characterization was performed with <sup>1</sup>H NMR spectroscopy and the degree of functionalization was determined using the colorimetric Ellman's test (for more details about the synthetic procedure, the amounts of reactants used and the characterizations performed see **Chapter 3**).<sup>42</sup>

*Cell cytotoxicity.* We tested the biosafety of the nano-emulsions by carrying out cytotoxicity tests on the system loaded with curcumin. As resulted from MTT test, cell viability was demonstrated, thus indicating the biosafety of the tested nanocarrier towards Caco-2 cells.

*Effect on monolayer dynamic.* Transepithelial electrical resistance (TEER), a widely accepted quantitative technique to measure the integrity of tight junction dynamics in cell culture models epithelial monolayers, was used to evaluate the transport of drugs or chemicals.<sup>53</sup> The reduction of the electrical resistance observed during the first 4 h of contact with the nano-emulsion, compared with the starting value ( $\sim 400 \text{ ohm} \cdot \text{cm}^2$ ), suggested that the nano-delivery system crossed the epithelial barrier. However, the TEER value became again comparable to the starting

value once the nano-emulsion had passed and the tight junction returned to the starting conformation.

As further confirmation, tight junctions of Caco-2 cells monolayer were stained using a primary antibody (ZO-1).<sup>54</sup> Comparing the sample treated with the nano-emulsion and the control (**Figure 2.17**) it is clear that the contact with the thiolated chitosan induces an opening of the tight junction, thus promoting the crossing of the intestinal barrier.<sup>16</sup>

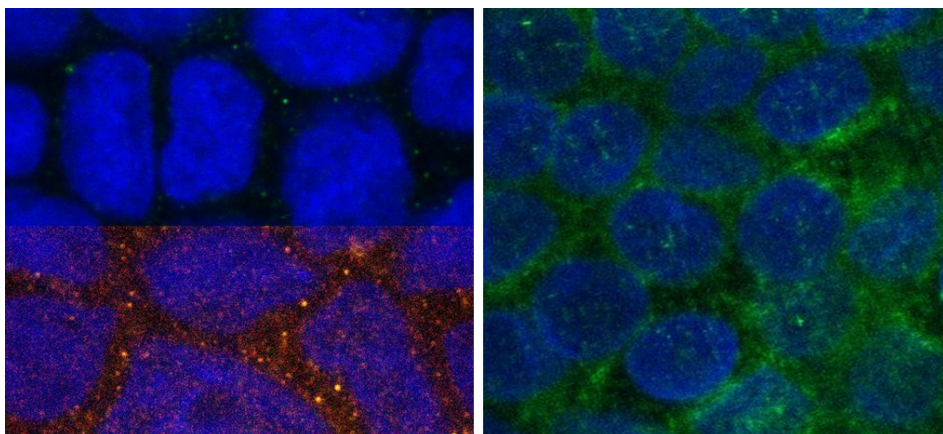


**Figure 2.17.** Confocal images of Caco-2 monolayer: nuclei (blue color) and tight junction (green color) have been selectively stained with DRAQ5 and ZO-1, respectively. On the left, cells in contact with nanoemulsion coated with labelled chitosan (red color, only half of the image, on bottom, includes the matching with the Rhodamine-B).

*Transport of nano-emulsion.* Confocal analysis allowed to evaluate the presence, the localization and the transport of our nano-delivery system. Preliminary tests were performed with Dextran-FITC,<sup>55</sup> thus demonstrating that the epithelial monolayer, as a consequence of the AIL

polarization, develops all the morphological and functional features of the *in vivo* intestinal epithelium (tight junctions, microvilli, brush borders, see **Figure 2.18**, right). Indeed, as shown in **Figure 2.18**, dextran crossed the cells monolayer, through a para- and trans-cellular transport.

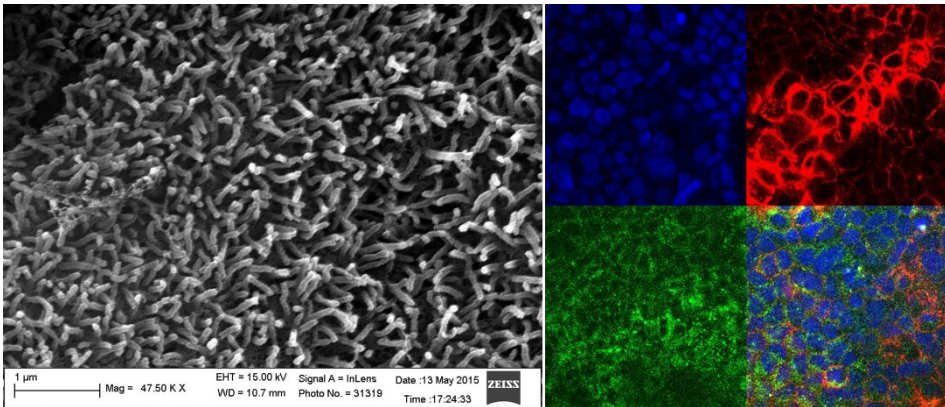


**Figure 2.18.** Left: SEM images of Caco-2 monolayer (top view). Right: confocal images of Caco-2 monolayer: cytoskeleton (red), nuclei (blue), dextran (green) and matching

In order to understand the transport of the nano-emulsion, glycol chitosan coating was covalently labelled with Rhodamine B. This labelling, together with the specific staining of the biological sample, allowed to discriminate between the nano-emulsion (red channel), the nuclei (blue channel) and the cytoskeleton (green channel), as shown in **Figure 2.19**, left. Confocal analysis clearly shows that the nanocarrier resulted to be fully distributed on the surface of the cell monolayer, thus demonstrating that the thiolation at the interface of the nanocapsule results in an increase of mucoadhesivity.<sup>16, 23</sup> In addition, the Z-view image (**Figure 2.19**, right)

shows that the nano-emulsion is able to cross the monolayer of cells through the opening of the tight junctions, as discussed above, but also to enter the cell thus, exploiting both the para- and trans- cellular transport.

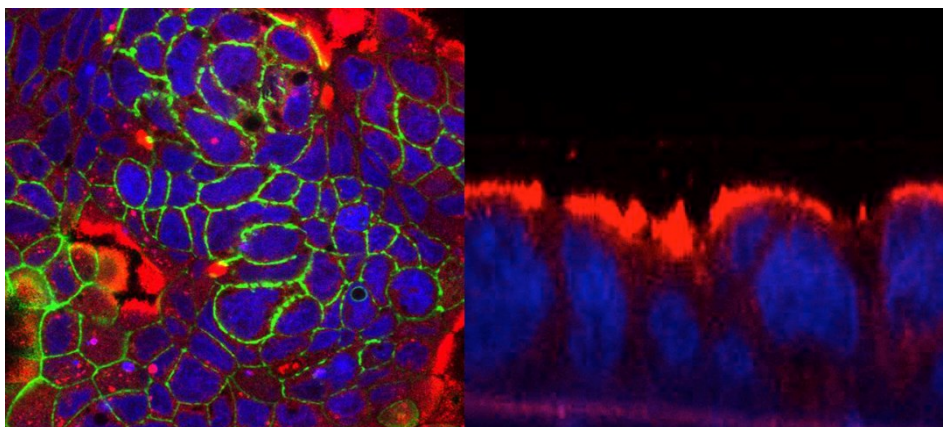


**Figure 2.19.** Confocal images of Caco-2 monolayer: Y-view matching on the left and Z-view matching on the right.

*Quantitative analysis of curcumin content.* Preliminary tests were performed to understand if the selected Transwell, and in particular the 3.0  $\mu\text{m}$  polycarbonate membrane, results to be permeable to the passage of the nano-emulsion. DLS measurement of the upper and lower solutions demonstrate that capsules are stable in the medium and are able to pass the membrane (**Table 2.3**).

**Table 2.3.** DLS analysis of coated nanoemulsion at different time of incubation (3 and 24 h) in Transwell.

Sample name	Time (h)	Size (d.nm)	PDI
Coated nanoemulsion	3	106.3	0.100
Upper	3	115.0	0.070
Lower	3	138.0	0.300
Coated nanoemulsion	24	114.0	0.090
Upper	24	113.6	0.070
Lower	24	118.9	0.130

In addition, HPLC measurements were performed to quantify the amount of curcumin that passed through the membrane: after 24 h of incubation the curcumin is distributed between the upper compartment (63%) and the lower one (37%). HPLC quantification was also performed on the Caco-2 monolayer in Transwell. Results are summarized in **Table 2.4** and show that the curcumin content is reduced with the time in the upper solution, probably because the nanocapsules pass through the cell monolayer or enter the cells. However, the decrease in the curcumin content of the upper solution is not followed by complementary increase of the drug content in lower solution: essentially the amount of curcumin did not change. This suggests that a perceptible amount of curcumin is included within the cell as nanocapsules content or as metabolites. Further study– HPLC assays of the curcumin amount and its related metabolites found in the cell, and antioxidant effect of curcumin – will be performed to obtain a complete understanding of the curcumin administration in the intestinal epithelium.

**Table 2.4.** HPLC analysis of the curcumin content in the upper and lower solutions.

Sample	Time (h)	Curcumin (ng/ml)	Percentage
Coated nanoemulsion		37.97	100 %
Upper	3	28.40	74.8 %
Lower	3	0.36	0.95 %
Not detected	3	9.21	24.2 %
Upper	24	7.30	19.2 %
Lower	24	0.43	1.13 %
Not detected	24	30.24	79.6 %

## ***Conclusions***

In this section an *in vitro* testing platform was presented. Morphological analysis demonstrated that the epithelial monolayer realized in Transwell, as a consequence of the AIL polarization, develops all the morphological and functional features of the *in vivo* intestinal epithelium (tight junctions, microvilli, brush borders). In addition, confocal imaging and related investigation allowed to understand the route of the nanosystem here studied. The designed oral nano-delivery system, an oil in water nano-emulsion loaded with curcumin and coated with a thiolated glycol chitosan, represents an interesting tool for the oral delivery of lipophilic drugs. In particular, by modifying the glycol chitosan with a thiol moiety it is possible to increase the adhesion to the intestinal mucosa and to open the tight junction, so as to make the nanocapsule more performing.

## ***Materials and Methods***

Below in this paragraph the materials and methods used for this supplementary work are presented: these are in addition or partially substitution of the materials and methods used for the main work presented above in this chapter.

*Materials.* 1-hydroxybenzotriazole hydrate (HOBt), *N*-acetyl-L-cysteine (NAC), Rhodamine B isothiocyanate (RBITC) were purchased from Sigma-Aldrich. 1-(3-dimethylaminopropyl)-3-ethyl-carbodiimide hydrochloride (EDC) was purchased from Iris Biotech. Glycol chitosan (GC) was purchased from Wako Chemicals. Caco-2 cells were obtained from American Type Cell Culture (ATCC, Usa). Dulbecco's Modified Eagle's Medium (DMEM, Gibco, Life Technologies), supplemented with 10% Fetal Bovine Serum (FBS, Sigma Aldrich), 1% Penicillin/Streptomycin and 1% L-Glutamine (Lonza, Milan) and 2% nonessential amino-acids NEEA (Euroclone, Milan). Hank's Balanced Salt Solution (HBSS) was purchased from Gibco, Life Technologies). Transwell Permeable Supports (12-well plates with polycarbonate membrane 3.0  $\mu\text{m}$  and 24-well plates with polyester membrane 0.4  $\mu\text{m}$ ) were purchased from Corning<sup>®</sup> Costar. FITC-Dextran was purchased from Molecular probes, Life Technologies.

*Glycol chitosan modifications.* Modification of GC with NAC was reported in detail in **Chapter 3, Materials and Methods** section. In one case, GC was previously modified with RBITC, thus obtaining a labelled polymer (GC-RBITC), and then modified with NAC. The procedure used to obtain GC-RBITC was the same proposed for GC-FITC (glycol

chitosan modified with fluorescein isothiocyanate), reported in **Chapter 3, Materials and Methods** section.

*Realization of nanocapsules.* Oil in water nano-emulsion was obtained as previously described in **Materials and Methods** section. The nano-emulsion was then coated with GC-NAC or GC-RBITC-NAC by adding 1.5 ml of polymer solution (0.033 % (w/v) in acidified water at pH 4) to 1 ml of water suspensions of O/W nanoemulsion (5 % (w/w) in acidified water at pH 4) under vigorous stirring.

*Cell Lines and Culture Conditions.* Caco-2 cells, a human colonic epithelial cell line, were grown in DMEM at 37°C with 5 % CO<sub>2</sub> – 95 % air in Transwell 12-well plates, that consisting of two chambers separated by a polycarbonate membrane (12 mm diameter, 3 µm pore size). The cells were seeded at 1x10<sup>5</sup> in 1.12 cm<sup>2</sup> in either insert and grown on polycarbonate membrane for two weeks. During the first week cells grew till to completely cover all the membrane surface, thus leading to a submerged layer; during the second week the upper medium is removed and cells were capable to polarize, thus leading to an Air Liquid Interface (ALI). Medium was replaced every 48 h: for two weeks in the basolateral chamber and for the first week only in apical chamber.

*Transepithelial electrical resistance assay.* TEER (Ohm) of Caco-2 cells cultured in Transwell was measured using the Millicell-ERS (Electrical Resistance System, Millipore Corporation). The measured value was multiply by the area of the membrane ( $1.12 \text{ cm}^2$ ) to obtain a TEER value expressed in  $\text{Ohm} \cdot \text{cm}^2$  in order to evaluate the cell monolayer integrity during permeation experiments.

*Apical-to-basal permeability assay.* The permeability of Caco-2 cell monolayers was performed by measuring in dynamic and static mode the trans-epithelial passage of the O/W nano-emulsion coated with GC-RBITC-NAC, of a blank sample (HBSS/DMEM, 1:1) and of FITC-Dextran solution (1 mg/ml diluted in HBSS), generally used like positive control.<sup>55</sup> Cells monolayers were incubated for 24 h at  $37^\circ\text{C}$  with 5 %  $\text{CO}_2$  – 95 % air; for dynamic mode a rotator at 80 rpm was used. A certain volume of HBSS/DMEM was placed in the basolateral chamber in order to guarantee the dipping of the lower side of the membrane. The passage was determined by confocal imaging (Leica SP5 II Laser Scanning Confocal Microscope) and fluorescence emission of rhodamine and fluorescein, respectively (Perkin Elmer 2300 Enspire plate reader  $\lambda_{\text{ex}}=555$

nm,  $\lambda_{em}=565$  nm and ). RP-HPLC was used as indirect permeability assay by detecting the presence of curcumin when used.

*Confocal imaging.* The monolayer of Caco-2 cells was washed with PBS solution and fixed with paraformaldehyde 4% (v/v) at room temperature for 20 minutes. Permeabilization was performed using a 0.01% Triton solution in PBS for 5 minutes, washing three times with PBS and incubating with specific staining. Actin filaments were stained with Phalloidin-Alexa Fluor® 488 conjugate (1:50 in PBS). Nuclei were stained with DRAQ5™ (1:10000 in PBS). Cellular morphology of the Caco-2 cells was observed with a Leica SP5 II laser scanning confocal microscope using a 63X oil immersion objective (HCX PL APO CS 63.0x1.40 OIL UV). Samples were observed with the following specific fluorescence channels: cytoskeleton (Phalloidin-Alexa Fluor® 488)  $\lambda_{ex}=488$  nm (Argon Laser) and  $\lambda_{em}=500-530$  nm, nanoemulsions coated with GC-RBITC-NAC (rhodamine B)  $\lambda_{ex}=543$  nm (Helium Laser)  $\lambda_{em}=560-610$  nm; nuclei (DRAQ5™)  $\lambda_{ex}=633$  nm  $\lambda_{em}=650-750$  nm. Z-Stack and Y-Stack image series were acquired to study the localization of labeled-drug in the caco-2 cells. Section thickness was set to 0.7  $\mu$ m for all the images. Images analysis was performed using Fiji (Image J, plugin) and LAS AF (Laica Applications System).

*Confocal analysis of nanoemulsions.* Samples containing nano-emulsions coated with GC-RBITC-NAC were opportunely diluted with HBSS/DMEM buffer and 200  $\mu$ l were put in a FD3510 dish for 30 min to allow it to adhere to the glass surface. Sample in excess was washed twice by replacing it with 130  $\mu$ l of HBSS/DMEM solution every 10 min and, in the end, with 130  $\mu$ l of 5% (w/v) DABCO anti-fade solution (needed to avoid the bleaching effect of the Rhodamine B).

*Electron microscopy.* For imaging analysis of nanocapsules samples were first exposed to vapors of OsO<sub>4</sub> water solution (1% wt.) as oil core dopant for not less than 4 h. After that, a small drop of solution containing silica nanocapsules was spread onto the surface of an aluminum stub covered by a carbon tape or a glass plate.

For imaging analysis of cells sample was first fixed with a sodium cacodylate 0.1 M in 2.5% wt. glutaraldehyde solution at room temperature for 2h. Sample was washed with a solution of 0.1 M sodium cacodylate - 0.1 M sucrose (3 times in an ice bath for 10 min). Sample was then fixed with OsO<sub>4</sub> (1% wt. in 0.1 M sodium cacodylate - 0.1 M sucrose) and washed again with a solution of 0.1 M sodium cacodylate - 0.1 M sucrose (3 times in an ice bath for 10 min). In the end sample was dehydrate by

replacing the water solution with a series of ethanol solutions (30%, 50%, 75%, 95%, 95%, 100%, 100%, 100% (v/v)) and dried with a Critical Point Drier (Leica EM CPD300).

The samples, both nano-emulsions that cells, were then sputter-coated with a thin Pt/Pd or Au layer (10 nm) in a Cressington sputter coater 208HR. The aluminum stub containing the Pt/Pd or gold -coated sample was then placed in a FEG-SEM scanning electron microscope and imaged using 20 kV accelerating voltage.

*Immunofluorescence assay.* Tight junctions of the monolayer of Caco-2 cells were stained using a primary antibody (ZO-1). Cells were washed with PBS solution and fixed with paraformaldehyde 4% (v/v) at room temperature for 20 minutes. Permeabilization was performed using a 0.01% Triton solution in PBS for 10 minutes, washing three times with PBS and first incubating with a blocking solution (PBS, BSA 5% and Triton 0.01%) for 2h in a wet chamber. After washing with PBS, cells were incubated with ZO-1 antibody (1:50 in PBS) overnight at + 4°C. Finally, cytoskeleton and nuclei are stained with Phalloidin-Alexa Fluor® 488 and DRAQ5™ solutions, as previously reported.

*Cell cytotoxicity experiments.* The cytotoxicity of the nano-emulsions was assessed on Caco-2 cells using the MTT method according to the manufacturer's instructions (Dojindo Molecular Technologies Inc., Rockville, MD). Cells were seeded in 6-well plates at a density of 200000 cells per well in complete medium at 37 °C in a humidified 5% CO<sub>2</sub> atmosphere. After 24 h of appropriate growth, we started the drug test and after 24 h we tested the viability of both cells (Treated and untreated) incubated one day, under standard conditions. At the end of the incubation period, cells were washed three times with PBS at pH 7.4 and incubated with 300 µl of a MTT solution (5 mg/ml in cell culture medium) for 4 h at 37 °C. In the end 150 µl of DMSO were added and samples were incubated for 1 h at 37 °C. The absorbance measurements were acquired at 570 nm (Perkin Elmer 2300 Enspire plate reader,  $\lambda_{\text{abs}}=570$  nm).

*Histochemical Analysis.* The monolayer of CaCo-2 cells on a polycarbonate membrane was fixed in formalin and then dehydrated by replacing the water solution with a series of ethanol solutions (30%, 50%, 75%, 95%, 95%, 100%, 100%, 100% (v/v)). After dehydration, sample was embedded in paraffin, cut in 5-10 µm thin slides by using an ultramicrotome (HM 355S Automatic Microtomes, Thermo Scientific) and put on a glass slide. Paraffin was de-waxed in xylene, and finally

sample was rehydrated and stained with Alcian Blue and Eosin according to the specific staining protocols.

*RP-HPLC.* Analysis of samples was performed using a Waters 2535 Quaternary Gradient Module, equipped with a 2489 UV/Visible detector. Separation was achieved with a C8 column (6 mm × 250 mm) kept at 25°C. The mobile phase was a linear gradient consisting of two components: A: 0.1% TFA CH<sub>3</sub>CN, B: 0.1% TFA water. The linear gradient ranges from 45% to 99% over 30 min. The retention time was 4.6 min. The flow rate was 1.0 ml/min. Curcumin and conjugated metabolites were detected at 426 nm and reduced curcumin metabolites at 280 nm.

## 2.6 References

1. B. B. Aggarwal, C. Sundaram, N. Malani and H. Ichikawa, in *The molecular targets and therapeutic uses of curcumin in health and disease*, Springer, 2007, pp. 1-75.
2. S. Anuchapreeda, S. Tima, C. Duangrat and P. Limtrakul, *Cancer chemotherapy and pharmacology*, 2008, **62**, 585-594.
3. A. Suhag, J. Dixit and P. Dhan, *Perio*, 2007, **4**, 115-121.
4. S. Shishodia, G. Sethi and B. B. Aggarwal, *Annals of the New York Academy of Sciences*, 2005, **1056**, 206-217.
5. P. Anand, A. B. Kunnumakkara, R. A. Newman and B. B. Aggarwal, *Molecular pharmaceutics*, 2007, **4**, 807-818.
6. G. Appendino, G. Belcaro, U. Cornelli, R. Luzzi, S. Togni, M. Dugall, M. Cesarone, B. Feragalli, E. Ippolito and B. Errichi, *Panminerva Med*, 2011, **53**, 43-49.
7. P. K. Mohan, G. Sreelakshmi, C. Muraleedharan and R. Joseph, *Vibrational Spectroscopy*, 2012, **62**, 77-84.
8. B. Antony, B. Merina, V. Iyer, N. Judy, K. Lennertz and S. Joyal, *Indian journal of pharmaceutical sciences*, 2008, **70**, 445.
9. Q. Jia, I. Ivanov, Z. Z. Zlatev, R. C. Alaniz, B. R. Weeks, E. S. Callaway, J. S. Goldsby, L. A. Davidson, Y.-Y. Fan and L. Zhou, *British journal of nutrition*, 2011, **106**, 519-529.
10. W. W. Epstein, D. F. Netz and J. L. Seidel, *Journal of chemical education*, 1993, **70**, 598.
11. G. Shoba, D. Joy, T. Joseph, M. Majeed, R. Rajendran and P. S. S. R. Srinivas, *Planta Med*, 1998, **64**, 353-356.
12. X. Wang, Y. Jiang, Y.-W. Wang, M.-T. Huang, C.-T. Ho and Q. Huang, *Food Chemistry*, 2008, **108**, 419-424.
13. L. Zhongfa, M. Chiu, J. Wang, W. Chen, W. Yen, P. Fan-Havard, L. D. Yee and K. K. Chan, *Cancer chemotherapy and pharmacology*, 2012, **69**, 679-689.
14. H. Sasaki, Y. Sunagawa, K. Takahashi, A. Imaizumi, H. Fukuda, T. Hashimoto, H. Wada, Y. Katanasaka, H. Kakeya and M. Fujita, *Biological and Pharmaceutical Bulletin*, 2011, **34**, 660-665.
15. M. Dash, F. Chiellini, R. M. Ottenbrite and E. Chiellini, *Progress in polymer science*, 2011, **36**, 981-1014.
16. Vijapur.L.S., S. S.A., Patil.S.H., Vijapur.P.V., Patwari.P.K. and Saraswathi, *International Research Journal of Pharmacy*, 2012, **3**, 51.

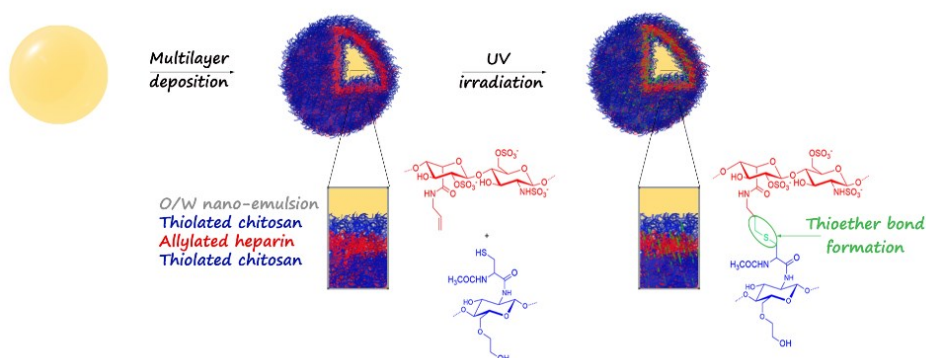
17. F. Kesisoglou, S. Panmai and Y. Wu, *Current Nanoscience*, 2007, **3**, 183-190.
18. D. J. McClements, *Soft Matter*, 2011, **7**, 2297-2316.
19. E. Acosta, *Current Opinion in Colloid & Interface Science*, 2009, **14**, 3-15.
20. R. Vecchione, U. Ciotola, A. Sagliano, P. Bianchini, A. Diaspro and P. Netti, *Nanoscale*, 2014, **6**, 9300-9307.
21. R. Vecchione, G. Iaccarino, P. Bianchini, R. Marotta, F. D'Autilia, V. Quagliariello, A. Diaspro and P. Netti, *Small*, 2016.
22. A. Bernkop-Schnürch, *Advanced drug delivery reviews*, 2005, **57**, 1569-1582.
23. A. Anitha, N. Deepa, K. Chennazhi, S. Nair, H. Tamura and R. Jayakumar, *Carbohydrate Polymers*, 2011, **83**, 66-73.
24. J. Ravindran, S. Prasad and B. B. Aggarwal, *The AAPS journal*, 2009, **11**, 495-510.
25. S. Sreenivasan and S. Krishnakumar, *Current eye research*, 2014, 1-13.
26. B. Vinod, J. Antony, H. Nair, V. Puliappadamba, M. Saikia, S. S. Narayanan, A. Bevin and R. J. Anto, *Cell death & disease*, 2013, **4**, e505.
27. Q. Du, B. Hu, H.-M. An, K.-P. Shen, L. Xu, S. Deng and M.-M. Wei, *Oncology reports*, 2013, **29**, 1851-1858.
28. M. Huang, E. Khor and L.-Y. Lim, *Pharmaceutical research*, 2004, **21**, 344-353.
29. J. Singh, R. Dubey and C. Atal, *Journal of Pharmacology and Experimental Therapeutics*, 1986, **236**, 488-493.
30. M. Ferrari, *Nature Reviews Cancer*, 2005, **5**, 161-171.
31. N. R. West, S. McCuaig, F. Franchini and F. Powrie, *Nature Reviews Immunology*, 2015.
32. M. Esquivel-Velázquez, P. Ostoa-Saloma, M. I. Palacios-Arreola, K. E. Nava-Castro, J. I. Castro and J. Morales-Montor, *Journal of Interferon & Cytokine Research*, 2015, **35**, 1-16.
33. G. Aust, M. Heuer, S. Laue, I. Lehmann, A. Hofmann, N. E. HELDIN and W. Scherbaum, *Clinical & Experimental Immunology*, 1996, **105**, 148-154.
34. A. M. Lewis, S. Varghese, H. Xu and H. R. Alexander, *Journal of translational medicine*, 2006, **4**, 48.
35. Y. Ning, P. C. Manegold, Y. K. Hong, W. Zhang, A. Pohl, G. Lurje, T. Winder, D. Yang, M. J. LaBonte and P. M. Wilson, *International Journal of Cancer*, 2011, **128**, 2038-2049.

36. A. K. Sasser, N. J. Sullivan, A. W. Studebaker, L. F. Hendey, A. E. Axel and B. M. Hall, *The FASEB Journal*, 2007, **21**, 3763-3770.
37. M. J. Waldner, S. Foersch and M. F. Neurath, *Int J Biol Sci*, 2012, **8**, 1248-1253.
38. H. Sang, G. L. Wallis, C. A. Stewart and Y. Kotake, *Archives of biochemistry and biophysics*, 1999, **363**, 341-348.
39. C. C. Barton, E. X. Barton, P. E. Ganey, S. L. Kunkel and R. A. Roth, *Hepatology*, 2001, **33**, 66-73.
40. J.-W. Hong, G.-E. Yang, Y. B. Kim, S. H. Eom, J.-H. Lew and H. Kang, *BMC complementary and alternative medicine*, 2012, **12**, 1.
41. T. Kawai and S. Akira, *Cell Death & Differentiation*, 2006, **13**, 816-825.
42. V. Calcagno, R. Vecchione, A. Sagliano, A. Carella, D. Guarnieri, V. Belli, L. Raiola, A. Roviello and P. A. Netti, *Colloids and Surfaces B: Biointerfaces*, 2016, **142**, 281-289.
43. P. W. Riddles, R. L. Blakeley and B. Zerner, *Analytical Biochemistry*, 1979, **94**, 75-81.
44. I. Fotticchia, T. Fotticchia, C. A. Mattia, P. A. Netti, R. Vecchione and C. Giancola, *Langmuir*, 2014, **30**, 14427-14433.
45. K. Maiti, K. Mukherjee, A. Gantait, B. P. Saha and P. K. Mukherjee, *International journal of pharmaceuticals*, 2007, **330**, 155-163.
46. S. Prasad, A. K. Tyagi and B. B. Aggarwal, *Cancer research and treatment: official journal of Korean Cancer Association*, 2014, **46**, 2.
47. T. H. Marczylo, R. D. Verschoyle, D. N. Cooke, P. Morazzoni, W. P. Steward and A. J. Gescher, *Cancer chemotherapy and pharmacology*, 2007, **60**, 171-177.
48. A. P. Walczak, P. J. Hendriksen, R. A. Woutersen, M. van der Zande, A. K. Undas, R. Helsdingen, H. H. van den Berg, I. M. Rietjens and H. Bouwmeester, *Journal of Nanoparticle Research*, 2015, **17**, 1-13.
49. K. Loeschner, J. Navratilova, C. Købler, K. Møhlhave, S. Wagner, F. von der Kammer and E. H. Larsen, *Analytical and bioanalytical chemistry*, 2013, **405**, 8185-8195.
50. Y.-M. Tsai, W.-L. Chang-Liao, C.-F. Chien, L.-C. Lin and T.-H. Tsai, *International journal of nanomedicine*, 2012, **7**, 2957.
51. G. Mathiak, G. Grass, T. Herzmann, T. Luebke, C. C. Zetina, S. A. Boehm, H. Bohlen, L. F. Neville and A. H. Hoelscher, *British journal of pharmacology*, 2000, **131**, 383-386.

52. P. Bulpitt and D. Aeschlimann, *Journal of biomedical materials research*, 1999, **47**, 152-169.
53. B. Srinivasan, A. R. Kolli, M. B. Esch, H. E. Abaci, M. L. Shuler and J. J. Hickman, *Journal of laboratory automation*, 2015, **20**, 107-126.
54. A. S. Fanning, B. J. Jameson, L. A. Jesaitis and J. M. Anderson, *Journal of Biological Chemistry*, 1998, **273**, 29745-29753.
55. C. Dalla Pellegrina, C. Rizzi, S. Mosconi, G. Zoccatelli, A. Peruffo and R. Chignola, *Toxicology and applied pharmacology*, 2005, **207**, 170-178.

# Chapter 3

## Biostability Enhancement of Oil Core - Polysaccharide Multilayer Shell via Photoinitiator Free Thiol-ene 'Click' Reaction<sup>1</sup>



<sup>1</sup> This work has been accepted for publication: V. Calcagno, R. Vecchione, A. Sagliano, A. Carella, D. Guarnieri, V. Belli, L. Raiola, A. Roviello and P. A. Netti, Biostability enhancement of oil core — polysaccharide multilayer shell via photoinitiator free thiol-ene 'click' reaction. *Colloids and Surfaces B: Biointerfaces*, 2016, **142**, 281-289. The Supplementary Section is not included in the publication.

**Abstract.** Layer-by-Layer of polyelectrolytes has emerged as one of the easiest and most controlled techniques to deposit ultrathin polymer layers mainly driven by electrostatic interactions. However, this kind of interaction results to be weak and easily breakable in physiological environment. Here we report on the preparation of nanocapsules completely made of natural biomaterials: a lipophilic core (soybean oil and egg lecithin as surfactant) as nanometric template and a polysaccharide-based multilayer shell (glycol chitosan and heparin) covalently cross-linked. We first modified glycol chitosan with a thiol moiety and heparin with an alkene moiety, respectively, and then we built a polymer multilayer film with a covalent cross-linkage among layers, exploiting the light initiated thiol-ene reaction, known as click chemistry. We showed the possibility to perform the covalent cross-linkage without any photoinitiator or metal catalyst, thus avoiding cytotoxic effects and further purification steps. The so realized nanocapsules resulted to be stable and completely biocompatible and, therefore, of interest for the biotechnology fields, mainly for drug delivery.

### 3.1 Introduction

Layer-by-layer (LbL) assembly is a versatile and robust technique for fabricating customized thin films of diverse composition.<sup>1-4</sup> It provides a high level of control on properties such as thickness, composition and nanostructure.<sup>2-6</sup> The method has predominantly been used to assemble films using electrostatic,<sup>1-4</sup> hydrogen-bonding<sup>7-9</sup> interactions or electrochemical deposition<sup>10, 11</sup> and, recently, to fabricate polyelectrolyte multilayer capsules.<sup>12</sup> The latter ones have attracted widespread interest in the field of drug delivery due to their control in the preparation procedure and their multifunctional features.<sup>13-16</sup> In addition, polyelectrolytes are also emerging as bio-functional interfaces in tissue engineering.<sup>17</sup>

However, the main forces stabilizing LbL assembled systems are based on electrostatic interactions, making such systems very sensitive to environmental conditions, such as variations in the ionic strength or temperature of the medium, and thus susceptible to disassembly,<sup>18, 19</sup> which represents an important limitation for some biomedical applications. Recent approaches have developed LbL polymer capsules whose synthesis combines electrostatic forces *via* LbL assembly and covalent cross-linking *via* click chemistry.<sup>20</sup> Click reactions are performed under mild conditions, are highly quantitative and inert to other chemical moieties,<sup>21</sup> allowing the

elegant design of diverse materials with varied functionality. Systems with layers linked covalently *via* click chemistry demonstrated increased stability to disassembly under varying conditions thanks to the formation of a cross-linked network structure.<sup>22-24</sup> The main issue concerning click chemistry is that most reactions applied in LbL assembly of capsules are catalyzed by copper, thus leading to cytotoxic effects.<sup>25</sup> Recently, a metal catalyst-free approach to covalently link the multilayer of microcapsules made of poly(methacrylic acid) using a particular click reaction, named thiol-ene click reaction, has been proposed.<sup>26</sup> This chemistry is versatile and has been used for a range of applications.<sup>27-34</sup>

Despite natural polymers, in particular polysaccharides<sup>35</sup> are largely used as biomaterials in LbL applications,<sup>36</sup> a free catalyst ‘click’ strategy applied to such polymers has never been proposed to the best of our knowledge. Although polysaccharides display a perfect biocompatibility and biodegradability, which are the basic characteristics for polymers used as biomaterials, and have several characteristics not found in other natural polymers,<sup>37</sup> the chemical modification can be a real challenge in comparison with synthetic polymers.<sup>36</sup>

In this paper, we report the fabrication of a completely biocompatible nanocarrier with enhanced biostability. In particular, an oil-in-water (O/W) nanoemulsion composed of natural material, i.e. soybean oil and

egg lecithin as surfactant, was used as lipophilic nano-carrier and coated with a polymeric multilayer film composed of polysaccharides, i.e. glycol chitosan and heparin. Alternating layers of glycol chitosan and heparin respectively modified with thiol and allylic moieties were covalently bonded with an UV irradiation by virtue of the thiol-ene reaction, leading to the formation of stable thioether cross-links between the successive layers. The reaction was previously characterized on polystyrene nanoparticles (PS NPs), a rigid template that can be centrifuged in order to be investigated by a properly modified Ellman's test and because the rigidity is necessary to carry out Magic Angle Spinning (MAS) NMR spectroscopy.

O/W nano-emulsions represent an ideal nano-carrier to conveying and releasing powerful poorly water-soluble drugs.<sup>38-40</sup> The covalently bound multilayer resulted to have an increased biostability, for both PS NPs and, more interestingly, O/W nano-emulsions templates. Moreover, the possibility to perform the cross-linkage without any photoinitiator, as demonstrated through cytotoxicity assays, and the choice of natural and biodegradable components make this approach highly biocompatible and efficient in the field of bio-applications.

## 3.2 Results and discussions

### *Polymer functionalization*

Preliminary tests were performed to obtain the highest degrees of functionalization of the two polymers: glycol chitosan (GC) and heparin. Polymer functionalization was obtained through amidation of N-acetyl-L-cysteine (NAC) for GC and allylamine for heparin, in both cases with a water soluble carbodiimide (EDC, ethyl-3-(3-dimethylaminoisopropyl)-carbodiimide) and 1-hydroxy-1,2,3-benzotriazole (HOBt) as additive.<sup>41</sup> This chemistry is very common, but the application to polysaccharides can result in low degrees of functionalization like in the case of chitosan due to poor reactivity of the functional groups and poor solubility of the polymer, which may justify the lack of a free catalyst cross-linkage applied to such natural polymers.

The first attempts of chitosan functionalization were conducted on chitosan and depolymerized chitosan, but the low water solubility limited the degree of functionalization (see **Table 3.1**).<sup>42</sup> Indeed, the best results were obtained using glycol chitosan, a modified chitosan that results to be soluble in water even at neutral pH due to the ethylene glycol moiety.<sup>43</sup> Such increase of solubility resulted in a very high content of free thiols (up to 650  $\mu\text{mol/g}$ ).

**Table 3.1.** Free and total thiol groups for thiolated CT determined by Ellman's test

Synthesized CT-NAC	HOBt:CT <sup>a</sup> :NAC:EDC (molar ratio)	Free Thiols groups ( $\mu\text{mol/g}$ )	Total Thiol groups ( $\mu\text{mol/g}$ )	Oxidized thiols (%)
CT 1	1:1:0.5:6	37.6	38.2	1.6%
CT 2	2:1:0.5:6	21.8	36	39.4%
CT 3	5:1:0.5:6	9.7	35.8	73%
CT 4	1:1:1:6	75.6	78	3.1%
CT 5	2:1:1:6	50.4	69	27%
CT 6	5:1:1:6	24.1	73.5	67.2%
CT 7	1:1:4:8	136.0	138.2	1.5%
CT 8	1:1:4:16	294.0	328.5	10.5%
CT-B 1	1:1:4:16	319.0		
CT-B 2 <sup>b</sup>	1:1:4:16	347.0		
GC-1	1:1:4:16	515.6		
GC-2 <sup>b</sup>	1:1:4:16	581.2		
GC-3 <sup>b</sup>	1:1:4:16 <sup>c</sup>	651.3		

<sup>a</sup> for chitosan, the moles of its repeating units are considered in the molar ratio with the other components of the reaction solution

<sup>b</sup> pH was adjusted at a value of 6.8

<sup>c</sup> EDC was added gradually (half amount was added at  $t=0$ ; a quarter was added at  $t=2$  h and the final amount was added at  $t=4$  h)

Heparin was chosen as the polyanionic component to establish the cross-linkage among layers (**Figure 3.1**). Thanks to its high solubility in water (the negative charge is maintained also in acid conditions due to the presence of sulfate groups),<sup>44</sup> till 80 % of carboxylic group could be functionalized (as determined with <sup>1</sup>H-NMR analysis).

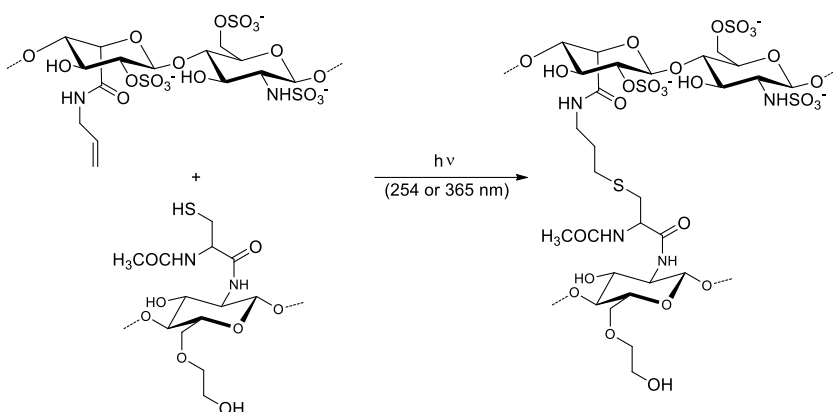


**Figure 3.1.** Thiol-ene reaction between allylated heparin and thiolated glycol chitosan. Reaction was triggered throughout UV irradiation.

More in detail, as shown in **Figure 3.2**, the signal at 5.72 ppm related to CH proton of terminal olefin is not overlapped with heparin signals. By the integration of the area of this peak and the area between 2.9 and 4.4 ppm, related to 10 protons of iduronic and glucosamine units, it is possible to determine the degree of functionalization, that results being 80.0 %.

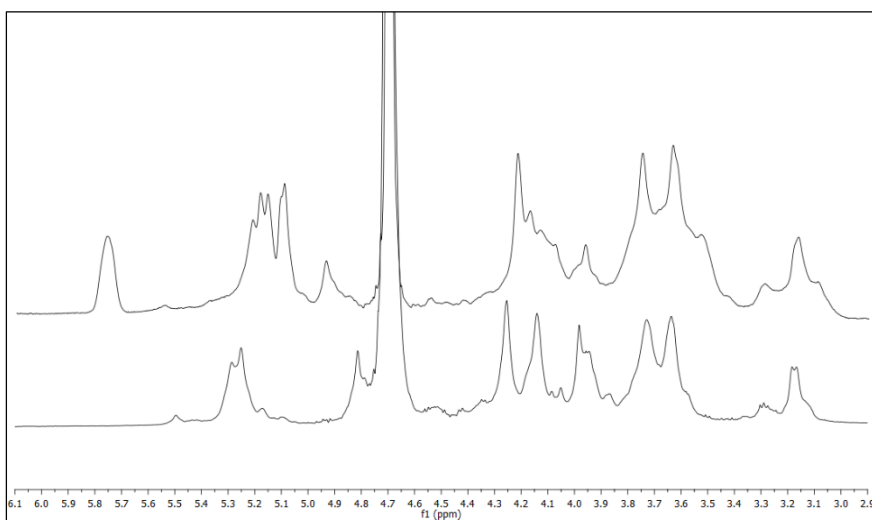


**Figure 3.2.**  $^1\text{H}$  NMR spectrum of heparin (below) and modified heparin (on top).

*Investigation of thiol-ene like reaction on modified polymers and on polymer multilayer shells*

Modification of polymers was needed to perform a covalent cross linkage among successive layers, exploiting the thiol-ene reaction (**Figure 3.1**). This reaction can be photo-initiated (at 365 nm or 254 nm), can be performed at room temperature in the presence of oxygen<sup>45</sup> and does not require potentially toxic metal catalysts. In order to determine the best reaction conditions, the modified glycol chitosan (GC-3, see **Table 3.1**) was first made to react with allylamine in solution and the experimental conditions (light source, wavelength, time irradiation, presence of oxygen and photoinitiator) were investigated. Once added allylamine Ellman's test was performed before and after irradiation and the relative reduction of free thiol groups was determined.

The results (**Table 3.2**) confirm that the reaction is not sensitive to the ambient light and to the presence of oxygen.<sup>45</sup> This means that it is possible to store and process the functionalized multilayer without any precautions in terms of light shielding and inert atmosphere. Moreover, comparing the two wavelengths used, it is evident that the irradiation at 254 nm is preferable as it is possible to perform effectively the reaction with low power irradiation (TLC lamp), without temperature control of the solution

and photoinitiators, even though the presence of the photoinitiator determines higher yields.

**Table 3.2.** Degree of reduction of thiol group by irradiation of thiolated glycol chitosan (with 13% of free thiols content) in presence of allylamine

Test	Irradiation source (nm)	Time exposure	Experimental condition	Photoinitiator	reduction free thiols
1	Sunlight	2h	N <sub>2</sub>	No	1.4 %
2	365 (Hg lamp)	2h	N <sub>2</sub>	Yes	49.4%
3	365 (TLC lamp)	2h	N <sub>2</sub> , pH 4	Yes	34.7%
4	365 (Hg lamp)	2h	In N <sub>2</sub>	No	17.2 %
5	365 (TLC lamp)	2h	N <sub>2</sub> , pH 4	No	< 1%
6	365 (Hg lamp)	2h	25 °C, pH4	No	12.1%
7	254 (TLC lamp)	2h	N <sub>2</sub> , pH 4	No	39.8 %
8	254 (TLC lamp)	2h	pH 4	No	35.3%
9	254 (TLC lamp)	2h	pH 4	Yes	76.8%
10	254 (TLC lamp)	2h	N <sub>2</sub> , pH 4	Yes (1/2)	45.5%
11	254 (TLC lamp)	1h	N <sub>2</sub> , pH 4	Yes	45.3%

To prove that the thiol-ene reaction can be effectively performed not only in solution but also on particulate substrates, a bilayer composed of glycol chitosan and heparin was deposited on PS NPs by LbL technique, as previously described. The amount of polymers needed to coat the nanoparticles was determined using the saturation method.<sup>46</sup> PS NPs were used instead of O/W nano-emulsion because the rigidity of the former template is required to characterize cross-linkage among layers, as it will be discussed below.

The bilayer on PS NPs was irradiated using the best conditions previously found (254 nm, 2 h) in an open container. A modified Ellman's test (see

**Figure 3.3)** was used to determine the decrease of free thiol groups that corresponds to the amount of thioether bonds formed.

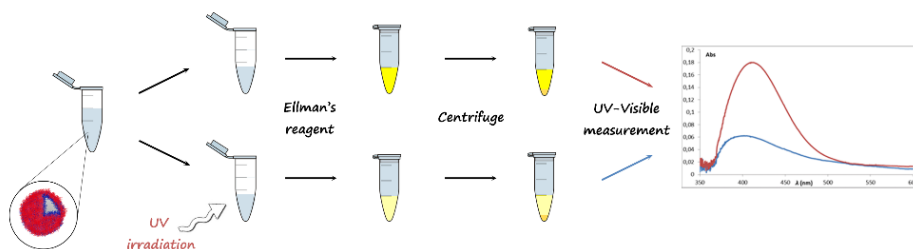


**Figure 3.3.** Schematic representation of the modified Ellman's test. The relative reduction of free thiols indicates the amount of thioether bond formed

In particular, the test was performed both on irradiated (2 h at 254 nm) and non-irradiated bilayer films. The test was opportunely modified in order to be applied to a system containing a particle suspension. Indeed, the Ellman's reagent was added to both suspensions, letting them to react for 2 h, and then the two samples were centrifuged collecting the supernatant for the spectrophotometric measurement. It was possible to obtain a solution containing only  $\text{TNB}^{2-}$  useful for UV measurement. As expected, the degree of cross-linkage was higher when using the photoinitiator ( $54.6 \pm 2.0 \%$  against  $25.4 \pm 0.9 \%$ ). We verified that the amount of photoinitiator was not above the saturation limit ensuring to not affect forcedly following cytotoxicity tests (**Figure 3.4**).

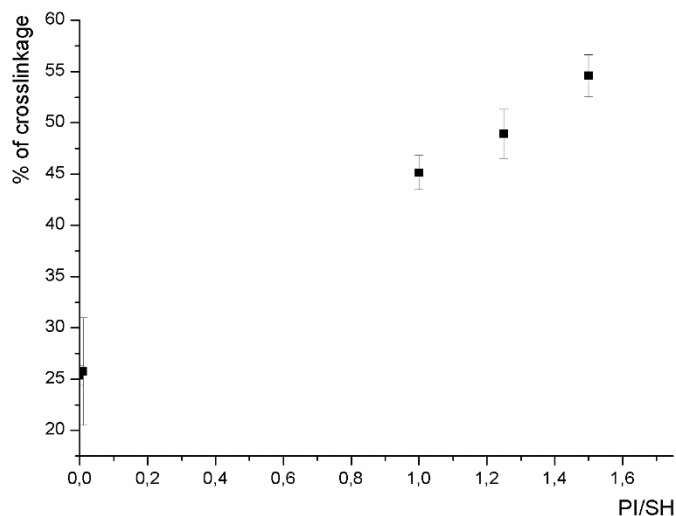


**Figure 3.4.** Free thiol reduction after cross-linkage (UV irradiation at 256 nm for 2h) of bilayer coating on PS NPs varying the photoinitiator content. Error bars indicate the standard deviation.

However, a sufficient reduction of free thiol occurs in absence of photoinitiator, demonstrating cross-linkage also in absence of photoinitiator. The possibility to trigger the reaction without the use of a photoinitiator is a remarkable advantage for bio-applications in which the presented systems is subsequently employed.

The formation of the thiol-ether bond was further proved using Magic-Angle Spinning  $^1\text{H-NMR}$  (MAS NMR) Spectroscopy. This technique is a powerful tool to study the polymers structure on the surface of rigid nanoparticles.<sup>47</sup> The reduction of allyl group signals in the spectrum confirms the cross-linkage between the allylated heparin and the thiolated glycol chitosan adsorbed on the PS nanoparticles surface. In **Figure 3.5** the superimposition of the spectra obtained before and after the UV

irradiation is shown. Allyl proton signal at 5.87 ppm is significantly decreased, suggesting again that the photoreaction occurs.

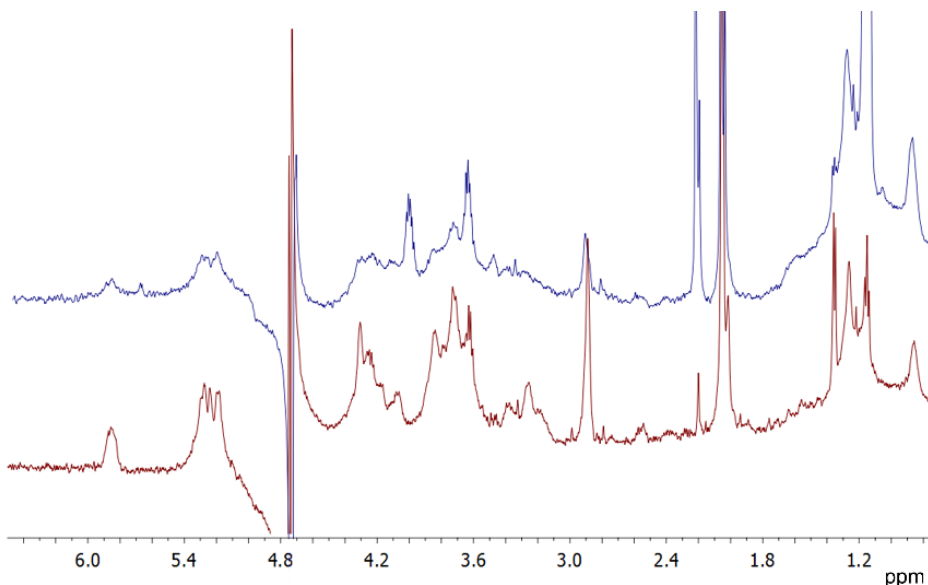


**Figure 3.5.** 1D <sup>1</sup>H MAS NMR spectra of PS nanoparticles suspension coated with polymer bilayer before (red line) and after (blue line) irradiation with UV light. Allyl proton signal at 5.87 ppm is decreased after irradiation.

### *Cytotoxicity results*

The cytotoxicity of the above bilayer coated PS NPs was investigated in order to verify the effect of the cross-linking process and, in particular, the effect of a hypothetical residual presence of the photoinitiator on cell viability (photoinitiator is removed dialyzing samples against water overnight, as previously reported). To this aim, mouse brain endothelial bEnd.3 cells were exposed to bilayer coated PS NPs for 24 h.

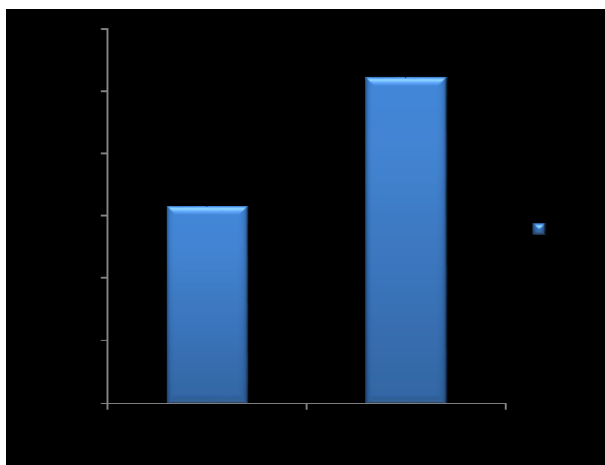


**Figure 3.6.** Viability of bEnd.3 cells 24 h after exposure to suspensions of bilayer-coated nanoparticles with a photoinitiator (BL + PI) and the same suspensions without a photoinitiator (BL) evaluated by the Alamar Blue assay. Viability of nanoparticle-treated cells is normalized to untreated control cells. Error bars indicate the standard deviation.

As shown in **Figure 3.6**, no significant cytotoxicity was observed for bilayer systems cross-linked without photoinitiator. Conversely, samples prepared in presence of a photoinitiator and after purification by dialysis provided a decrease of about 35-40% in cell viability. Moreover, confocal microscopy images demonstrated the capability of the bilayer coated PS NPs to enter cells after 24 h incubation as shown by the intracellular green spots mainly localized around the nucleus (**Figure 3.7**).

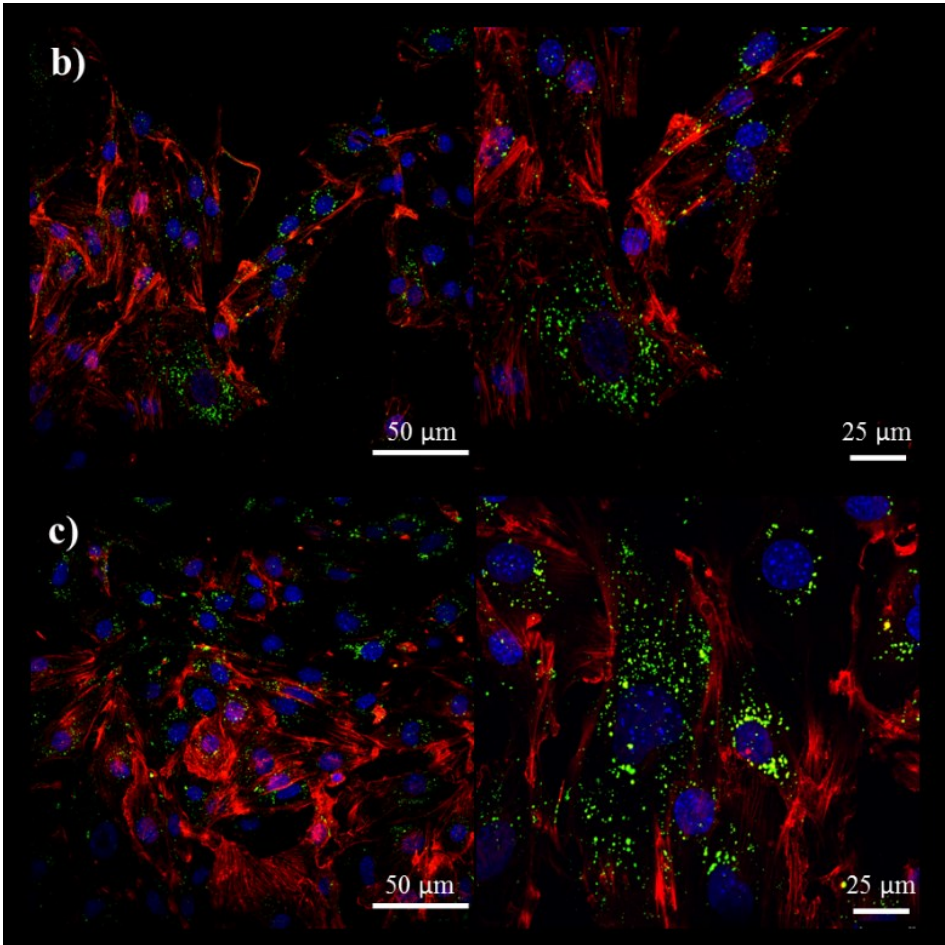


**Figure 3.7.** Confocal images of bEnd.3 cells incubated with suspensions of bilayer-coated nanoparticles with a photoinitiator (b) and the same suspensions without a photoinitiator (c) for 24 h at 37 °C.

Taken altogether, these preliminary results suggest that this strategy is promising in order to obtain stable and biocompatible nanosystems valid for bio-applications.

### ***Biostability tests on multilayer***

To highlight the enhanced stability of the cross-linkage on polymeric coating prepared *via* LbL, we compared two systems made respectively

with functionalized and not functionalized polymers on PS NP as template. Since chitosan is more sensitive of the heparin to physiological conditions, we used chitosan as last layer thus preparing a trilayer coating. Both systems were irradiated at 256 nm without the photoinitiator. The trilayer was based on a first layer of glycol chitosan, a second layer of heparin and again a layer of glycol chitosan. The values of size, PDI and  $\zeta$ -Potential for the starting template and the layers sequentially deposited are shown in **Table 3.3**.

**Table 3.3.** DLS analysis of trilayer coating on PS NPs of modified polymers (entries 2-4) and non-modified polymers (entries 5-7).

		Size (d.nm)	PDI	$\zeta$ -Potential (mV)	$\zeta$ -Deviation (mV)
1	Template	120.0	0.026	- 35.4	$\pm$ 10.8
2	Monolayer	126.7	0.067	+ 39.8	$\pm$ 8.39
3	Bilayer	133.5	0.087	- 30.4	$\pm$ 13.3
4	Trilayer	139.9	0.064	+29.8	$\pm$ 8.13
5	Monolayer	129.6	0.064	+ 44.8	$\pm$ 8.35
6	Bilayer	141.3	0.073	- 35.0	$\pm$ 7.47
7	Trilayer	165.8	0.111	+30.3	$\pm$ 6.87

It is noteworthy that chitosan is a weak polycation, and the increase of pH leads to the loss of positive charges and to the consequent destabilization of the entire system.<sup>48</sup> For this reason, stability was monitored checking the size of the sample over time in media with different pH and ionic strength.

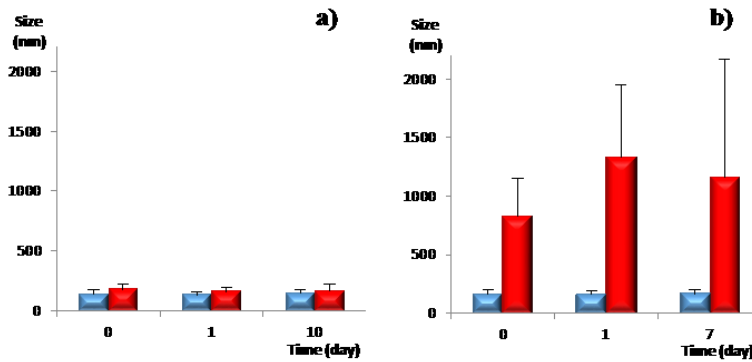


**Figure 3.8.** Comparison of size measurement between sample cross-linked (blue bars) and non (red bar) in different media: a) sample dispersed in water at pH 4; b) sample dispersed in 10 mM phosphate buffer solution at pH 7.3. Error bars indicate the standard deviation.

From **Figure 3.8 a** it is evident how stability is similar for both systems if samples are stored in water at pH 4, where there is no significant ionic strength and the pH is ideal to maintain the first and the outer layer positively charged. The same comparison was performed in phosphate buffer solution at neutral pH to simulate a physiological environment where pH and ionic strength increase. In **Figure 3.8 b** it is shown that the not cross-linked sample is sensibly unstable in such conditions: size increases dramatically disclosing a fast destabilization. Conversely, the sample previously cross-linked resulted to be stable over several days. The notable difference between the samples is also macroscopically evident

(**Figure 3.9**), proving that the cross-linkage positively affects the stability of the LbL multilayer.

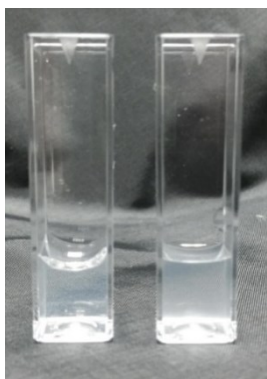


**Figure 3.9.** Macroscopic comparison between samples dispersed in phosphate solution: the sample cross-linked (on the left) is not subject to aggregation phenomena and the suspension remains clear.

### ***Multilayer nanocapsule on O/W nano-emulsion***

In the end we realized the same trilayer coating an O/W nano-emulsion, a liquid template already developed in our lab,<sup>49, 50</sup> to show the utility and the promising application of the above results. O/W nano-emulsions were prepared by using a high-pressure homogenizer and a formulation based on natural materials, i.e. soy-bean oil and lecithin as surfactant. Depending on the relative amount of oil and surfactant, it was possible to realize nano-emulsions, ranging from 100 to 200 nm. The liquid template represents a promising platform for imaging and drug delivery since it was already demonstrated its capability to encapsulate lipophilic drugs (e.g. curcumine), dyes (e.g. Nile red, fluorescein) or contrasting agents (e.g. SPION, QDs; see **Figure 3.10**).<sup>49, 51</sup>

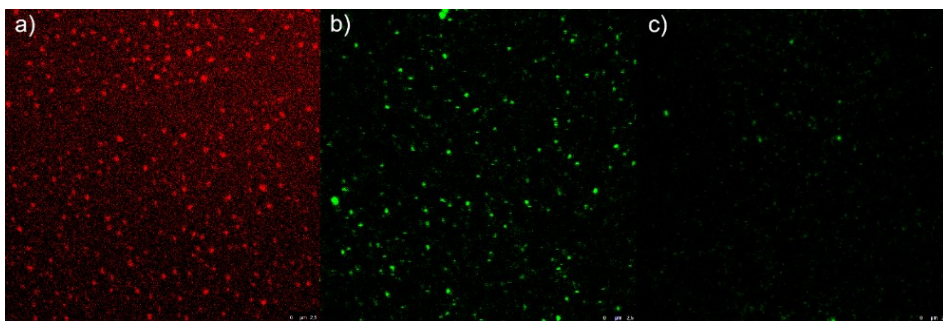


**Figure 3.10.** Confocal and STED image of Oil-in-Water nanoemulsion loaded with: a) Nile Red (confocal); b) CdSe QDs (STED); c) FITC (STED). Scale bar 2.5 micron.

Consequently, several advantages are related to the use of this template: i) the core removal is not required; ii) the deposition of few layers is sufficient to obtain a stable carrier;<sup>52</sup> iii) particle large enough to be centrifuged and pelleted are not needed; iv) a post-production step of encapsulation is avoided. These advantages result in an approach significantly less time-consuming and less labor-intensive to obtain nano-sized capsules.<sup>53</sup>

**Table 3.4.** DLS analysis of multilayer deposition of modified polymers (entries 2-4) on O/W nano-emulsion template (entry 1) and of trilayer after irradiation and dispersion in PBS (entries 5 and 6).

		Size (d.nm)	PDI	Z-Potential (mV)	Z-Deviation (mV)
1	O/W nano-emulsion	132.0	0.048	- 38.7	± 6.15
2	Monolayer	137.7	0.072	+ 26.0	± 6.87
3	Bilayer	141.8	0.116	- 30.8	± 3.04
4	Trilayer	166.4	0.138	+ 38.1	± 4.76
5	Trilayer cross-linked	170.9	0.144	+ 31.6	± 4.52
6	Trilayer in PBS	169.8	0.126		

**Table 3.4**, summarizes the particle size and Z-potential measurement for the starting template and for the resulting trilayer built up with functionalized glycol chitosan and heparin. The trilayer was irradiated and dispersed in PBS to confirm, also in this case, the enhanced stability due to covalent cross-linkage among layers (see entry 6 in **Table 3.4**). Also for this sample, after 24 hours of contact with cells, no cytotoxicity was observed (% viability = 95.6 %; SD = 13.0%). Further biological tests are presently under investigation in order to use this system in specific biomedical applications, in particular in drug delivery applications.

In addition to size measurements, the glycol chitosan of the last layer was labelled with fluorescein. In **Figure 3.11** it is shown a confocal image of cross-linked trilayer coating O/W nanoemulsions dispersed in PBS that clearly demonstrate persistence of the outer layer even after disappearance of the electrostatic stabilization. DLS of the above nanocapsules is also reported in **Figure 3.11** to show monomodality and narrow distribution (average size in **Table 3.4**, entry 6).

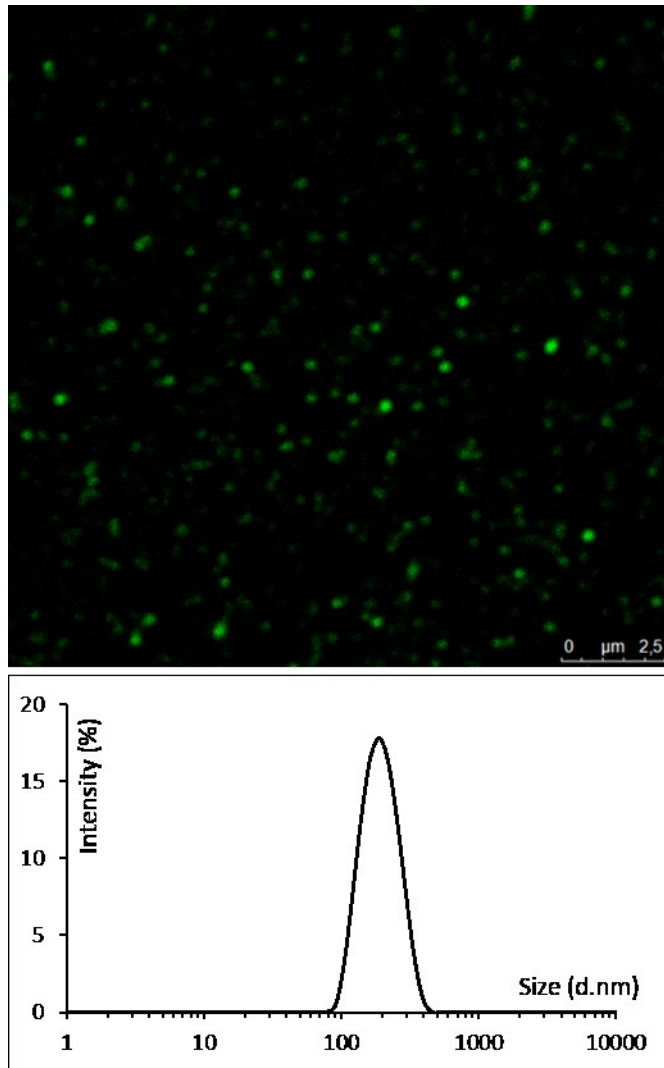


**Figure 3.11.** Confocal and DLS analysis of a trilayer coatings on O/W nano-emulsion after cross-linkage and dispersion in PBS. The outer layer, labelled with fluorescein, remains attached to the nanocapsules also if ionic forces are weak in this conditions.

It is noteworthy that for the first time we propose the use of natural based materials, like polysaccharides, stabilized by a thiol-ene click reaction. At the same time, we demonstrate that this reaction can be applied to oil core based capsules made of completely biodegradable polymers which is an

highly wished requisite in drug delivery<sup>54</sup> together with the size requirement below 200 nm.<sup>55</sup> Very interestingly, the degree of cross-linkage reached in this work was enough for the final aim to stabilize the nanocapsules in physiological medium even with no photoinitiator due to the high degree of functionalization of the starting polymers and with a limited number of polymer layers. Moreover, the oil based nanocarrier here proposed is very useful for drug delivery, due to the possibility of conveying and releasing bioactive hydrophobic substances.

### **3.3 Conclusions**

In this work we showed how the stability of biopolymer multilayers obtained via layer by layer can be enhanced introducing covalent bonds among layers by means of a metal catalyst-free, light initiated 'click' reaction, namely the thiol-ene reaction. In particular, a thiol moiety on chitosan and an allylic moiety on heparin were introduced analyzing the related degree of functionalization. High degrees of thiolation (up to 650  $\mu\text{mol/g}$ ) could be reached using glycol chitosan. NMR analysis and colorimetric tests were performed to demonstrate the occurring of the thiol-ene reaction among modified polymers. Interestingly, the reaction resulted effective even without a photoinitiator, mainly due to the high degree of modification of the biopolymers, providing a completely non-

cytotoxic final product, as demonstrated through in vitro tests. Cross-linked multilayers resulted in more stable systems than those stabilized with just electrostatic forces, even when they experienced perceptible variations in pH and ionic strength. Therefore, we provide an efficient and biocompatible approach to fabricate very stable polymer multilayer capsules made via LbL technique. In addition, the application of this approach to biopolymers surrounding an O/W nano-emulsion demonstrates that thiol-ene cross-linkage can be nicely exploited in the field of completely biocompatible and biodegradable nanocarriers. Other bio-applications where LbL multilayers have to be stabilized may also benefit from the proposed approach.

### **3.4 Materials and Methods**

#### *Materials*

Chitosan low molecular weight (CT-LMW, 90-150 kDa), heparin sodium salt (from porcine intestinal mucosa), 1-hydroxybenzotriazole hydrate (HOBt), acetic acid, sodium acetate, sodium chloride, N-acetyl-L-cysteine (NAC), allylamine, sodium nitrite, methanol, ammonium hydroxide solution, sodium borohydride, hydrochloric acid, sodium hydroxide, deuterium oxide (D<sub>2</sub>O), trifluoroacetic acid (TFA), 5,5'-dithiobis(2-nitrobenzoic acid) (DTNB, also known as Ellman's reagent) and

Fluorescein 5(6)-isothiocyanate (FITC) were purchased from Sigma-Aldrich. Soy-bean oil (density at 20 °C of 0.922 g ml/1) and Lipoid E80 lecithin (egg lecithin powder 80–85% enriched with phosphatidyl choline and 7–9.5% content in phosphatidyl ethanolamine) were purchased from Lipoid. Glycol chitosan (GC) was purchased from Wako Chemicals. 1-(3-dimethylaminopropyl)-3-ethyl-carbodiimide hydrochloride (EDC) was purchased from Iris Biotech. Carboxyl latex beads (4% (w/v), 0.1 µm) and FluoSpheres® (Carboxylate-Modified Microspheres, 0.1 µm, yellow-green fluorescent (505/515), 2% solids) were purchased from Invitrogen. Irgacure® 2959 was purchased by Ciba Specialty Chemicals. Dialysis membranes were purchased from Spectrum Laboratories Inc.

### ***Oil-in-Water nanoemulsion***

The O/W nano-emulsion was prepared as previously described.<sup>49</sup> Briefly, the oil phase was prepared by adding an exact amount of Lipoid E 80 to the soy-bean oil at 60 °C and then sonicated with an immersion sonicator (Ultrasonic Processor VCX500 Sonic and Materials). To obtain the pre-emulsion, the oil phase was added dropwise to a weighted amount of aqueous phase (Milli-Q water) and mixed using the immersion sonicator. The pre-emulsion was finally passed at 2000 bar through the high-pressure valve homogenizer (Microfluidics M110PS) to obtain the final nano-emulsion.

*Modification of glycol chitosan with N-Acetylcysteine*

Thiolation was performed on different chitosan substrates in order to identify the best degree of functionalization: chitosan low molecular weight (CT-LMW,  $M_v = 126.0$  kDa), depolymerized chitosan (dCT,  $M_v = 17.5$  kDa, depolymerization was performed using nitrous acid)<sup>56, 57</sup> and glycol chitosan (GC, chitosan conjugated with ethylene glycol). In the typical procedure, 0.5 mmol of the chitosan substrate were dissolved in 10 ml of Milli-Q water. Different amounts of HOBt (see **Table 3.1**) were added and pH was at first adjusted to a value of 4 with HCl 1 M to allow complete dissolution. Then, different amounts of NAC and EDC (see **Table 3.1**) were added to the solution. The pH was adjusted and maintained to a value of 6.8 (pH was kept at pH 5 for CT-LMW to prevent the precipitation) throughout the reaction time (3 h). The reactions proceeded at room temperature. The product was then purified by dialysis four times against water containing 1% (w/v) NaCl and acidified with HCl at pH = 3, four times against water acidified at pH = 3. Finally, the purified product was freeze-dried for 48 h (Freeze Dryer CHRIST Alpha 1-4 LSC).

Total and free thiols were determined using a colorimetric assay, the Ellman's test.<sup>58-60</sup> In particular, after reaction of thiolated chitosan with a DTNB solution at 25 °C for 2 h, absorbance was registered at 412 nm using a Varian Cary Scan 100 Spectrophotometer. For total thiols evaluation,

reduction of disulphide bond with  $\text{NaBH}_4$  was needed before adding DTNB solution.

### ***Modification of heparin with allylamine***

Heparin (100 mg, 0.150 mmol of  $-\text{COOH}$  groups) was dissolved in 10 ml of Milli-Q water. After the rapid dissolution of the polymer, allylamine (112.5  $\mu\text{L}$ , 1.5 mmol) was added to the solution and pH adjusted to 6.8 value. Then, HOBt (81.22 mg, 0.6 mmol) and EDC (115.2 mg, 0.6 mmol) were added. The pH was adjusted again to 6.8 and maintained at this value throughout the reaction time (6 h, RT). Sample was then dialyzed (dialysis tubing of 6-8 kDa) against water and freeze-dried for 48 h. The degree of functionalization was determined with  $^1\text{H-NMR}$  spectra (**Figure 3.2**).

### ***Modification of glycol chitosan with fluorescein isothiocyanate***

Glycol chitosan (GC, 100 mg, 0.20 mmol) was dissolved in 10 ml of 0.1 M of acetic acid solution. After complete dissolution, a solution of FITC (5.0 mg in 500  $\mu\text{l}$  of DMSO) was added dropwise. The reaction proceeded over night at room temperature. Sample was then dialyzed (dialysis tubing of 6-8 kDa) against water till no dye was detected (using Perkin Elmer 2300 Enspire Plate Reader,  $\lambda_{\text{ex}} = 488 \text{ nm}$ ,  $\lambda_{\text{em}} = 510 \text{ nm}$ ). Finally, the purified product was freeze-dried for 48 h.

### ***Solution Nuclear Magnetic Resonance spectroscopy***

1D  $^1\text{H}$ -NMR experiments were performed using an Agilent 600 MHz spectrometer equipped with a DD2 console and an OneNMR HX probe. Samples containing CT or GC were prepared at 10 mg/ml in  $\text{D}_2\text{O}$ , containing 1 % (v/v) of TFA. Samples containing heparin were prepared at 10 mg/ml in deuterium oxide. NMR spectra were recorded with a total of 64 transients and a PRESAT sequence was used to saturate the water residual peak. Spectra analysis was performed using VNMRJ 4.0 software.

### ***LbL deposition of functionalized polymers on polystyrene carboxylated nanoparticles***

*Monolayer deposition.* 1 ml of a water suspension (pH 4) of carboxyl latex beads (PS NPs, 0.5 % w/v) were added, under vigorous stirring for 15 min to 2 ml of a solution of GC (0.04 % w/v) in water at pH = 4.

*Bilayer deposition.* 2.5 mL of a water solution of heparin (0.128 % w/v) at pH = 4 were added to 2.5 ml of monolayer-coated nanoparticles suspension (0.16 % w/v PS NPs; 0.0256 % w/v GC) under vigorous stirring for 15 min.

*Trilayer deposition.* 2.5 ml of a water solution of GC (0.064 % w/v) at pH = 4 were added to 2.5 ml of bilayer-coated nanoparticles suspension (0.08 % w/v PS NPs; 0.0128 % w/v GC; 0.064 % w/v Hep) under vigorous stirring for 15 min.

### ***LbL deposition of functionalized polymers on O/W nano-emulsion***

Monolayer, bilayer and trilayer were obtained with the same procedure explained above, with the following final concentration: 0.25 % (w/v) O/W nano-emulsion, 0.0025 % (w/v) GC, 0.005 % (w/v) Hep, 0.01 % (w/v) GC-FITC.

### ***$\zeta$ -potential measurements***

The  $\zeta$ -potential was determined using a particle electrophoresis instrument (Zetasizer zs nano series ZEN 3600, Malvern Instruments Ltd., Malvern, U.K.). Samples were diluted up to a concentration of approximately 0.025 % (w/v) using the proper buffer solution. The  $\zeta$ -potential analysis was carried out by setting 50 runs for each measurement.

### ***Particle size measurements***

Suspensions were characterized using a laser dynamic light scattering (DLS) instrument ( $\lambda = 632.8$  nm). A detecting angle of  $173^\circ$  was used. All the samples were diluted up to a droplet concentration of approximately 0.025 w/v % by using Milli-Q water acidified at pH 4. A default refractive index ratio (1.5900) and 5 runs for each measurement (1 run lasting 100 s) were used in the calculations of the particle size distribution.

### ***Photoreaction of the multilayer***

The suspensions of PS NPs coated with polymer multilayer were irradiated with UV light for 2 h. Two different UV light sources were used: a UV Hand Lamp Spectroline® E-Series UV lamp (output 6 W, wavelength 254 and 365 nm), or a High Intensity Lamp Blak-Ray® UV (Ultraviolet Lamp with Spot Bulb, output 100 W, wavelength 365 nm). For the UV Hand lamp, the light source was at 3 cm distance. For the High Intensity Lamp the distance was increased to 10 cm and a water bath was used to avoid overheating of the solution. Photoreaction was conducted both with a final concentration of photoinitiator of 0.3 mg/ml and without a photoinitiator. Samples for cytotoxic assays were dialyzed against water overnight.

*Ellman's test.* To determine the reduction of free thiols after irradiation (corresponding to the degree of cross-linkage), 50 ml of PS NPs coated with a bilayer were concentrated to 2 ml by centrifuge (13000 rpm, 10 min, 4 °C), and sonicated (10 min, 40 MHz, 50 % of power, 4 °C). Half volume was stored at room temperature for 2 h in presence of natural light and atmospheric oxygen, while half volume was irradiated. Then, 0.5 ml of each sample were added to a solution containing the Ellman's reagent. After 2 h, each sample was centrifuged (13000 rpm, 15 min) and supernatant was collected for UV measurement. (**Figure 3.3**)

*MAS NMR Analysis.* To confirm the reduction of allyl groups after irradiation an NMR analysis was performed. A suspension of PS NPs

coated with polymer bilayer was centrifuged, resuspended in 100  $\mu$ l of D<sub>2</sub>O and then sonicated. The same procedure was used for sample irradiated with the UV light. 1D <sup>1</sup>H-NMR experiments were performed using an Agilent 600 MHz spectrometer equipped with a DD2 console and a gHX Nanoprobe. The MAS spin rate was set at 2.7 kHz and the number of transients used for spectra acquisition was 4096. A DPGFSE<sup>61</sup> sequence was used to saturate the water residual peak. Spectra were transformed, superimposed and analyzed using the software VNMJ 4.0.

### ***Stability tests on normal and cross-linked trilayer***

The stability over time of the system was determined dispersing PS NPs coated with the trilayer in different media, i.e. water at pH = 4, PBS 10 mM pH = 7.3. Stability was determined monitoring by DLS particle size variations over time.

### ***Cytotoxicity test***

The Alamar Blue assay was used to test the cytotoxicity of the PS NPs coated with a bilayer in presence or not of the residual photoinitiator. Immortalized mouse cerebral endothelial cells, bEnd.3 cells (American Type Culture Collection, Manassas, VA), grown in DMEM with 4.5 g/l glucose, 10 % w/v Fetal Bovine Serum (FBS), 3.7 g/l sodium bicarbonate, and 4 mM glutamine, 1 % w/v non-essential amino acids, 100 U/ml

penicillin and 0.1 mg/ml streptomycin in 100 mm diameter cell culture dish, in a humidified atmosphere at 37 °C and 5 % v/v CO<sub>2</sub>, were chosen as a model of endothelium. Briefly, cells were seeded in 96-well microplates (Costar) at a density of  $8 \times 10^3$  cells/well at a final volume of 100 µl and incubated for 24 h at 37 °C. Cells were then treated with PS NPs coated with two polymer layers (GC-Hep) at a concentration of 0.002 % w/v in a final volume of 150 µl for each well. The metabolic activity of all cell cultures was determined after 24 hours of exposure by using standard Alamar Blue assay (Invitrogen) as described elsewhere.<sup>62</sup> The Alamar Blue reagent reduction of the sample solutions was analysed with a spectrophotometer (Perkin Elmer 2300 Enspire Plate Reader,  $\lambda_{\text{ex}} = 570$  nm,  $\lambda_{\text{em}} = 600$  nm). Data were reported as a percentage of cell viability normalized to untreated control cells. Statistical analyses of significance were performed using ANOVA test. p values equal or lower than 0.05 were considered statistically significant. Experiments were repeated three times in triplicates.

For the observation of multilayer cellular uptake, bEnd.3 cells were incubated with the same bilayer on PS NPs at a final concentration of 0.002 % w/v for 24 h at 37 °C. After each time, samples were washed two times with PBS and fixed with 4 % v/v paraformaldehyde for 20 min. Then, cell nuclei were stained with DAPI (Sigma-Aldrich) and cytoskeleton

microfilaments with red fluorescent phalloidin (Sigma-Aldrich). Samples were observed by confocal and multiphoton microscope system (Leica TCS SP5 MP) equipped with an oil-immersion 40× objective. Images were acquired with a resolution of 1024×1024 pixels.

### ***Confocal analysis***

Trilayer on O/W nano-emulsion was diluted 1:25 to a final oil concentration of 0.01 % w/v in an Eppendorf with PBS 10 mM at pH 7.2 and 200 µl were put in a FD3510 dish for 30 min to allow it to adhere to the surface of the dish. After that, several washes were performed replacing the sample twice with 120 µl of water and in the end with 120 µl of 5 % w/v DABCO antifade solution, taking care to let always wet the central part of the dish. DABCO antifade was needed to avoid the bleaching effect of the fluorescein. Samples were imaged with a Leica TCS STEDCW microscope (Leica-Microsystems, Mannheim, Germany) equipped with an oil immersion 100× objective. Images were acquired with a field of view of 25.6 × 25.6 µm for a pixel size of 25 × 25 nm. The analysis of the images was carried out using LAS AF software.

### 3.5 Supplementary Section<sup>2</sup>

In this section a parallel work performed using chitosan instead of glycol chitosan is reported. The limit illustrated for chitosan thiolation with *N*-acetyl-L-cysteine are here overcome using a different synthetic approach.

#### *Chitosan functionalization with 2-iminothiolane*

Chitosan functionalization was obtained using the Traut's reagent, namely 2-iminothiolane (2-IT), a heterocyclic thioimidate compound (**Figure 3.12**).

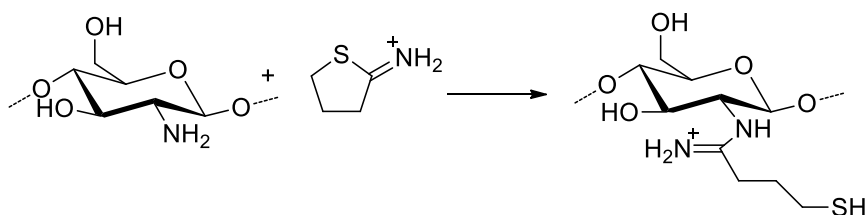


**Figure 3.12.** Schematic representation of the coupling reaction between chitosan and 2-iminothiolane to obtain chitosan-4-thio-butyl-amidine conjugate (CT-TBA)

Due to its structure, 2-IT shows angle, torsional and steric strain and, therefore, it results to have high reactivity towards amine. In addition, reaction with primary amine - in this case, with chitosan - leads to a chitosan-4-thio-butyl-amidine conjugate (CT-TBA) which still possesses a positive charge.<sup>42, 63</sup> This feature represents an advantage for LbL

<sup>2</sup> The work here illustrated has been realized with the precious help of Dr. Giusi Liberatore Ilardi and Dr. Luigi Angellillo, with whom I had the pleasure to collaborate during their respective Master Degree Thesis.

application, in that the charge density positively effects on the polymer deposition. In addition, the reaction does not require any condensing agent or catalyst, the yield strictly depends on the relative amount of 2-IT added and thus result to be very high (up to 17.7 % of functionalization). However, as reported,<sup>64, 65</sup> the major limits related to the formation of chitosan-TBA conjugate are the formation of disulfide bonds – resulting in the formation of covalent cross-linked gel – and a side reaction that involves a cyclization of TBA with the loss of ammonia and the formation of *N*-substituted 2-iminothiolane – the loss of ammonia makes the side reaction irreversible and the side product results to be without the positive charge and the thiol moiety (**Figure 3.13**).

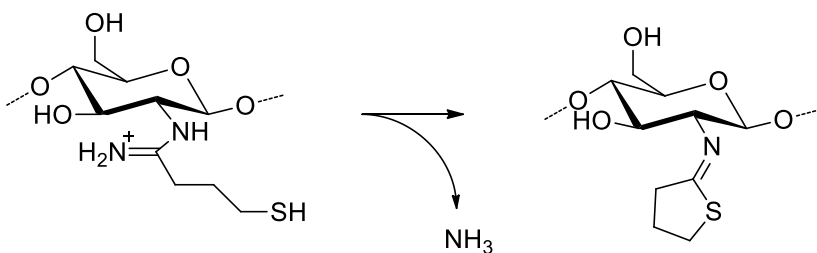


**Figure 3.13.** Schematic representation of the side reaction occurring with CT-TBA. At higher pH value (< 3-4) the loss of an ammonia molecules brings to the formation of a stable and thiol-free specie, the *N*-substituted 2-iminothiolane.

The synthetic procedure has been planned in order to minimize as much as possible these problems. In particular, reactions were conducted in inert atmosphere by using nitrogen, a mild reducing agent (DTT, dithiothreitol) was added to the solutions to remove disulphide bonds and pH was

lowered to 3.5 just prior to the purification step to reduce re-oxidation of thiols to disulphide and the irreversible loss of ammonia. The so modified polymer has been characterized both with  $^1\text{H-NMR}$  spectroscopy and with the colorimetric Ellman's test.

Further information about the materials and methods used for the synthesis, the characterizations and the degrees of functionalization obtained are more fully reported in the previous chapter.

### ***Biostability test on multilayer with CT-TBA***

As for thiolated glycol chitosan, also CT-TBA was employed to realize multilayer coating on colloidal nanoparticles *via* LbL and the effectiveness of the thiol-ene reaction to enhance the stability of the final system as a result of the cross-linkage has been evaluated.

Firstly, a trilayer systems made with functionalized polymers on PS NP as template was realized. The trilayer was based on a first layer of chitosan-TBA, a second layer of allylated heparin and again a layer of chitosan-TBA. The values of size, PDI and  $\zeta$ -Potential for the starting template and the layers sequentially deposited are shown in **Table 3.5**. The sample was splint in two aliquots, one of which was irradiated at 256 nm without any photoinitiator.

**Table 3.5.** DLS analysis of trilayer coating on PS NPs with modified polymers

		Size (d.nm)	PDI	$\zeta$ -Potential (mV)
1	Template	120.5	0.042	- 35.1
2	Monolayer	162.5	0.057	+ 25.4
3	Bilayer	148.6	0.060	- 44.9
4	Trilayer	196.8	0.057	+23.2

Finally, both the samples were dispersed in medium with varied pH and ionic strength, namely PBS (10 mM, pH 7.2) and DMEM, to detect any difference in the stability of the system before and after the cross-linkage. As shown in **Table 3.6**, system submitted to irradiation shows a higher stability, in that size results to be unchanged – or even slightly reduced – compared to the system dispersed in the starting acidic medium. On the other side, system not irradiated shows an increase in size and/or PDI. Thus comparison suggests that cross-linkage effects on the stability of the system, even if the differences are not so striking as in the case of the thiolated glycol chitosan.

**Table 3.6.** DLS analysis of trilayer coating on PS NPs submitted or not to UV irradiation. The comparison of the size and PDI measured illustrates that cross-linkage stabilize the system.

	Sample	Medium	Size (d.nm)	PDI	$\zeta$ -Potential (mV)
1	Irradiated	PBS	187.6	0.071	+ 22.7
2	Not irradiated	PBS	274.5	0.071	+ 23.5
3	Irradiated	DMEM	185.5	0.102	+ 23.6
4	Not irradiated	DMEM	225.9	0.211	+24.7

Subsequently, the same trilayer coating was realized on an O/W nanoemulsion. In **Table 3.7** are reported the values of size, PDI and  $\zeta$ -Potential for the starting oil-core, the layers sequentially deposited and the final system dispersed in DMEM and PBS. Results shows that the cross-linkage does not sufficiently strengthen the system, in that size and PDI increase dramatically.

**Table 3.7.** DLS analysis of cross-linked trilayer coating on O/W nanoemulsion.

		Size (d.nm)	PDI	$\zeta$ -Potential (mV)
1	O/W nanoemulsion	126.5	0.049	- 32.1
2	Monolayer	142.1	0.092	+ 27.6
3	Bilayer	174.6	0.125	- 32.6
4	Trilayer	186.7	0.092	+ 28.2
5	Trilayer in DMEM	423.8	1.000	
6	Trilayer in PBS	546.9	1.000	

In order to further enhance the stability of the system two possible strategy have been hypnotized, both aimed to increase the amount of cross-linkage: to increase the number of the layers or to increase the thickness of each layer. We oriented to realize the latter hypothesis because it results to be easier achievable – by increasing the ionic strength during the realization of the layer<sup>46</sup> – and without the complications related to the increase of the number of layers. In detail, layers' deposition is performed in an Acetic Acid buffer solution (20 mM, pH 4) containing a precise amount of NaCl (5 mM). In **Table 3.8** are reported the values of size, PDI and  $\zeta$ -Potential

for the starting oil-core, the layers sequentially deposited in this new conditions. Results clearly show the increase of size compared to the previous system (~ 35 nm for the final trilayer, see **Table 3.7** for a comparison). Entries 5 e 6 in **Table 3.8** also show that the greater thickness of the layer positively effects on the stability of the system. Indeed, the trilayer maintain the values of size and PDI after dispersion in DMEM e PBS.

**Table 3.8.** DLS analysis of cross-linked trilayer coating on O/W nanoemulsion obtained by increasing the ionic strength of the medium during the LbL deposition. Sizes result to be increased up to 35 nm in these conditions (compared with results in **Table 3.7**).

		Size (d.nm)	PDI	ζ-Potential (mV)
1	O/W nanoemulsion	126.5	0.049	- 32.1
2	Monolayer	158.4	0.133	+ 21.9
3	Bilayer	176.0	0.108	- 43.4
4	Trilayer	212.6	0.106	+ 18.6
5	Trilayer in DMEM	211.8	0.118	
6	Trilayer in PBS	226.0	0.127	

## ***Conclusions***

In this Section we briefly showed an alternative approach to prepare biocompatible nanocapsules with enhanced stability. As discussed above, modification of chitosan with N-acetyl-L-cysteine can be very challenging and degrees of functionalization result to be very low. The use of 2-iminothiolane as coupling agent allowed to reach higher percentage of thiolation, even if some problems have been encountered. In particular,

compared with GC-NAC, CT-TBA resulted to be less stable over time and, therefore, difficult to store. Nevertheless, results obtained with this different biopolymer further confirm the efficacy of the thiol-ene cross-linkage to realize very stable polymer multilayer capsules made *via* LbL technique.

## 3.6 References

1. G. Decher and J.-D. Hong, *Makromolekulare Chemie. Macromolecular Symposia*, 1991, **46**, 321-327.
2. G. Decher, *Science*, 1997, **277**, 1232-1237.
3. P. Bertrand, A. Jonas, A. Laschewsky and R. Legras, *Macromolecular Rapid Communications*, 2000, **21**, 319-348.
4. G. Decher and J. B. Schlenoff, *Multilayer thin films: sequential assembly of nanocomposite materials*, John Wiley & Sons, 2006.
5. C. S. Peyratout and L. Dähne, *Angewandte Chemie International Edition*, 2004, **43**, 3762-3783.
6. G. Decher and J. D. Hong, *Berichte der Bunsengesellschaft für physikalische Chemie*, 1991, **95**, 1430-1434.
7. W. B. Stockton and M. F. Rubner, *Macromolecules*, 1997, **30**, 2717-2725.
8. L. Wang, Z. Wang, X. Zhang, J. Shen, L. Chi and H. Fuchs, *Macromolecular rapid communications*, 1997, **18**, 509-514.
9. E. Kharlampieva and S. A. Sukhishvili, *Journal of Macromolecular Science, Part C: Polymer Reviews*, 2006, **46**, 377-395.
10. M. B. Zakaria, V. Malgras, T. Takei, C. Li and Y. Yamauchi, *Chemical Communications*, 2015, **51**, 16409-16412.
11. H. Wang, S. Ishihara, K. Ariga and Y. Yamauchi, *Journal of the American Chemical Society*, 2012, **134**, 10819-10821.
12. G. B. Sukhorukov, A. L. Rogach, M. Garstka, S. Springer, W. J. Parak, A. Muñoz-Javier, O. Kreft, A. G. Skirtach, A. S. Susha and Y. Ramaye, *Small*, 2007, **3**, 944-955.
13. S. De Koker, R. Hoogenboom and B. G. De Geest, *Chemical Society Reviews*, 2012, **41**, 2867-2884.
14. P. R. Gil, L. Loretta, A. Muñoz\_Javier and W. J. Parak, *Nano Today*, 2008, **3**, 12-21.
15. A. P. Johnston, C. Cortez, A. S. Angelatos and F. Caruso, *Current Opinion in Colloid & Interface Science*, 2006, **11**, 203-209.
16. Y. Yan, G. K. Such, A. P. Johnston, H. Lomas and F. Caruso, *ACS Nano*, 2011, **5**, 4252-4257.
17. Z. Tang, Y. Wang, P. Podsiadlo and N. A. Kotov, *Advanced Materials*, 2006, **18**, 3203.
18. L. Loretta, P. Rivera-Gil, A. Z. Abbasi, M. Ochs, C. Ganas, I. Zins, C. Sönnichsen and W. J. Parak, *Nanoscale*, 2010, **2**, 458-467.

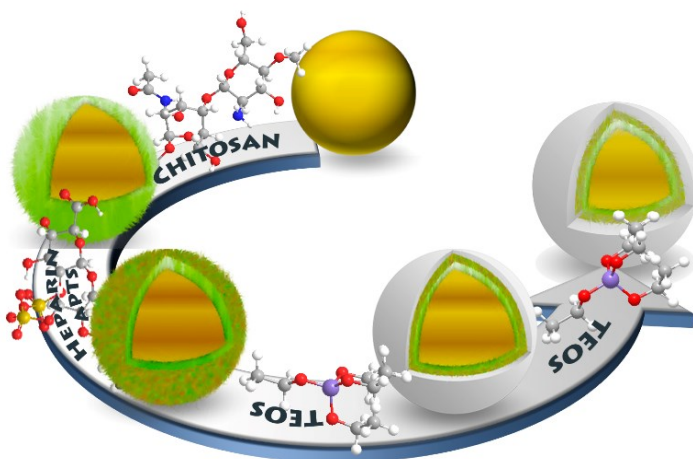
19. J. F. Quinn, A. P. Johnston, G. K. Such, A. N. Zelikin and F. Caruso, *Chemical Society Reviews*, 2007, **36**, 707-718.
20. B. G. De Geest, W. Van Camp, F. E. Du Prez, S. C. De Smedt, J. Demeester and W. E. Hennink, *Chemical Communications*, 2008, 190-192.
21. V. D. Bock, H. Hiemstra and J. H. Van Maarseveen, *European Journal of Organic Chemistry*, 2006, **2006**, 51-68.
22. P. Kohli and G. Blanchard, *Langmuir*, 2000, **16**, 4655-4661.
23. P. Kohli and G. Blanchard, *Langmuir*, 2000, **16**, 8518-8524.
24. T. Serizawa, K. Nanameki, K. Yamamoto and M. Akashi, *Macromolecules*, 2002, **35**, 2184-2189.
25. C. J. Ochs, G. K. Such, B. Städler and F. Caruso, *Biomacromolecules*, 2008, **9**, 3389-3396.
26. L. A. Connal, C. R. Kinnane, A. N. Zelikin and F. Caruso, *Chemistry of Materials*, 2009, **21**, 576-578.
27. J. Justynska, Z. Hordyjewicz and H. Schlaad, *Polymer*, 2005, **46**, 12057-12064.
28. A. Gress, A. Völkel and H. Schlaad, *Macromolecules*, 2007, **40**, 7928-7933.
29. K. L. Killops, L. M. Campos and C. J. Hawker, *Journal of the American Chemical Society*, 2008, **130**, 5062-5064.
30. C. D. Heidecke and T. K. Lindhorst, *Chemistry-a European Journal*, 2007, **13**, 9056-9067.
31. E. C. Hagberg, M. Malkoch, Y. Ling, C. J. Hawker and K. R. Carter, *Nano Letters*, 2007, **7**, 233-237.
32. L. M. Campos, I. Meinel, R. G. Guino, M. Schierhorn, N. Gupta, G. D. Stucky and C. J. Hawker, *Advanced Materials*, 2008, **20**, 3728-3733.
33. P. Jonkheijm, D. Weinrich, M. Köhn, H. Engelkamp, P. Christianen, J. Kuhlmann, J. C. Maan, D. Nüsse, H. Schroeder and R. Wacker, *Angewandte Chemie*, 2008, **120**, 4493-4496.
34. V. S. Khire, A. W. Harant, A. W. Watkins, K. S. Anseth and C. N. Bowman, *Macromolecules*, 2006, **39**, 5081-5086.
35. Z. Liu, Y. Jiao, Y. Wang, C. Zhou and Z. Zhang, *Advanced Drug Delivery Reviews*, 2008, **60**, 1650-1662.
36. T. Crouzier, T. Boudou and C. Picart, *Current Opinion in Colloid & Interface Science*, 2010, **15**, 417-426.
37. S. Dumitriu, *Polymeric Biomaterials, Revised and Expanded*, CRC Press, 2001.
38. C. Lovelyn and A. A. Attama, *Journal of Biomaterials and Nanobiotechnology*, 2011, **2**, 626.

39. A. Gianella, P. A. Jarzyna, V. Mani, S. Ramachandran, C. Calcagno, J. Tang, B. Kann, W. J. Dijk, V. L. Thijssen and A. W. Griffioen, *ACS Nano*, 2011, **5**, 4422-4433.
40. W. He, Y. Tan, Z. Tian, L. Chen, F. Hu and W. Wu, *Int J Nanomedicine*, 2011, **6**, 521-533.
41. P. Bulpitt and D. Aeschlimann, *Journal of biomedical materials research*, 1999, **47**, 152-169.
42. A. Bernkop-Schnürch, M. Hornof and T. Zoidl, *International journal of pharmaceutics*, 2003, **260**, 229-237.
43. K. Kurita, Y. Yoshida and T. Umemura, *Carbohydrate Polymers*, 2010, **81**, 434-440.
44. H. G. Garg, R. J. Linhardt and C. A. Hales, *Chemistry and biology of heparin and heparan sulfate*, Elsevier, 2011.
45. C. E. Hoyle, T. Y. Lee and T. Roper, *Journal of Polymer Science Part A: Polymer Chemistry*, 2004, **42**, 5301-5338.
46. D. Guzey and D. J. McClements, *Advances in Colloid and Interface Science*, 2006, **128**, 227-248.
47. T. M. Alam and J. E. Jenkins, *HR-MAS NMR spectroscopy in material science*, INTECH Open Access Publisher, 2012.
48. N. Kubota, N. Tatsumoto, T. Sano and K. Toya, *Carbohydrate Research*, 2000, **324**, 268-274.
49. R. Vecchione, U. Ciotola, A. Sagliano, P. Bianchini, A. Diaspro and P. Netti, *Nanoscale*, 2014, **6**, 9300-9307.
50. I. Fotticchia, T. Fotticchia, C. A. Mattia, P. A. Netti, R. Vecchione and C. Giancola, *Langmuir*, 2014, **30**, 14427-14433.
51. A. Jakhmola, R. Vecchione, D. Guarnieri, V. Belli, D. Calabria and P. A. Netti, *Advanced Healthcare Materials*, 2015, DOI: 10.1002/adhm.201500588, n/a-n/a.
52. S. F. Chong, R. Chandrawati, B. Städler, J. Park, J. Cho, Y. Wang, Z. Jia, V. Bulmus, T. P. Davis and A. N. Zelikin, *Small*, 2009, **5**, 2601-2610.
53. J. J. Richardson, M. Björnmalm and F. Caruso, *Science*, 2015, **348**, aaa2491.
54. S. Mizrahy and D. Peer, *Chemical Society Reviews*, 2012, **41**, 2623-2640.
55. M. Gaumet, A. Vargas, R. Gurny and F. Delie, *European journal of pharmaceutics and biopharmaceutics*, 2008, **69**, 1-9.
56. G. G. Allan and M. Peyron, *Carbohydr Research*, 1995, **277**, 257-272.
57. G. G. Allan and M. Peyron, *Carbohydrate Research*, 1995, **277**, 273-282.

58. G. L. Ellman, *Archives of Biochemistry and Biophysics*, 1958, **74**, 443-450.
59. P. W. Riddles, R. L. Blakeley and B. Zerner, *Analytical Biochemistry*, 1979, **94**, 75-81.
60. P. Eyer, F. Worek, D. Kiderlen, G. Sinko, A. Stuglin, V. Simeon-Rudolf and E. Reiner, *Analytical biochemistry*, 2003, **312**, 224-227.
61. T.-L. Hwang and A. Shaka, *Journal of Magnetic Resonance, Series A*, 1995, **112**, 275-279.
62. M. Biondi, D. Guarnieri, H. Yu, V. Belli and P. A. Netti, *Nanotechnology*, 2013, **24**, 045101.
63. M. Roldo, M. Hornof, P. Caliceti and A. Bernkop-Schnürch, *European Journal of Pharmaceutics and Biopharmaceutics*, 2004, **57**, 115-121.
64. K. Kafedjiiski, A. H. Krauland, M. H. Hoffer and A. Bernkop-Schnürch, *Biomaterials*, 2005, **26**, 819-826.
65. R. Singh, L. Kats, W. A. Blättler and J. M. Lambert, *Analytical biochemistry*, 1996, **236**, 114-125.

# Chapter 4

## Multilayered silica-biopolymer nanocapsules with hydrophobic core and hydrophilic tunable shell thickness<sup>1</sup>



---

<sup>1</sup> This work has been accepted on *Nanoscale*: R. Vecchione, G. Luciani, V. Calcagno, A. Jakhmola, B. Silvestri, D. Guarnieri, V. Belli, A. Costantini, P. A. Netti. "Multilayered silica-biopolymer nanocapsules with hydrophobic core and hydrophilic tunable shell thickness". The Supplementary Sections are not included in the submitted publication.

**Abstract.** Stable, biocompatible, multifunctional and multicompartiment nanocapsules are highly wished in the nanomedicine field. Here, we report a simple, novel, strategy to design an engineered nanocarrier system featuring an oil-core/hybrid polymer/silica-shell. Silica shells with tunable thickness are grown in situ, directly around a highly mono-disperse and stable oil-in-water emulsion system, stabilized by a double bio-functional polyelectrolyte heparin/chitosan layer. Such silica has shown a complete degradation in a physiological medium (SBF) in a time frame of three days. Moreover, the outer silica shell has been coated with polyethylenglycol (PEG), in order to confer antifouling properties to the final nanocarrier. The outer silica layer, combines its properties of being an optimal bio-interface for bio-conjugations and for the embedding of hydrophilic drugs in the porous structure- with the capability to stabilize the oil core for confining high payloads of lipophilic tracers (e.g. CdSe quantum dots, Nile Red) and drugs. In addition, polymer layers – beside conferring stability to the emulsion while building the silica shell - can be independently exploited if properly functionalized, as demonstrated by conjugating chitosan with fluorescein isothiocyanate. Such features into a single nanocarrier system make it very intriguing as a multifunctional platform for smart diagnosis and therapy.

## 4.1 Introduction

A great deal of effort has been spent in searching for new materials for the development of smart nanocarriers<sup>1-3</sup> with high stability, biocompatibility,<sup>4, 5</sup> biodegradability,<sup>5</sup> together with high payloads of contrast agents and/or drugs,<sup>4-6</sup> selective cell targeting<sup>7, 8</sup> and release of active compounds at the molecular level.<sup>2, 9-13</sup> In this race, inorganic systems based on silica have been highlighted as one of the most interesting bio-interfaces since they couple interesting properties with a reduced toxicity.<sup>13, 14</sup> Silica is one of the few inorganic materials recognized as 'safe' by the US FDA. In addition, the endogenous nature of silica,<sup>15</sup> its functional versatility<sup>16</sup> - makes it as one of the most intensively investigated among inorganic materials in the field of biotechnology, health and medicine both for imaging and delivery.<sup>16-19</sup> Indeed, silica shells can be porous if synthesized on polymer templates, thus allowing the embedding of hydrophilic drugs or tracers.<sup>20, 21</sup> Moreover, silica permeability can be tuned by tailoring synthesis conditions<sup>22</sup> and post etching treatment.<sup>23</sup> Furthermore, it is biocompatible and easy to functionalize to guarantee active targeting, as well as long circulation times.<sup>13, 24</sup>

It is widely recognized that, due to molecular complexity of many diseases (in particular, cancer, cardiovascular diseases, neurological disorders, malaria, and AIDS), smart combination of drugs can better modulate cell-signaling network and maximize therapeutic effect, reducing drug resistance as well as side effects.<sup>25</sup> Therefore, developing novel systems that could jointly encapsulate two different types (hydrophilic and/or hydrophobic) of drugs into a single vehicle is still a major challenge for smart drug delivery.<sup>26</sup> To this end, a capsule-like configuration with different compartments to encapsulate both hydrophilic and hydrophobic agents is highly desirable. Furthermore, the presence of a silica gel outside layer could act as hydrophilic biocompatible compartment for hydrophilic drugs.

In recent papers *in situ* synthesis of silica nanocapsules has been described using liposome templates.<sup>27, 28</sup> Although liposome templates can allow good monodispersion and nanometric size distribution, their fragile nature makes the coating process very delicate and time consuming. Alternatively, emulsion droplets have also been reported as templates for the synthesis of oil-core silica capsules.<sup>29-33</sup> Nano-emulsions are now emerging as intriguing carrier systems for theranostic tests as they give an opportunity to embed high payloads of lipophilic compounds in the oil phase. However, some major concerns are typically associated to this

method such as polydispersion and low stability coming from the use of emulsions as templates,<sup>34</sup> or the use of toxic materials and high temperatures during the synthesis process.<sup>29</sup> At the same time, among the available procedures to produce multifunctional nanocapsules, layer-by-layer (LbL) method is one of the most controlled.<sup>35</sup> By using LbL technique capsules with well-controlled size and shape, finely tuned shell thickness and variable shell compositions can be obtained. Furthermore, the multilayer structure of the capsules allows achieving multifunctionality, through the combination of different properties in one system. However, as a major issue, LbL assembly, as a multistep procedure, is generally time-consuming which limits its industrial applications.<sup>36</sup>

Here, we propose a synthetic strategy to obtain oil core- multilayered shell nanocapsules. *In situ* deposition of tunable silica shells was carried out directly around a mono-disperse oil in water nano-emulsion system,<sup>37-39</sup> stabilized by polymer layers via LbL, but limiting the deposition to only two layers, chitosan and heparin respectively, as shown in **Figure 4.1** and depositing them in saturation conditions to avoid any purification steps. Each step was optimized through physical-chemical characterization of reacting mixture, thus allowing to carry out an in-situ procedure. The silica shell was prepared by an *in situ* short (2-4 h) synthesis process, using a

modified Stöber sol-gel method<sup>19, 40</sup> which employs 3-Aminopropyl triethoxysilane (APTS) as a coupling agent<sup>41</sup> to ensure covalent grafting to heparin.<sup>42</sup> Obtained silica nanocapsules were coated by PEG in order to improve their half-life.<sup>43</sup>

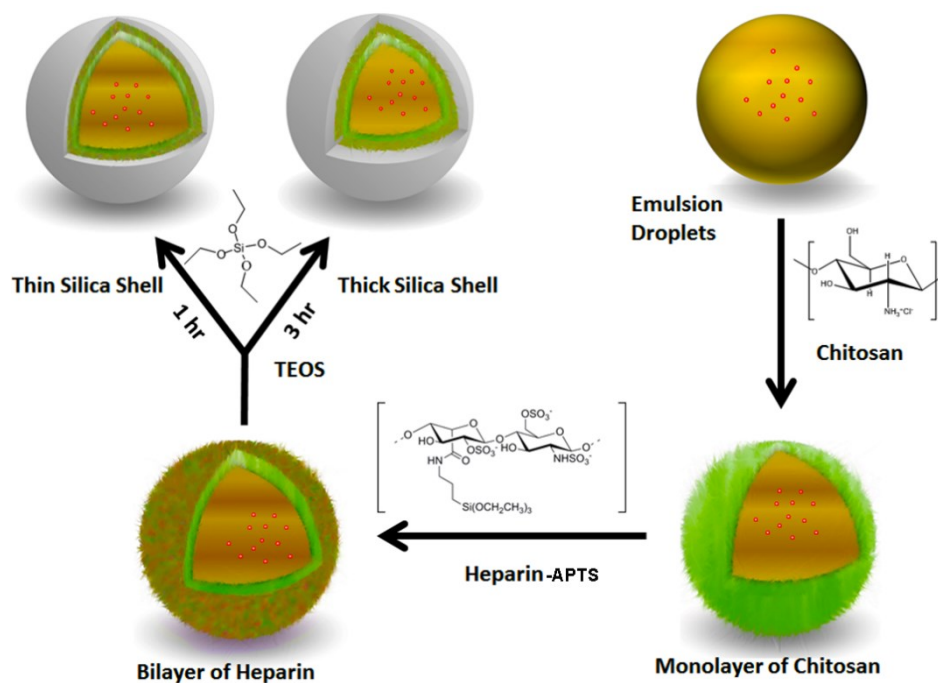


**Figure 4.1.** Schematic synthesis protocol of silica based nanocarrier system with core/shell type morphology. Red dots denote hydrophobic materials which can be safely encapsulated inside nanocapsules.

The synthetic strategy was optimized to easily tune the thickness of the shell which represents a hydrophilic compartment for polar compounds as demonstrated by embedding sulforhodamine B. On the other side, we assessed the embedding of hydrophobic fluorescent compounds such as CdSe quantum dots as nanoparticles as well as Nile Red as molecules in

the oil core while preserving size and PDI of the final nanocapsules. Silica nanostructures were characterized by a variety of analytical and spectroscopic techniques like Raman Spectroscopy, Dynamic Light Scattering (DLS), Electron microscopy (SEM, TEM), and fluorescence microscopy (Confocal and STED). Furthermore, *in vitro* degradation of silica shell was also assessed. Then, they were biologically characterized to prove their capability to be internalized and to have no cytotoxicity on three different cell lines.

## 4.2 Results and discussions

As shown in **Figure 4.1** monodisperse O/W emulsion was chosen as the morphology-deciding template to obtain silica nanocapsules. Highly monodisperse O/W nano-emulsions with droplet size of around  $170 \div 190$  nm with polydispersity index (PDI)  $< 0.1$  and  $\zeta$ -potential  $\sim -35 \pm 8$  mV as measured by DLS were used. Our main goal was to control the size of the silica nanocapsules which should be small enough to pass through the human capillaries without any hindrance, coagulation and clogging. In fact, the fate of nano-materials for *in vivo* experiments is closely related to their morphology as well as size, which determines different sequestering efficiencies.<sup>44</sup>

Starting nano-emulsions respect the requirements of size and monodispersion, but emulsions are quite delicate systems when used as templates and can readily destabilize during the formulation process itself. However, before silica shell deposition emulsions were protected and stabilized with polyelectrolyte layers. In particular, a layer of chitosan was deposited as a first layer and heparin as a second layer (**Figure 4.1**). This was a sensitive process and required optimization beforehand as any excess could result in free chitosan molecules in solution resulting in precipitation or aggregation in the following steps. When chitosan and heparin are added to O/W emulsion, the deposition takes place very quickly (within 15 min); this is mainly due to the strong electrostatic interaction between surfactant layer and chitosan, and that between heparin and chitosan. The amount of heparin was also carefully optimized to prevent any excess of polymer in solution as this could either act as free sites of silica nuclei formation and subsequent growth of solid silica nanoparticles or could also result in agglomeration during the next activation process. The hydrodynamic diameter of the emulsion before and after deposition of the bilayer, in one example, was 175 nm (PDI=0.055) and 211 nm (PDI=0.083) respectively; these results give a rough idea about the thickness of polyelectrolytes layers (below 20 nm) and monodispersion feature of the template. The  $\zeta$ -potential measurements

confirmed that the charge of the chitosan and heparin layers were  $> +30$  mV and  $< -40$  mV, respectively. Then, heparin was coupled to APTS, so that silanol ( $\equiv\text{Si-OH}$ ) groups from its hydrolysis act as preferential sites for condensation of TEOS,<sup>45, 46</sup> thus driving the selective growth of silica onto the bilayer, as schematized in **Figure 4.1**.

The activation of carboxylates for reaction with amines is commonly achieved with N-(3-dimethylaminopropyl)-N'-ethylcarbodiimide hydrochloride (EDC hydrochloride) and N-hydroxy succinimide (NHS) as catalysts in the amidation reaction.<sup>47</sup> The O-acylisourea group generated via activation by the carbodiimide is converted into the NHS-activated carboxylic acid group, which is less susceptible to hydrolysis than the O-acylisourea and improves conversion. The use of this strategy for the modification of heparin has therefore been widely employed.<sup>43, 47</sup> Reaction conditions (time, temperature) were accurately designed with the support of literature<sup>48</sup> as well as NMR and UV-Vis analysis. Temperature was kept low to avoid undesirable side reactions.

Furthermore, <sup>1</sup>H-NMR spectra of the reacting mixture **Figure 4.2a** showed the presence of ethanol as well as a marked change of the signals of hydrogen within ethoxy chains, suggesting that hydrolytic processes of APTS are quantitative within 20 min. Moreover, a closer look to NMR spectra (**Figure 4.2b**) evidenced a marked decrease of the characteristic

signals of heparin, in the range 3.5-4.5 ppm, that are no longer appreciated after 1 h. Since any denaturation/degradation process involving heparin can be excluded in the operating conditions for reaction, this disappearance must be due to some precipitation phenomena of heparin.

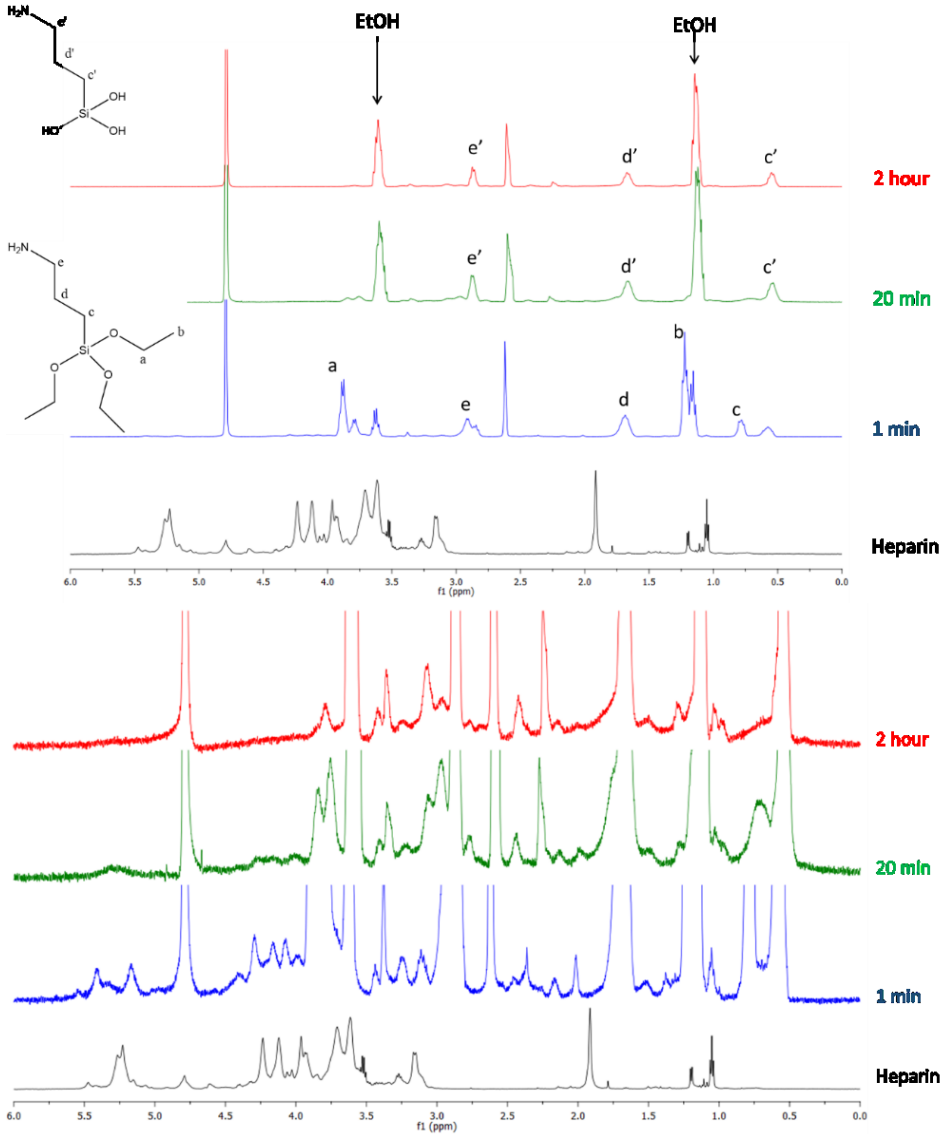


**Figure 4.2.** (a)  $^1\text{H-NMR}$  spectra of heparin (black line) and of the reacting mixture (heparin, EDC, NHS and APTS) at 3 different times. (b) Expanded  $^1\text{H-NMR}$  spectra showing the characteristic heparin signals. Mixture was kept at  $4^\circ\text{C}$ .

As a support to this hypothesis, the reacting mixture containing heparin, EDC, APTS and NHS lost transparency after 1 h, as proven by pictures of reaction batch (inset in **Figure 4.3**) and UV-Vis spectra (**Figure 4.3**), showing a broad absorption increase in the visible region, due to scattering phenomena. Therefore, the reaction time was set at 15 min in order to limit collateral side reactions involving heparin.

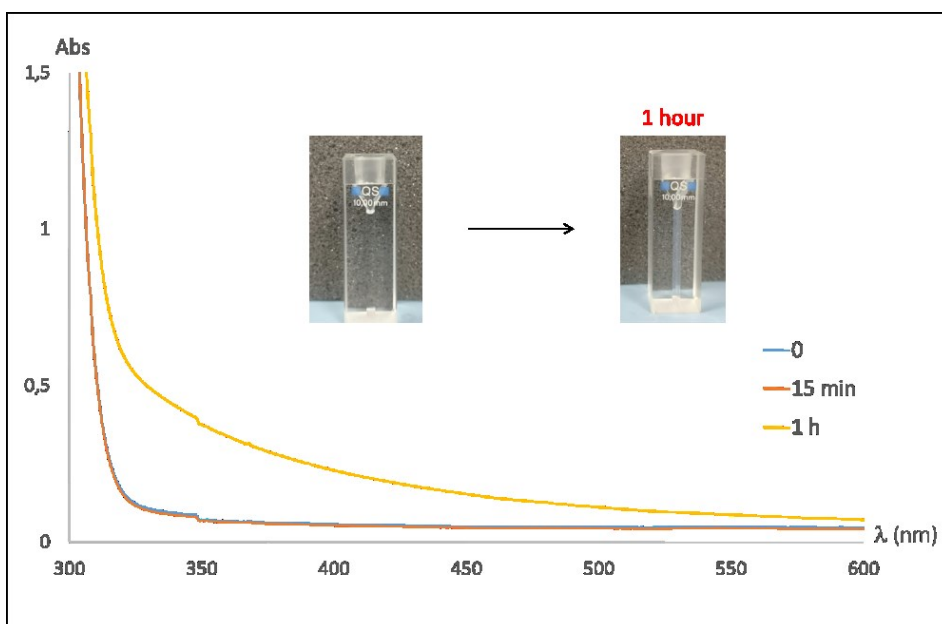


**Figure 4.3.** UV-Vis spectra of reaction mixture containing heparin, EDC, NHS and APTS at different times (blue and red line are overlapped). In the inset, the reaction batch just mixed and after 1 hour are compared, thus showing the appearance of opalescence in the solution.

In order to confirm the key role played by APTS in the nucleation of silica shell, systems where the heparin layer was not conjugated to APTS before

silica synthesis were also produced as a control experiment. Confocal micrographs of these samples show only large irregular fluorescence patches (**Figure 4.4 a**). The images also display non fluorescent nanosized objects in the bright field STED camera (**Figure 4.4 b**), which can be simple silica nanoparticles without any oil core as evidenced by the no matching between the two images (**Figure 4.4 c**).

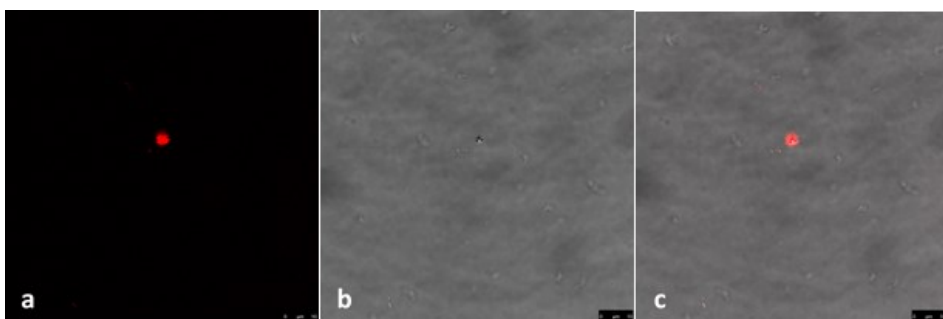


**Figure 4.4.** Confocal analysis of nanocapsules stained with Nile Red in the oil core: in fluorescence analysis (a), in bright field (b); matching of the two images.

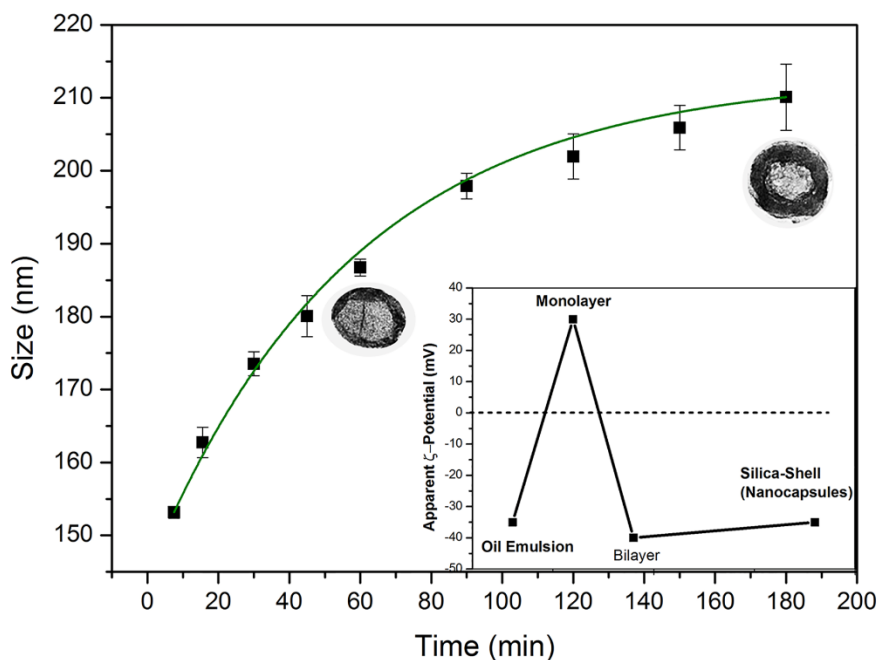


**Figure 4.5.** Size dependence as a function of seeded growth time. Inset:  $\zeta$ -potential measurements during the synthesis steps.

Therefore, these control experiments further proved that the coupling reaction between heparin and APTS is strictly required to have silica shell grown on the template. The size of silica nanocapsules obtained from the seeded growth was measured through DLS and reported as a function of seeded growth time in **Figure 4.5**.

**Table 4.1.** DLS data of silica nanocapsules collected at different reaction time intervals.

Time (min)	Size 1 (nm)	PDI	Size 2 (nm)	PDI	Size 3 (nm)	PDI
7,5	153,3	0,042	152,3	0,036	153,9	0,031
15	165,1	0,028	161,2	0,015	161,9	0,057
30	175,4	0,019	172,2	0,017	173,0	0,045
45	182,3	0,044	181,0	0,018	176,9	0,042
60	187,8	0,043	186,9	0,037	185,5	0,035
90	198,7	0,036	199,1	0,022	195,9	0,055

120	198,4	0,060	203,6	0,050	203,9	0,030
150	203,8	0,054	209,4	0,036	204,5	0,054
180	205,7	0,045	209,8	0,044	209,8	0,057

The results (**Table 4.1**) displayed a peculiar trend, a sharp increase in the hydrodynamic diameter was noticed for the first 60 min; thereafter, the process slowed down and after 3 h of reaction no further changes were noticed. The PDI was found to be  $\leq 0.06$  in all the cases. Samples collected at 1 and 3 h of seeded growth were submitted to Electron microscopy (FESEM, TEM) for morphological analysis. Samples collected at shorter times (1 h of seeded growth) had very thin silica shell and therefore not enough mechanical strength to sustain the low pressure inside the scanning electron microscope; as a matter of fact, they rapidly collapsed due to vacuum inside the microscopes **Errore. L'origine riferimento non è stata trovata. a.**

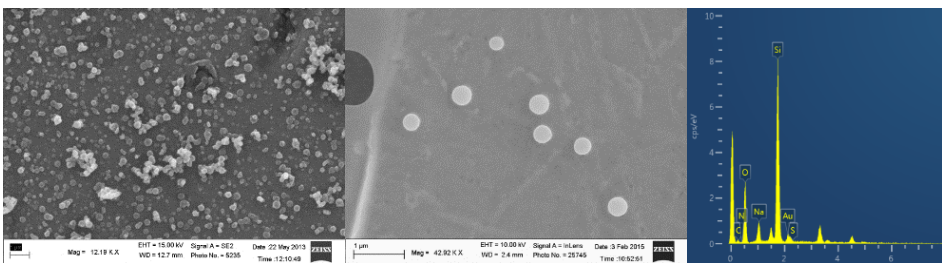


**Figure 4.6.** SEM micrographs (a) of silica nanocapsules after 1 h of seeded growth; TEM tomography of a single silica nanocapsule after 1h (scale bar 500 nm) (b) and 3h (scale bar 200 nm) (c) of seeded growth

On the contrary, as shown in SEM micrograph of silica nanocapsules after 3 h of seeded growth (**Errore. L'origine riferimento non è stata trovata. b**), a continuous shell formed around the bilayer. Narrow size distribution can also be appreciated from the SEM micrograph in agreement with DLS results (**Table 4.1**). Energy dispersive X-Ray (EDX) spectra of nanocapsules (**Errore. L'origine riferimento non è stata trovata. c**) show presence of elements like carbon, oxygen of oil and bilayer together with silicon, thus confirming the formation of a silica shell. The presence of small amounts of nitrogen and sulfur in the EDX measurements further confirms the presence inside the nanocapsule of chitosan and heparin polyelectrolyte layer. **Figure 4.7** shows TEM images on samples with different shell thickness collected after 1 h (**Figure 4.7 a**) and 3 h (**Figure 4.7 b**) of seeded growth.

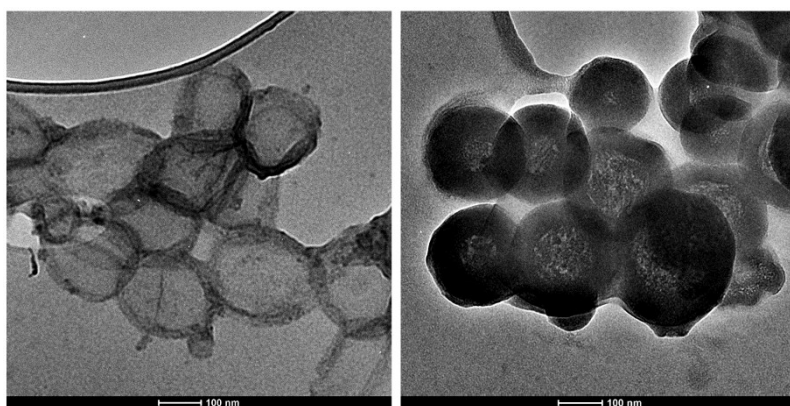


**Figure 4.7.** TEM micrographs of silica nanocapsules after 1 h (a) and 3 h (b) of seeded growth time.

As seen, samples with just 1 h of reaction (**a**) had thin and continuous shells with a thickness of around 20 nm; particles after 3 h of reaction (**b**) possessed a thicker continuous shell of about 45 nm, which sustained spherical morphology and did not collapse even under high vacuum or high voltage of the electron beam indicating enhanced mechanical strength. Evaluation of silicon amount, obtained deriving the amount of silica gel from the shell thickness after 1 h and 3 h of seeded growth and comparing the values with the starting TEOS amount, allowed to estimate a yield around 36 and 82 %, respectively.

To further confirm the spherical structure and core-shell morphology of silica nanocapsules, experiments were also performed using TEM tomography, which is a reconstruction from a series of tilted two-dimensional TEM images. For this experiment a single isolated particle was chosen in the grid and tomography was carefully carried out to obtain a detailed 3D structure of the silica nanocapsules with thick stable shells able to withstand low pressure inside TEM.

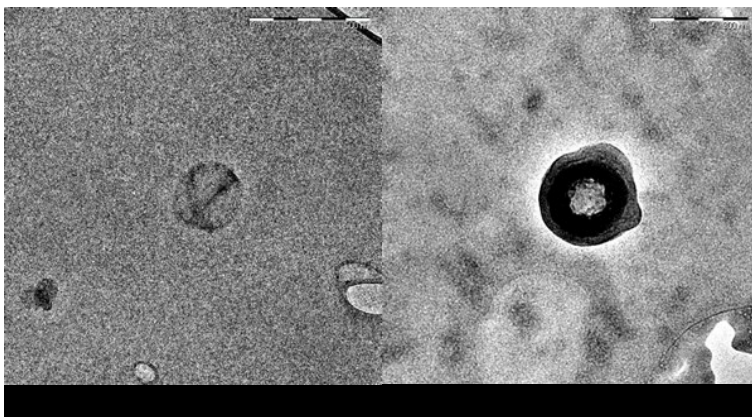


**Figure 4.8.** TEM tomography of a single silica nanocapsule after 1h (scale bar 500 nm) (a) and 3h (scale bar 200 nm) (b) of seeded growth. (Click on the black strip to play the videos).

Tomography analysis provided important results regarding the mechanical strength of shell. After 1 h seeded growth the shell was around 20 nm and its mechanical strength was not strong enough to hold the spherical size at low pressure environment inside the microscope. Particles therefore appeared as flattened discs when rotated between  $\pm 50^\circ$  (**Figure 4.8 a**). The shell of the samples after 3 h of seeded growth was thicker and was strong enough to hold its spherical shape (**Figure 4.8 b**). The relatively smooth surface texture of the silica shell, as observed with SEM and TEM, provides valuable insight of the formation mechanism of the silica shell, and it strongly suggests that the silica growth is initiated by an *in situ* direct deposition mechanism effectively coating organic scaffolds with an inorganic layer. The SEM images also ruled out any grown seed in solution

deposited on the template afterwards, as seen in the case of silica colloidosomes.<sup>49</sup>

In order to confirm nano-confinement of solid hydrophobic materials in the oil core, we performed characterization with fluorescence microscopy. For this analysis, two different sets of experiments were designed. The first was carried out with hydrophobic CdSe quantum dots (~3.5 nm, Hexyldecylamine used as capping agent) chosen in view of their high fluorescence; they were easily tracked by super resolution fluorescence microscopy to demonstrate the effective nano-confinement combined with no change in dimensional features. **Figure 4.9a** shows a STED image where the green pseudo color corresponds to the nanocapsules with entrapped CdSe quantum dots in the core. This experiment proved the nano-confinement capability of these capsules, where in place of CdSe also other types or nanoparticles, such as gold or iron oxide (which can make these capsules suitable for X-ray or MRI imaging, depending on the applications) may be used.

In the second experiment we used two different dyes; one, Nile Red, to tag the oil and FITC to tag the chitosan layer, as detailed in the experimental section. Fluorescent nanocapsules were irradiated with two different lasers to excite the dyes separately. **Figure 4.9b** displays emission of FITC dye (500 – 600 nm) excited with laser of frequency 488 nm while

L'origine riferimento non è stata trovata. **c** corresponds to emission of Nile Red (530 – 718 nm) excited with laser of frequency 543 nm always in confocal modality. **Figure 4.9d** corresponds to the overlay of two images. As can be seen there is a good match between the two colors, indicating the co-localization of the two chromophores therefore the core shell structure.

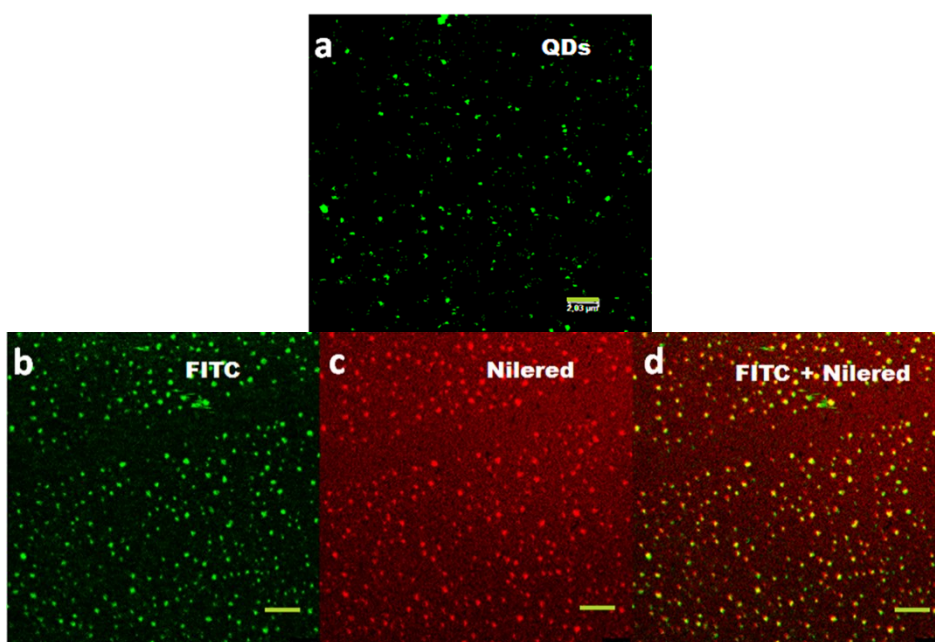


**Figure 4.9.** STED image of nanocarriers with oil confining QDs (a); nanocarriers stained with FITC labeling the first polymer layer (b); Nile Red nanoconfined in the oil phase (c) and matching of the two colors (d). Scale bar is 2  $\mu\text{m}$ .

These results suggest effective Nile Red nano-confinement and no variation of nanoparticle size. Both these experiments confirmed that these nanocapsules can act as efficient nanocarriers for various foreign materials, such as contrasting agents of nanometric size or lipophilic drugs.

The size calculated with STED micrograph in the case of nanocapsules containing CdSe quantum dots was nearly identical to the one seen in SEM or TEM.

In order to assess biodegradation of the silica nanocapsules, the 1 h and 3 h samples were exposed to SBF at constant temperature of 37 °C and stirring rate of 200 rpm. Free silicic acid was monitored by colorimetric assay as described in Materials and Methods section to follow the biodegradation; at the same way the complete dissolution was evaluated by adding to the samples a solution of NaOH 5M. In **Figure 4.10** the absorbance measured from the colorimetric assay for the two samples was plotted over time. Complete degradation, indicated by the straight lines reported in the graph, happened in both cases within three days even though 3 h sample shows a higher plateau, due to higher silica content, as expected by the thicker shell. Evaluation of silicon amount, obtained deriving the amount of silica gel from the shell thickness after 1h and 3h of seeded growth and comparing the values with the starting TEOS amount, allowed to estimate a yield around 36 % and 82, respectively.

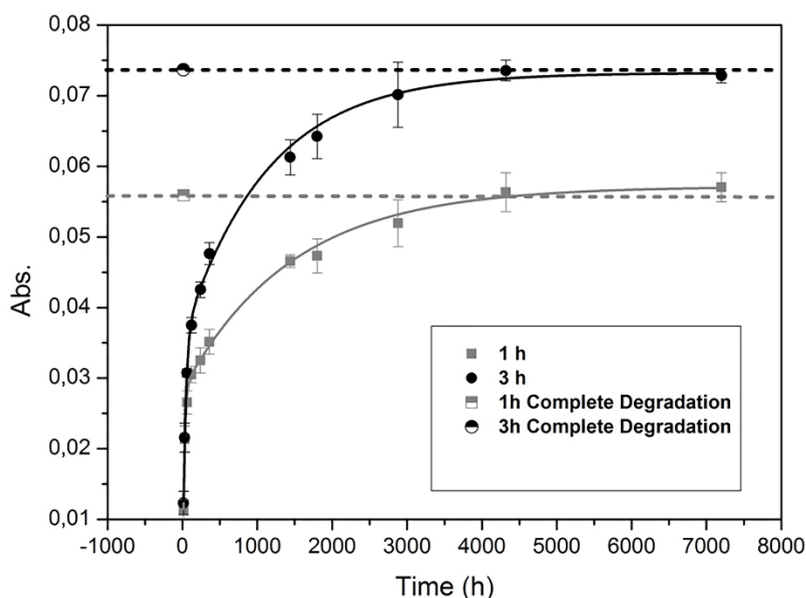


**Figure 4.10.** Degradation trend of silica shell by colorimetric assay for 1 h and 3 h samples.

Despite the different thickness a similar degradation rate was observed, thus suggesting the porous structure of the silica. Indeed, solution can enter the whole silica shell promoting in this way its complete degradation in the same time frame. Therefore, nanocarrier has enough time to accumulate in the target tissue before complete degradation of silica which in the meanwhile exerts a protection action of the inner nano-emulsion and its cargo. At the same time silica shell can also act as a biodegradable hydrophilic compartment. As an example of hydrophilic encapsulation sulforhodamine was loaded into the silica shell, as described in the Materials and Methods section. To demonstrate the effective encapsulation of the silica shell, chitosan was labelled with FITC so a co-localization test

by confocal microscopy between the two colors (FITC and rhodamine) was performed and a perfect match was found, **Figure 4.11**.

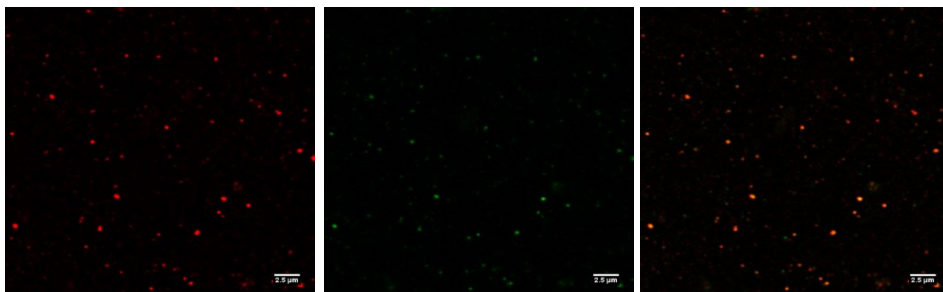


**Figure 4.11.** Confocal image of silica nanocapsules by exciting sulforhodamine B in the shell (a) and FITC on the chitosan (b) and the overlapped image of a and b (c). Scale bar 2.5  $\mu\text{m}$ .

A further proof of the porous structure of the silica shell was provided by carrying out an external sink release experiment where capsules of different thickness were put in contact under stirring with an organic solvent (hexane). The thinner the shell the higher the release of the hydrophobic oil core over time as shown in the **Figure 4.12**.

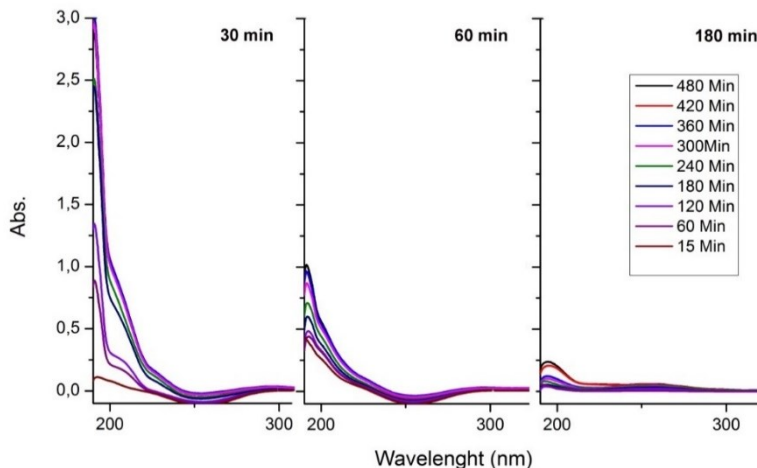


**Figure 4.12.** UV absorbance of soybean oil released from nanocapsules at different silica shell thickness (corresponding to 30, 60 and 180 min of seeded growth time) over stirring time in the mixture with hexane.

### *PEGylation of silica nanoparticles*

Although the negative surface charge, due to deprotonated silanol groups at neutral pH, provides extra colloidal stability to the nanocapsules, it also limits their efficacy due to increased interaction with blood proteins which can result in rapid capture and removal by reticuloendothelial system.<sup>13, 44</sup> The negative charge can also result in aggregation in highly ionic biological media. To potentially reduce these obstacles, we coated the surface of nanocapsules with PEG (MW 5000) (experimental section). PEG concentration within solution was set at a value (0.220 M) that, according to previous studies,<sup>43</sup> allowed long term stability of silica sols, without any aggregation phenomena due to interlocking of polymeric chains.<sup>43</sup>

The non-PEGylated samples could be easily precipitated at 6000 RPM in centrifuge, while the PEGylated ones were stable and it was not possible to precipitate them even at 14000 RPM.

In order to confirm PEGylation - as well as composition of the nanocapsules - Raman analysis was carried out on bare and PEGylated silica nanocapsules after dialysis. The spectra were normalized locally and reported, together with Raman spectra of pure PEG in **Figure 4.13** for ease of comparison.

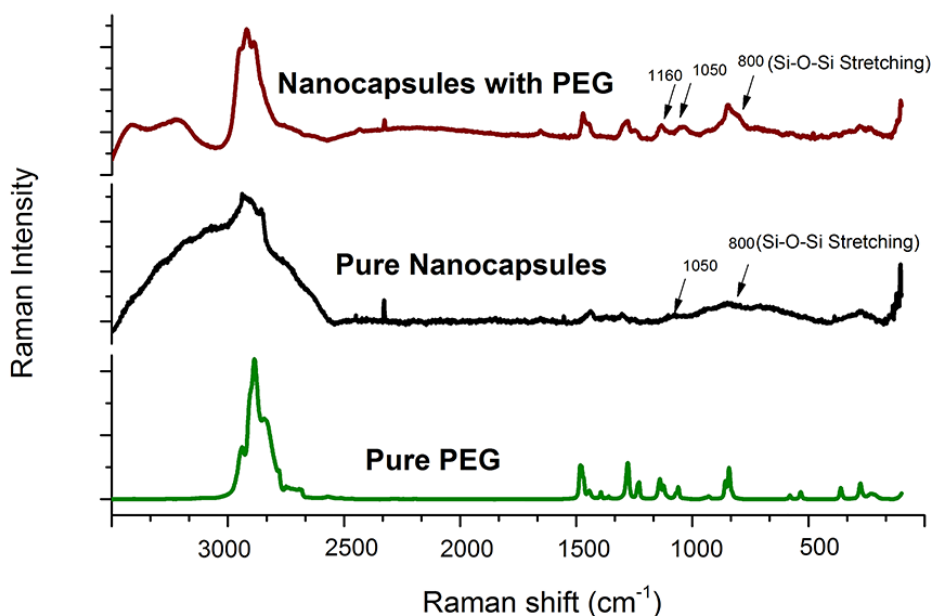


**Figure 4.13.** Raman spectra of nanocarriers with PEG, with no PEG and of pure PEG.

The presence of all the typical Raman bands observed for silica can be noticed.<sup>50</sup> In fact, stretching peaks centered at 800  $\text{cm}^{-1}$ , 1060  $\text{cm}^{-1}$  and

1200  $\text{cm}^{-1}$  are attributed to amorphous silica. PEG was also modified with FA (adsorption and emission spectra are reported in **Figure 4.15**) and deposited according to the same procedure on the silica shell. Its permanence on the shell after dialysis was then confirmed by spectrofluorimetry (**Figure 4.16**) and confocal analysis (**Figure 4.14**).

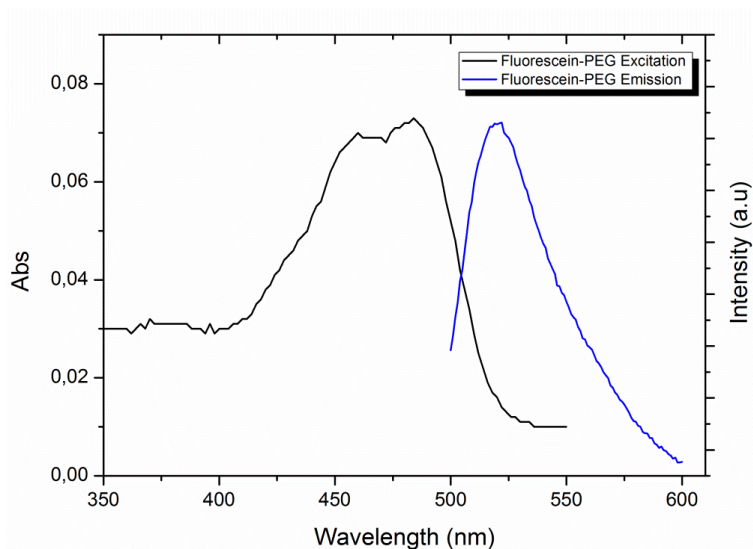


**Figure 4.15.** Excitation (black curve) and emission (blue curve) spectrum for FA modified PEG5000-COOH.

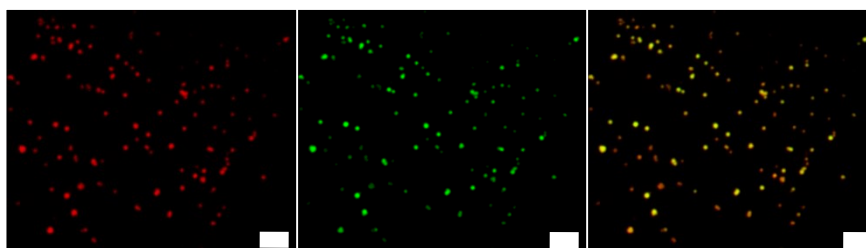


**Figure 4.14.** Confocal image of silica nanocapsules by exciting Nile Red in the oil core (a) and PEG-FA on the shell (b) and the overlapped image of a and b (c). Scale bar 2.5  $\mu\text{m}$ .

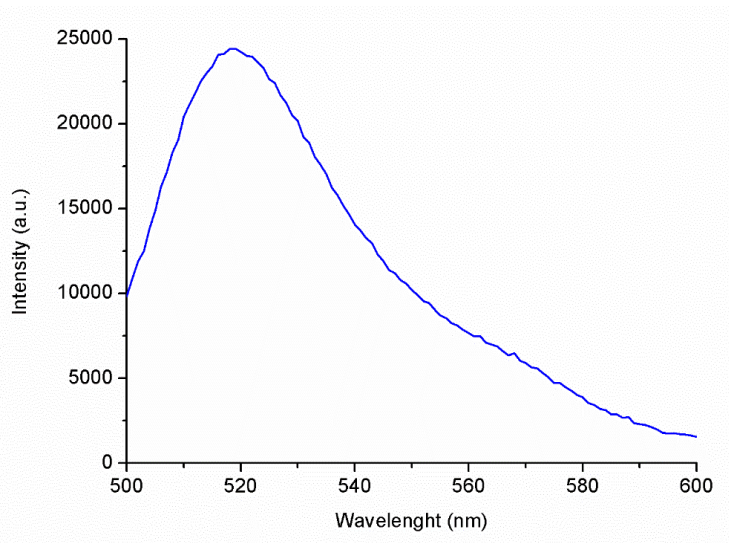


**Figure 4.16.** Emission spectra of silica nanocapsules coated with FA-labeled PEG5000-COOH after dialysis.

### *Cytotoxicity and cellular uptake*

We performed preliminary biological tests on three different cell lines, namely bEnd.3, HeLa and U87-MG cells, as models of endothelium and tumor tissues, in order to evaluate the biocompatibility of the nanocapsules. In particular, uptake and cytotoxicity of the PEGylated and non-PEGylated nanocapsules were investigated. As shown in **Figure 4.17**, **Figure 4.18** and **Figure 4.19**, both PEG and no-PEG nanocapsules entered cells after 2, 4 and 24 h exposure.

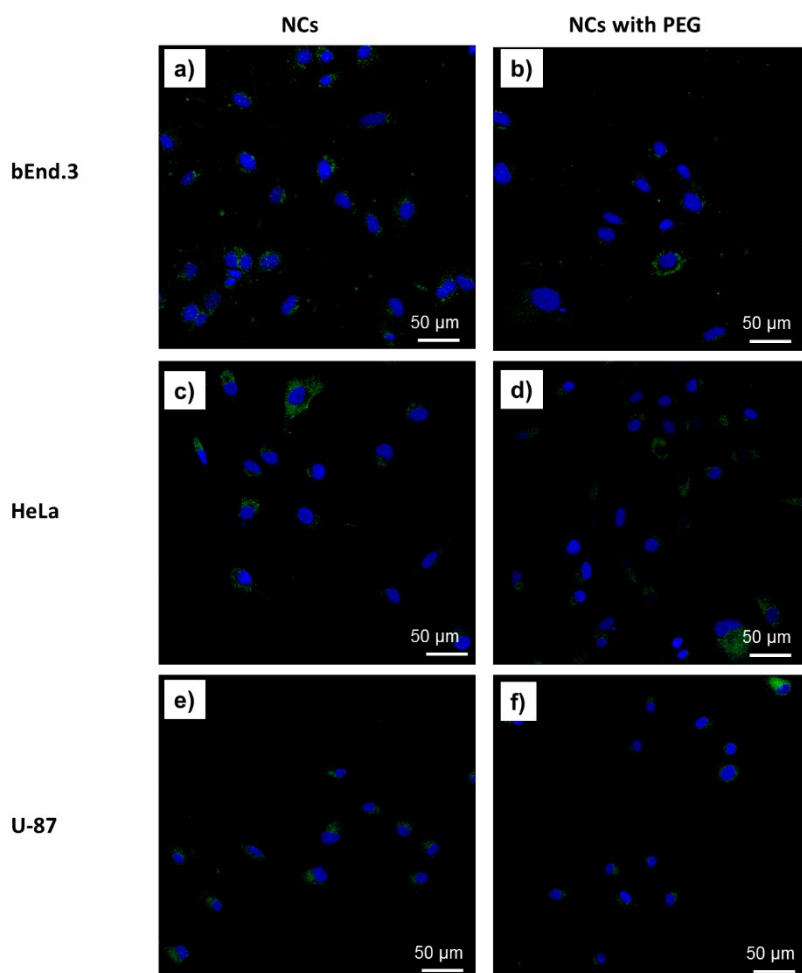


**Figure 4.17.** Confocal images of bEnd.3 (a and b), HeLa (c and d) and U87 (e and f) cells incubated with FITC-doped nanocapsules and PEGylated nanocapsules at the final concentration of 14.2 μg/ml for 2 hours at 37 °C.

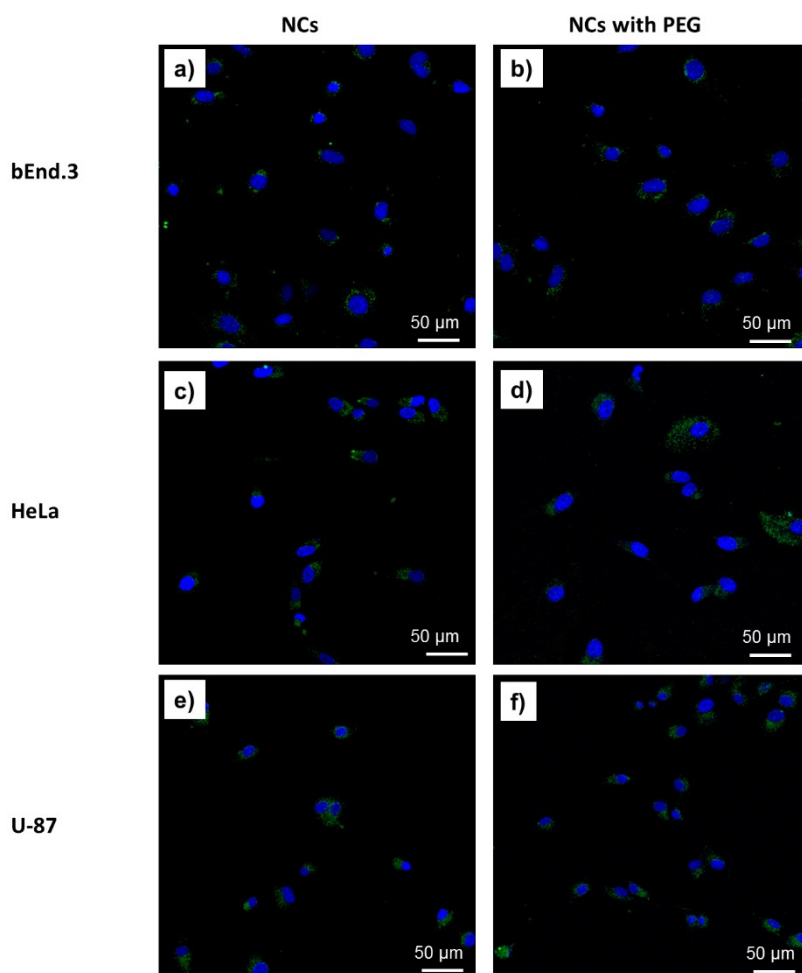


**Figure 4.18.** Confocal images of bEnd.3 (a and b), HeLa (c and d) and U87 (e and f) cells incubated with FITC-doped nanocapsules and PEGylated nanocapsules at the final concentration of 14.2 μg/ml for 4 hours at 37 °C.

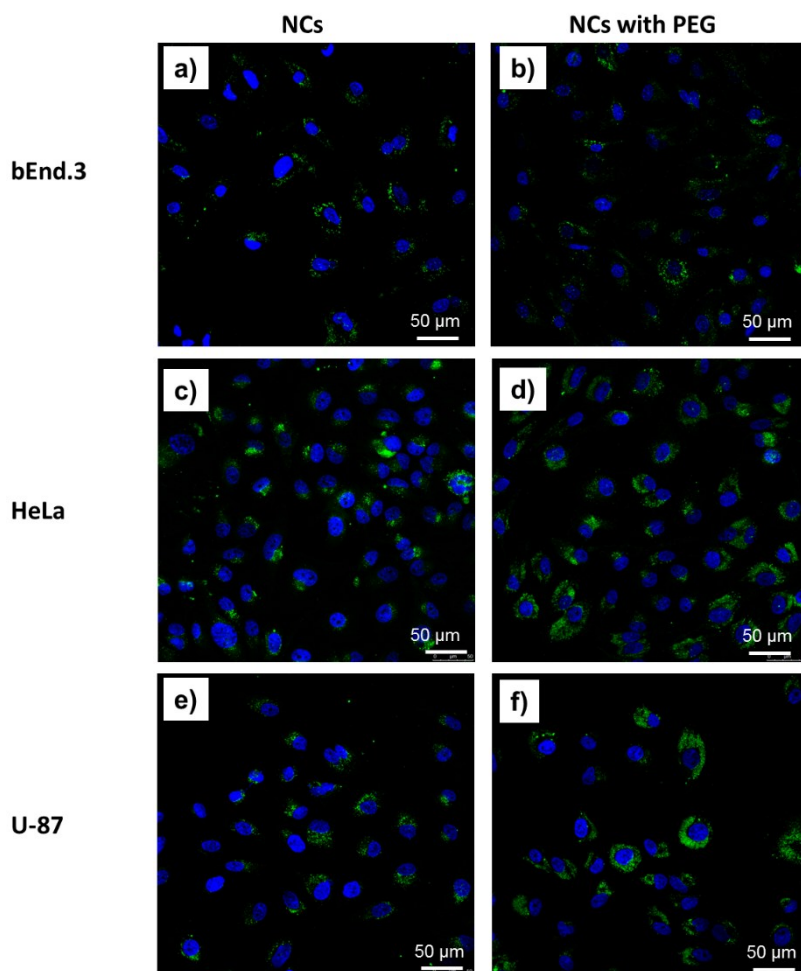


**Figure 4.19.** Confocal images of bEnd.3 (a and b), HeLa (c and d) and U87 (e and f) cells incubated with FITC-doped nanocapsules and PEGylated nanocapsules at the final concentration of 14.2  $\mu\text{g/ml}$  for 24 hours at 37  $^{\circ}\text{C}$ .

In all cases, the intracellular distribution of the nanocapsules appeared as small aggregates mainly localized in the perinuclear region. As previously demonstrated, silica nanoparticles enter cells mainly through endocytosis.<sup>51</sup> In our case, the spot-like intracellular distribution might suggest an endocytic mechanism of internalization and the confinement of

the nanocapsules within vesicular structures. Further investigations are necessary to better elucidate this issue. In addition, Alamar Blue assay was performed in order to verify the effect of NCs on cell metabolism and viability. Results, shown in **Figure 4.20**, indicate no cytotoxic effect for PEGylated and non-PEGylated nanocapsules after 24 and 48 h incubation for all cell lines at any used concentration. Only a very slight reduction of cell viability was observed for U87-MG cells at the higher concentration (14.2  $\mu\text{g/ml}$ ) of PEGylated nanocapsules.

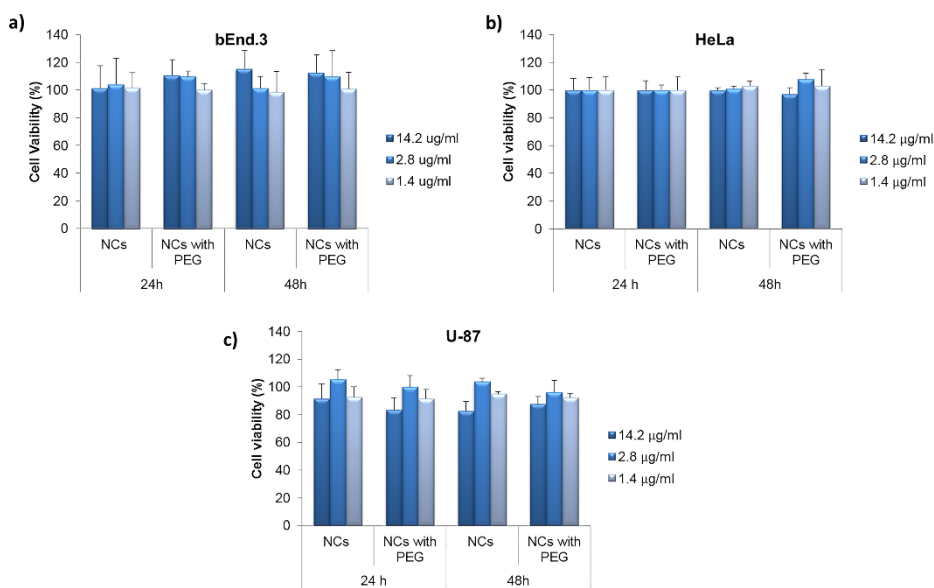


**Figure 4.20.** Cell viability of bEnd.3 (a), HeLa (b) and U87 (c) cells at 24 hours after the exposure to increasing doses of both PEGylated and non-PEGylated nanocapsules evaluated by the Alamar Blue assay. Viability of nanocapsule-treated cells is normalized to non-treated control cells. Error bars indicate the standard deviation.

Taken altogether, these data demonstrate the capability of these nanocapsules to enter the cells and not to affect cell viability. These findings were in agreement with others reported in literature indicating no significant effects on cell viability of silica nanoparticles with a diameter smaller than 200 nm on primary human endothelial cells.<sup>52</sup> Although preliminary, these promising results suggest that these nanocapsules could be used as safe nanosystems for biomedical applications.

### 4.3 Conclusions

One intriguing route for *in vivo* imaging, as well as drug delivery, is the use of core shell type structures that effectively allow confinement or protection of both tracers and/or drugs in the inner core. In the present work, oil core silica shell nanocapsules with narrow size distribution have been successfully prepared at room temperature. The synthetic strategy is based on a multistep process involving encapsulation of oil nanodroplets within a bilayer of chitosan and heparin followed by *in situ* synthesis of silica by using TEOS as a precursor. APTS has been chemically coupled to heparin, allowing condensation reaction of TEOS and therefore formation of silica just around oil droplets. Silica nanocapsules keep a narrow size distribution and average size of about 200 nm. We demonstrated the capability to effectively pre-load lipophilic molecules

(Nile Red) as a model drug, as well as inorganic nanoparticles (*e.g.*, CdSe), as a contrasting agent model, with no variation in the expected size. At the same time, hydrophilic molecules could also be loaded in the silica shell. These nanocapsules can be completely degraded in SBF at 37 °C under stirring in a time frame (3 days) compatible with drug delivery applications. Moreover, conjugation of chitosan to optical active molecules (FITC) proves the multifunctional behavior of nanocapsules. In addition, they were effectively conjugated with PEG for possible *in vivo* applications; cytotoxicity tests validated possible use of these systems both in the PEGylated and non-PEGylated form. Therefore, this is an innovative, low cost, effective and green way to produce new nanocarriers to be used in nanomedicine.

## 4.4 Materials and Methods

### *Materials*

Soy-bean oil (density at 20 °C of 0.922 g/ml), and Lipoid E80 Lecithin (egg lecithin powder 80-85% enriched with Phosphatidyl choline (PC) and 7-9.5% content in phosphatidyl ethanolamine (PE) as per the manufacturer's specifications), were both purchased from Lipoid and used without further purification. Chitosan (CT, LMW 90-150 kDa, DDA 84% determined *via* <sup>1</sup>H-NMR, pKa~6.7)<sup>53</sup> was purchased by Sigma Aldrich.

Heparin (Heparin sodium salt from porcine intestinal mucosa, 17-19 KDa),<sup>54</sup> poly(ethylene glycol) methyl ether (PEG, average  $M_n=5,000$ ), methoxypolyethylene glycol 5,000 acetic acid (PEG<sub>5000</sub>-COOH, average  $M_n=5,000$ ), N-(3-dimethylaminopropyl)-N'-ethyl-carbodiimide hydrochloride, (EDC, protein seq. grade), N-hydroxy succinimide (NHS, 98 %), 3-(aminopropyl)triethoxysilane (APTS), tetra ethyl orthosilicate metal basis (TEOS, 99.999 %), ammonium hydroxide (NH<sub>3</sub>, Lsg acs reagent 28-30 %), acetic acid ( $\geq 99.7$  %), 2-propanol, Lumidot™ CdSe 560 core-type quantum dots, (5 mg/ml in toluene), Nile Red (MW=318.37), sulforhodamine B sodium salt (MW=580.65), fluorescein isothiocyanate (FITC, MW=389.38) and Fluoresceinamine (FA, MW=347.32) were also purchased from Sigma Aldrich and used as such without any further purification. Dialysis tubing (RC, 25 kDa and 3.5 kDa MWCO) were purchased from Spectrum Laboratories Inc and used after being washed with water. For the colorimetric test to analyze silica degradation, ammonium molybdate tetrahydrate, oxalic acid, 4-(methylamino)phenol hemisulfate salt, sodium sulfite hydrochloric acid 37%, sulfuric acid were purchased from Sigma Aldrich.

### *Nanocarrier Synthesis*

Nano-emulsions were prepared through a three-step process; this was necessary to maintain stability and size distribution of oil droplets as narrow as possible. The initial step involved the preparation of homogenous oil phase by simply adding a certain amount of surfactant (Lipoid E 80, Lecithin (1.2g)) to a predetermined volume of soy-bean oil (20 ml) at 60 °C followed by sonication for a few min to homogenize and mix. In the second step, a pre-emulsion was prepared by a step-by-step addition of the as-prepared oil phase to a weighted amount of aqueous phase (Milli-Q water) so as to obtain a final concentration of 10 wt% in the oil phase. The mixture was thoroughly mixed through the immersion sonicator for a few minutes in a beaker. A low temperature was maintained throughout the process by keeping this assembly inside a larger beaker containing ice in form of a continuous ice jacket. Finally, in the third step, the pre-emulsions were passed at 1000 bar through a high-pressure homogenizer (Microfluidics M110PS) with a combination of individual cycles and continuous steps until a minimum size and PDI was reached.

After emulsion preparation, chitosan monolayer was deposited at a final concentration of 0.01% wt (at pH=4) whereas oil concentration was 1% wt. Bilayer emulsion was prepared by mixing 4 ml of monolayer to 2.5 ml of heparin solution (0.044% wt) in water. After the formation of the

bilayer, heparin carboxyl ( $-\text{COOH}$ ) groups, were coupled to amino groups of APTS molecules, through EDS/NHS chemistry.<sup>42</sup> In detail, first 50  $\mu\text{l}$  of EDC (6.42 mM) and NHS (74.8 mM) solution in water and then 50  $\mu\text{l}$  of APTS solution (15.0 mM) in 2-propanol were added to 1 ml of bilayer emulsion under continuous stirring. Reaction was allowed to proceed under stirring for 15 min at 4 °C in an ice bath.

Then, reaction mixture was removed from ice bath and silica shell synthesis was initiated at room temperature using a modified Stober method. In summary, we deposited silica *via* a two-step process. In the first step, the pH of dispersion was adjusted to 10.0 by adding 2.31 ml of  $\text{NH}_3$  solution in 2-propanol (0.119 M in  $\text{NH}_3$ ) followed by slow drop-wise addition of 2.31 ml of TEOS solution (in 2-propanol (0.0268 M)). Synthesis parameters were defined so as to have a 10 nm thick shell, in the former step. Moreover, alkoxide TEOS/APTS molar ratio was kept at 82.5 so as to avoid any aggregation phenomena.<sup>55</sup> Stirring was continued for another 1 h at room temperature after which seeded growth was carried out (second step). To this purpose, the dispersion was mixed with equal volumes of Milli-Q water and subjected to further stirring for variable timings, ranging from 5 min to 3 h. The second step was necessary for tuning shell thickness and making it suitable for specific applications. To carry out PEGylation of the nanocapsules, equal volumes of an aqueous PEG solution 0.220 M,

were added to the nanocapsule dispersion during the second step (1:2 dilution), thus obtaining a PEG grafting by means of a transesterification reaction.<sup>43</sup> Aliquots collected at different times were then dialyzed overnight against Milli-Q water to remove any unreacted reactants and solvents or physically adsorbed species (PEG). To exclude any presence of i-propanol residue we heated the aqueous colloidal sample in rotavapor at 50 °C for half an hour and then corrected the reduced volume by addition of fresh Milli-Q water. Thanks to the narrow size distribution of the silica nanocapsules prepared with this method, there was no need to filter it to remove aggregates. These particles had a shelf life of at least 2 months. As a control experiment, synthesis of silica was also carried according to the procedure detailed before, but leaving out the conjugation step of heparin to APTS.

Oil was also stained both with Nile Red, a lipophilic molecule (0.06 mg/ml of oil) used as a model drug, and with hydrophobic CdSe quantum dots (0.2 mg/ml of oil) used as a contrasting agent. In the former case emulsion was also coated with chitosan conjugated with fluorescein isothiocyanate (FITC), in order to show multifunctional behavior such as loading of core and shell for a possible theranostic approach. Silica shell preparation was completed by using the usual procedure as already described.

To obtain FITC modified chitosan, 500 mg of purified and dried chitosan were dissolved in 50 ml of aqueous acetic acid solution (0.10 M). After complete dissolution, 50 ml of methanol were added. Then 25 mL of a 1 mg/ml solution of FITC (fluorescein isothiocyanate) in anhydrous methanol was prepared. This solution was slowly added to chitosan solution and the reaction was allowed to proceed in the dark under magnetic stirring for 18 h at room temperature. Finally, chitosan was precipitated with a solution of NaOH and the precipitate was collected by centrifugation (9000 rpm; 4 °C; 15 min). The obtained FITC-chitosan was dispersed in Milli-Q water, washed and centrifuged 6 times until pH had a neutral value and no traces of FITC were visible in the waste washing solutions.

In one case, 3 h silica nanocapsules containing FITC modified chitosan were exposed to sulforhodamine B at a final concentration of 0.001 % w/v of such molecule (10 mg/l, 17.2  $\mu\text{mol/L}$ ) and 0,055 % w/v of nanocapsules. Then the sample was dialyzed with distilled water.

#### ***External sink release method***

Silica nanocapsules (2 ml) were collected during silica deposition process (30, 60, 180 min of seeded growth time) to get different shell diameters and placed in vials. In each of the vials 2 ml hexane was added and the

samples were stirred vigorously at 1500 rpm. After predetermined times hexane layer was collected and analyzed by UV-vis spectroscopy for the absorbance of soybean oil between 200-300 nm and then replaced back. With the growth of silica shell the release of soybean oil diminished and in case of thick silica shell (after 180 min of seeded growth time) only a slight increase in absorbance was observed with time even after 8 h of rigorous stirring.

### ***Spectrofluorimetry Analysis and Confocal imaging of PEGylated nanocapsules***

To confirm that shell PEGylation occur an experiment was performed using PEG modified with FA. Briefly, PEG<sub>5000</sub>-COOH (Methoxypolyethylene glycol 5000 acetic acid, 90.0 mg) and NHS (12.0 mg) were dissolved in 2.50 ml of MilliQ water. After 10 minutes EDC (10.0 mg) was added. In the meantime, 7.0 mg of 6-Aminofluorescein were dissolved in 100  $\mu$ l of DMSO. After 30 minutes the fluorescein solution was added dropwise to the PEG<sub>5000</sub>-COOH solution. pH was corrected to 6.7 adding NaOH 1 M. After 24 h the solution was dialyzed (dialysis tubing RCE, 3.5 kDa MWCO) against Milli Q water to remove solvent and unreacted reactants and freeze dried. An absorbance spectrum was recorded in order to select the correct excitation wavelength (480 nm)

and, then, the emission spectrum was recorded between 500 and 600 nm using an excitation wavelength of 480 nm and a flashes number of 1000 (**Figure 4.15**).

The so obtained PEG-FA was used instead of PEG to mark the sample, using the same procedure proposed. The marked sample was dialyzed (Dialysis tubing, RC, 25 kDa MWCO) against water to remove the excess of PEG-FA and dialysis was monitored recording the fluorescent emission of fluorescein in the washing water (EnSpire Multimode Plate Reader 2300-0000, Perkin Elmer). 10  $\mu$ l of NaOH solution 1 M were added to 300  $\mu$ l of water and loaded in a multi-well (3 replicates for each sample were prepared) and irradiated with a light source at 480 nm. Dialysis is kept until no significant emission is recorded in the water, also after sonication of the sample. Moreover, to show that PEG-FA is still present on the sample and, in particular on the shell, an emission spectrum of sample was recorded (10  $\mu$ l of sample were added to 10  $\mu$ l of NaOH solution 1 M and dilute to 300  $\mu$ l, **Figure 4.16**) together with a confocal images of silica nanocapsules with Nile Red in the core and PEG-FA on the shell surface (**Figure 4.14**).

### ***DLS and $\zeta$ -Potential characterization***

Size distribution and  $\zeta$ -potential were measured by Zetasizer (Nanoseries, Malvern) using laser dynamic scattering ( $\lambda = 632.8$  nm) and particle electrophoresis techniques, respectively. All the samples were diluted up to a droplet concentration of approximately 0.025% wt, by using acetic acid Milli-Q water solution (pH 4, 0.2M) in the case of chitosan coated emulsions and bare Milli-Q water in the case of primary emulsions, bilayer and oil core silica shell nanocapsules. A detecting angle of  $173^\circ$ , a default refractive index ratio of 1.52 and 5 runs for each measurement (1 run lasting 100 s) were used in the calculations of the particle size distribution. In the case of  $\zeta$ -potential, analyses were carried out by setting 50 runs for each measurement.

### ***Electron Microscopy***

For TEM analysis about 10  $\mu\text{l}$  of the sample was spread on a copper grid (200 mesh with carbon membrane). After removing carefully the excess of solution grids were left to dry overnight. Contrast for transmission electron microscopy (TEM) was also achieved by exposing the samples to vapors of  $\text{OsO}_4$  water solution (1% wt) as oil core dopant for not less than 4 h. TEM images were obtained using a TECNAI 20 G2: FEI COMPANY (CRYO-TEM-TOMOGRAPHY, Eindhoven) with a camera Eagle 2HS.

The images were acquired at 200 KV; camera exposure time: 1 s; size 2048 x 2048. For SEM and EDX measurements a small drop of solution containing silica nanocapsules was spread onto the surface of an aluminum stub covered by a carbon tape or a glass plate. The sample was then sputter-coated with a thin Pt/Pd or gold layer (10 nm) in a Cressington sputter-coater 208HR. The aluminum stub containing the Pt/Pd or gold -coated sample was then placed in a FEG-SEM scanning electron microscope and imaged using 20 kV accelerating voltage.

### ***Confocal and STED Analysis***

A FC3510 dish was first washed with ethanol and dried. Then a water solution of poly-L-lysine (0.1 % wt) was added in order to have the dish surface positively charged. After 10 min the dish was washed twice with water and 150  $\mu$ l of sample (diluted 1:20 with water) were poured onto it. The solution was washed out with water after 30 min and the dish was left full of water during sample observation. Laser sources of 488 and 543 nm were used to excite samples with CdSe QDs and chitosan-FITC from one side and Nile Red and sulforhodamine B from the other side. Samples were imaged with Leica TCS STED-CW microscope (Leica-Microsystems, Mannheim, Germany). Thanks to the use of QDs and FITC, it was possible to work in STED modality with super-resolution down to 100 nm in order

to resolve the real size of the samples. For each sample, the images were acquired with a field of view of 25.6 x 25.6  $\mu\text{m}$  for a pixel size of 25 x 25 nm with line average between 8 and 16. The STED-CW beam power was 430 mW, measured at objective back focal plane. The analysis of the images was carried out by LAS AF software.

### ***Colorimetric test for silica degradation analysis***

The degradation experiments in vitro were carried out by soaking a dialysis membrane containing a fixed volume (3 ml) of each sample into 30 ml of SBF at constant temperature of 37 °C and stirring rate of 200 rpm. Exactly 300  $\mu\text{l}$  of SBF were collected each time and replaced by an equal volume of fresh SBF. Sample solutions were monitored for free silicic acid,  $\text{Si}(\text{OH})_4$ , using the blue silicomolybdic acid (SMA) spectrophotometric method.<sup>56</sup> Briefly, 150  $\mu\text{l}$  of solution A (2% w/v ammonium molybdate tetrahydrate, 6% v/v of concentrated hydrochloric acid) are added to 300  $\mu\text{l}$  of the unknown concentration of silicic acid solution. After 10 min, 750  $\mu\text{l}$  of solution B (2% w/v oxalic acid, 0.667% w/v 4-methylaminophenol sulphate, 0.4% anhydrous sodium sulfite, 10% v/v concentrated sulphuric acid) are added to the assay solution. The blue colour is left to develop over 2 h at room temperature before measuring the absorbance at  $\lambda = 810$  nm. For the total amount of silicon, 10  $\mu\text{l}$  of NaOH 5M were added to the

sample 10 min before adding solution A to allow the complete dissolution of silica shell.

### ***Raman Spectroscopy***

Raman analysis was performed on Thermo Scientific DXR Raman microscope with point and shoot Raman microscopy equipped with 532 nm, 633 nm, and 780 nm laser. The 632.8 nm radiation from a 17 mW air-cooled He/Ne laser was used as excitation source. The acquisition time was 90 s. Experiments were performed by placing drops of sample on aluminum foil and drying them at room temperature. The spectra were recorded in range of 0÷3500  $\text{cm}^{-1}$ , within 3-5 min.

### ***Cell culture***

Immortalized mouse cerebral endothelial bEnd.3 cells (American Type Culture Collection, Manassas, VA) were grown in DMEM with 4.5 g/l glucose, 10 % Fetal Bovine Serum (FBS), 3.7 g/l sodium bicarbonate, and 4 mM glutamine, 1% non-essential amino acids, 100 U/ml penicillin and 0.1 mg/ml streptomycin. Human cervix adenocarcinoma HeLa cells (American Type Culture Collection, Manassas, VA) were cultured in DMEM with 4.5 g/l glucose, 10 % FBS, and 4 mM glutamine, 100 U/ml penicillin and 0.1 mg/ml streptomycin. Human glioma U87-MG cell line (American Type Culture Collection, Manassas, VA) was grown in Eagle's

Minimum Essential Medium (EMEM), 10 % FBS, and 4 mM glutamine, 100 U/ml penicillin and 0.1 mg/ml streptomycin. All cell lines were cultured in 100 mm diameter cell culture dish, in a humidified atmosphere at 37 °C and 5% CO<sub>2</sub>.

### ***Confocal microscopy for nanoparticle uptake***

Cells were incubated with FITC-doped nanocapsules with and without PEG at the final concentration of 14.2 µg/ml for 2, 4 and 24 h at 37 °C in 5% CO<sub>2</sub>. After each time, samples were washed two times with PBS to remove non internalized NPs and fixed with 4% paraformaldehyde for 20 min. Then, cell nuclei were stained with DAPI (Sigma-Aldrich). Samples were observed by confocal and multiphoton microscope system (Leica TCS SP5 MP) equipped with oil-immersion 40× and 63× objective. Images were acquired with a resolution of 1024×1024 pixels.

### ***Cytotoxicity tests***

Cells were seeded in 96-well microplates (Costar) at a density of  $8 \times 10^3$  cells/well at a final volume of 100 µl and incubated for 24 and 48 h in a humidified atmosphere at 37 °C and 5% CO<sub>2</sub> to obtain a subconfluent monolayer. Cells were treated with nanocapsules at concentrations of 14.2, 2.8 and 1.4 µg/ml in a final volume of 150 µl for each well. The metabolic activity of all cell cultures was determined after 24 h of exposure by using

standard Alamar Blue assay (Invitrogen). Briefly, after incubation time, cells were washed with PBS and 150  $\mu$ l of Dulbecco's modified Eagle's medium without phenol red (Gibco), containing 10% Alamar Blue reagent, were added to each well and samples were incubated for 4 h at 37 °C. The solution was subsequently collected from the wells and analyzed with a spectrophotometer (Perkin Elmer) at wavelengths of 570 and 600 nm. Statistical analyses of significance were performed by using ANOVA test. *p* values equal or less than 0.05 were considered statistically significant. Experiments were repeated three times in triplicates.

## 4.5 Supplementary Section

### *Realization of silica nanocapsules with reduced size*

As mentioned in the **Chapter 1**, one of the main advantages of the LbL technique is the high versatility and, in particular, the possibility to obtain a final nanosystem with the desired size by starting from a template with appropriate dimensions.<sup>36</sup> In this case, by reducing the size of the starting O/W nanoemulsion it is hypothetically possible to realize a nanocapsules with a final size further reduced. Indeed, the O/W nanoemulsion used in the typical procedure had a starting size of 175 nm (PDI < 0.1), but we realized O/W nanoemulsion with smaller droplet dimensions, up to 80 nm.<sup>38</sup> However, the transition of the whole synthetic procedure to a system with reduced size is not so obvious. The main difficulty is related to the realization of the polymeric bilayer (chitosan and heparin) with the same concentration, in order to maintain the relative quantities of the reactants unchanged. In addition, it is important that the system remain stable during the synthesis steps, in particular when *i*-propanol is added and pH is raised to 10.

Starting from these considerations, a bilayer was built up using the LbL technique and a silica shell was realized starting from it. Dimensional and Z-Potential data are reported in **Table 4.2**. DLS analysis confirms that,

even starting from a bilayer system with sizes and PDIs not exactly suitable, it is possible to obtain a final silica-nanocapsules with good monodispersity. Moreover, as also suggested from the reduction of the size in the beginning of the seeded growth, it is possible that during this synthesis step a disaggregation of droplets.

**Table 4.2.** Size, PDI and Z-Potential data related to the realization of the bilayer and Silica-NCs at different reaction time.

	Size	PDI	Z-Potential
O/W nanoemulsion	114.8	0.107	- 24.8
Monolayer	118.3	0.169	+ 16.0
Bilayer	145.4	0.190	- 16.9
Silica NCs (15 min)	114.7	0.044	- 35.8
Silica NCs (60 min)	126.8	0.057	- 32.5
Silica NCs (120 min)	129.8	0.088	- 32.3
Silica NCs (180 min)	129.4	0.068	- 32.5
Silica NCs (over night)	228.5	0.099	- 31.6

Focusing on the seeded growth, by comparing the seeded growth time for the systems with different initial O/W nanoemulsion (**Figure 4.21**), it is appreciable that the reduction of the size effects on the kinetic: seeded growth results slowed if the starting size is smaller, even if NCs keep on growing till to double the size if reaction go on overnight (**Table 4.2**).

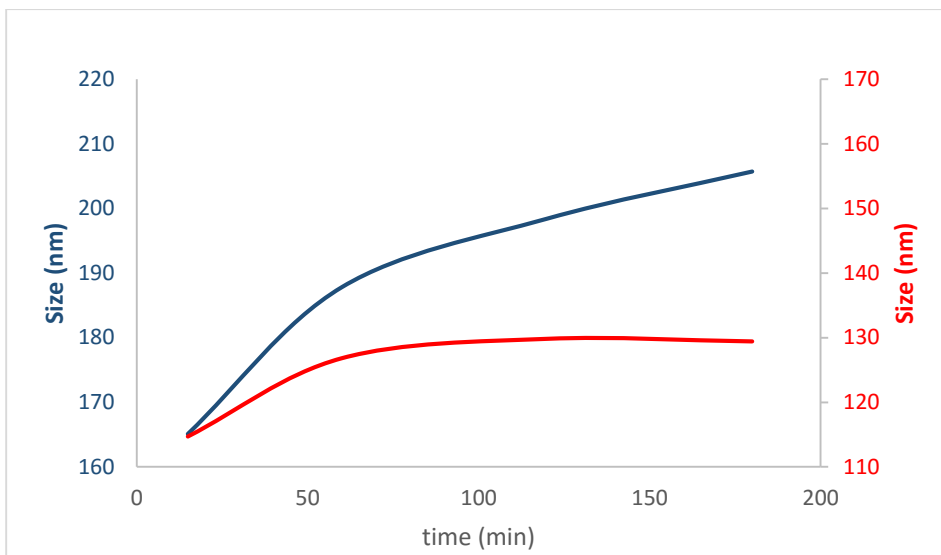


**Figure 4.21.** Comparison of the seeded growth time of the system realized on bigger sized O/W nanoemulsion (blue line) and on the smaller one (red line).

These smaller nanoparticles were further characterized using Electron Microscopy (samples have been stained with OsO<sub>4</sub> vapors, **Figure 4.23**) and NanoSight (NTA, Nanoparticle Tracking Analysis) measurements, whose results are summarized as follow (see also **Figure 4.23**):

Concentration (particle/ml)	6.07 E+08 ± 3.82 E+07
Mean size	134.5 ± 1.2 nm
Mode	127.7 ± 1.7 nm
SD	31.6 ± 5.5 nm
D10	68.3 ± 1.1 nm
D50	100.7 ± 0.5 nm
D90	142.8 ± 3.1 nm

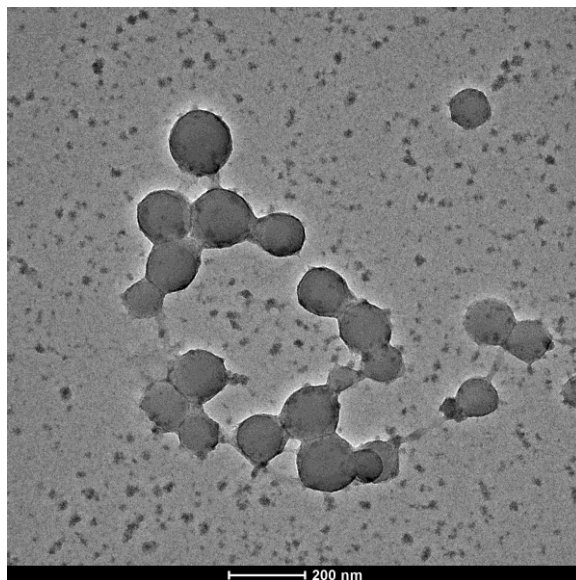


**Figure 4.22.** TEM micrograph of silica nanocapsules after 1 h of seeded growth time. Sample has been stained with  $\text{OsO}_4$  vapors.

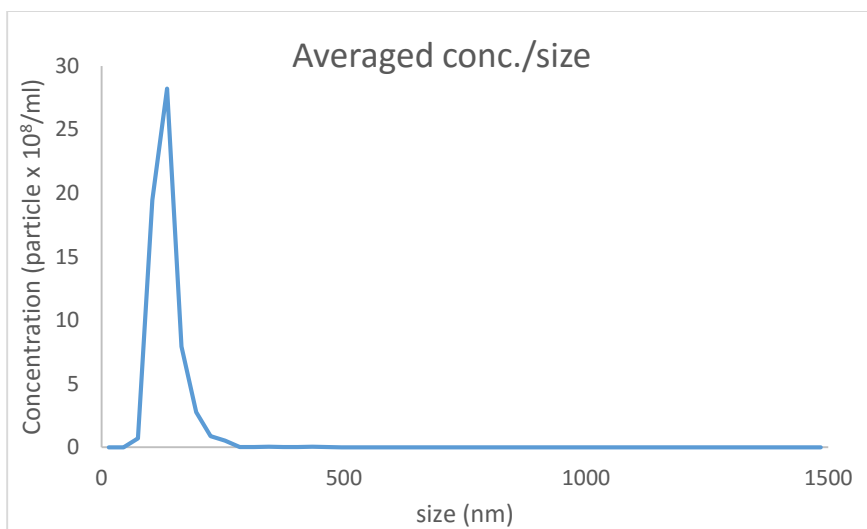


**Figure 4.23.** NTA plot of Silica-NCs (averaged concentration versus sizes).

NTA utilizes the properties of both light scattering and Brownian motion in order to obtain the particle size distribution of samples in liquid suspension.<sup>57</sup> In contrast to Dynamic Light Scattering, NTA approach makes possible to visualize and track individual particles and therefore

makes possible to determine the exact concentration of particles in the sample (and the distribution of concentrations, **Figure 4.23**) and to detect and quantify any aggregation. In particular, the possibility to determine the concentration of silica nanocapsules could be very important for further modification of the system, for example adding molecules for active targeting, since the procedure used does not allow to verify the final concentration of nanocapsules – due to the purification via dialysis and rotavapor that can increase or decrease the volume of the sample without any control.

## 4.6 References

1. D. Peer, J. M. Karp, S. Hong, O. C. Farokhzad, R. Margalit and R. Langer, *Nature nanotechnology*, 2007, **2**, 751-760.
2. F. M. Kievit and M. Zhang, *Advanced Materials*, 2011, **23**, H217-H247.
3. D.-E. Lee, H. Koo, I.-C. Sun, J. H. Ryu, K. Kim and I. C. Kwon, *Chemical Society Reviews*, 2012, **41**, 2656-2672.
4. R. M. Fratila, S. G. Mitchell, P. del Pino, V. Grazu and J. s. M. de la Fuente, *Langmuir*, 2014.
5. L. Zhang, Y. Li and C. Y. Jimmy, *Journal of Materials Chemistry B*, 2014, **2**, 452-470.
6. M. Colombo, S. Carregal-Romero, M. F. Casula, L. Gutiérrez, M. P. Morales, I. B. Böhm, J. T. Heverhagen, D. Prospero and W. J. Parak, *Chemical Society Reviews*, 2012, **41**, 4306-4334.
7. R. Rossin, S. Muro, M. J. Welch, V. R. Muzykantov and D. P. Schuster, *Journal of Nuclear Medicine*, 2008, **49**, 103-111.
8. M. Shokeen, E. D. Pressly, A. Hagooley, A. Zheleznyak, N. Ramos, A. L. Fiamengo, M. J. Welch, C. J. Hawker and C. J. Anderson, *ACS nano*, 2011, **5**, 738-747.
9. X. Guo, C. Shi, G. Yang, J. Wang, Z. Cai and S. Zhou, *Chemistry of Materials*, 2014, **26**, 4405-4418.
10. F. Tang, L. Li and D. Chen, *Advanced Materials*, 2012, **24**, 1504-1534.
11. V. P. Torchilin, *Advanced drug delivery reviews*, 2012, **64**, 302-315.
12. M. Ding, N. Song, X. He, J. Li, L. Zhou, H. Tan, Q. Fu and Q. Gu, *ACS nano*, 2013, **7**, 1918-1928.
13. C. Argyo, V. Weiss, C. Bräuchle and T. Bein, *Chemistry of Materials*, 2013, **26**, 435-451.
14. J. L. Vivero-Escoto, I. I. Slowing, B. G. Trewyn and V. S. Y. Lin, *Small*, 2010, **6**, 1952-1967.
15. S. V. Patwardhan, *Chemical Communications*, 2011, **47**, 7567-7582.
16. I. M. Rio-Echevarria, F. Selvestrel, D. Segat, G. Guarino, R. Tavano, V. Causin, E. Reddi, E. Papini and F. Mancin, *Journal of Materials Chemistry*, 2010, **20**, 2780-2787.
17. I. I. Slowing, B. G. Trewyn, S. Giri and V. Y. Lin, *Advanced Functional Materials*, 2007, **17**, 1225-1236.

18. M. Liong, S. Angelos, E. Choi, K. Patel, J. F. Stoddart and J. I. Zink, *Journal of Materials Chemistry*, 2009, **19**, 6251-6257.
19. B. Silvestri, D. Guarnieri, G. Luciani, A. Costantini, P. Netti and F. Branda, *Journal of Materials Science: Materials in Medicine*, 2012, **23**, 1697-1704.
20. K. K. Cotí, M. E. Belowich, M. Liong, M. W. Ambrogio, Y. A. Lau, H. A. Khatib, J. I. Zink, N. M. Khashab and J. F. Stoddart, *Nanoscale*, 2009, **1**, 16-39.
21. M. W. Ambrogio, C. R. Thomas, Y.-L. Zhao, J. I. Zink and J. F. Stoddart, *Accounts of chemical research*, 2011, **44**, 903-913.
22. J. van Wijk, J. W. Salari, N. Zaquen, J. Meuldijk and B. Klumperman, *Journal of Materials Chemistry B*, 2013, **1**, 2394-2406.
23. Q. Zhang, T. Zhang, J. Ge and Y. Yin, *Nano letters*, 2008, **8**, 2867-2871.
24. R. Kumar, I. Roy, T. Y. Ohulchanskyy, L. N. Goswami, A. C. Bonoiu, E. J. Bergey, K. M. Trampusch, A. Maitra and P. N. Prasad, *Acs Nano*, 2008, **2**, 449-456.
25. S.-H. Hu, S.-Y. Chen and X. Gao, *ACS nano*, 2012, **6**, 2558-2565.
26. C.-W. Su, C.-S. Chiang, W.-M. Li, S.-H. Hu and S.-Y. Chen, *Nanomedicine*, 2014, **9**, 1499-1515.
27. G. Tan, P. Xu, J. He, L. Lawson, G. L. McPherson and V. T. John, *Soft matter*, 2009, **5**, 3006-3009.
28. C. Wu, C. Yu and M. Chu, *International journal of nanomedicine*, 2011, **6**, 807.
29. C. Zoldesi, P. Steegstra and A. Imhof, *Journal of colloid and interface science*, 2007, **308**, 121-129.
30. M. O'Sullivan, Z. Zhang and B. Vincent, *Langmuir*, 2009, **25**, 7962-7966.
31. A. V. Jovanovic, R. S. Underhill, T. L. Bucholz and R. S. Duran, *Chemistry of materials*, 2005, **17**, 3375-3383.
32. T. J. Joncheray, P. Audebert, E. Schwartz, A. V. Jovanovic, O. Ishaq, J. L. Chávez, R. Pansu and R. S. Duran, *Langmuir*, 2006, **22**, 8684-8689.
33. L. Spornath and S. Magdassi, *Micro & Nano Letters*, 2010, **5**, 28-36.
34. D. Guzey and D. J. McClements, *Advances in Colloid and Interface Science*, 2006, **128**, 227-248.
35. J. Cui, M. P. van Koeven, M. Müllner, K. Kempe and F. Caruso, *Advances in colloid and interface science*, 2014, **207**, 14-31.

36. L. L. del Mercato, M. M. Ferraro, F. Baldassarre, S. Mancarella, V. Greco, R. Rinaldi and S. Leporatti, *Advances in colloid and interface science*, 2014, **207**, 139-154.
37. S. Sivakumar, V. Bansal, C. Cortez, S. F. Chong, A. N. Zelikin and F. Caruso, *Advanced Materials*, 2009, **21**, 1820-1824.
38. R. Vecchione, U. Ciotola, A. Sagliano, P. Bianchini, A. Diaspro and P. Netti, *Nanoscale*, 2014, **6**, 9300-9307.
39. I. Fotticchia, T. Fotticchia, C. A. Mattia, P. A. Netti, R. Vecchione and C. Giancola, *Langmuir*, 2014, **30**, 14427-14433.
40. R. Ciriminna, A. Fidalgo, V. Pandarus, F. o. Béland, L. M. Ilharco and M. Pagliaro, *Chemical reviews*, 2013, **113**, 6592-6620.
41. F. Hoffmann, M. Cornelius, J. Morell and M. Fröba, *Angewandte Chemie International Edition*, 2006, **45**, 3216-3251.
42. B. Silvestri, A. Pezzella, G. Luciani, A. Costantini, F. Tescione and F. Branda, *Materials Science and Engineering: C*, 2012, **32**, 2037-2041.
43. F. Branda, B. Silvestri, G. Luciani, A. Costantini and F. Tescione, *Colloids and Surfaces A: Physicochemical and Engineering Aspects*, 2010, **367**, 12-16.
44. F. Alexis, E. Pridgen, L. K. Molnar and O. C. Farokhzad, *Molecular pharmaceutics*, 2008, **5**, 505-515.
45. L. M. Liz-Marzán, M. Giersig and P. Mulvaney, *Langmuir*, 1996, **12**, 4329-4335.
46. H. Matsumori, S. Takenaka, H. Matsune and M. Kishida, *Applied Catalysis A: General*, 2010, **373**, 176-185.
47. T. Nie, A. Baldwin, N. Yamaguchi and K. L. Kiick, *Journal of Controlled Release*, 2007, **122**, 287-296.
48. U. Freudenberg, A. Hermann, P. B. Welzel, K. Stirl, S. C. Schwarz, M. Grimmer, A. Zieris, W. Panyanuwat, S. Zschoche and D. Meinhold, *Biomaterials*, 2009, **30**, 5049-5060.
49. H. Wang, X. Zhu, L. Tsarkova, A. Pich and M. Möller, *Acs Nano*, 2011, **5**, 3937-3942.
50. G. Walrafen, Y. Chu and M. Hokmabadi, *The Journal of Chemical Physics*, 1990, **92**, 6987-7002.
51. A. Lesniak, F. Fenaroli, M. P. Monopoli, C. Åberg, K. A. Dawson and A. Salvati, *ACS nano*, 2012, **6**, 5845-5857.
52. D. Guarnieri, M. A. Malvindi, V. Belli, P. P. Pompa and P. Netti, *Journal of nanoparticle research*, 2014, **16**, 1-14.
53. M. Dash, F. Chiellini, R. M. Ottenbrite and E. Chiellini, *Progress in Polymer Science*, 2011, **36**, 981-1014.

54. H. G. Garg, R. J. Linhardt and C. A. Hales, *Chemistry and biology of heparin and heparan sulfate*, Elsevier, 2011.
55. F. Branda, B. Silvestri, G. Luciani and A. Costantini, *Colloids and Surfaces A: Physicochemical and Engineering Aspects*, 2007, **299**, 252-255.
56. T. Coradin, D. Eglin and J. Livage, *Journal of Spectroscopy*, 2004, **18**, 567-576.
57. B. Carr and M. Wright, *Innovations in Pharmaceutical Technology*, 2008, **26**, 38-40.

# Chapter 5

## Conclusions

The field of Nanomedicine, and the related nanotechnologies and drug delivery systems (DDSs), is facing a critical juncture in both academic and industrial research centers.<sup>1</sup> It has been over 40 years since the advent of use of nanoparticles as site specific drug delivery systems. During the last decades there have been some notable successes, namely the reformulation of doxorubicin, amphotericin B and paclitaxel into the lower toxicity versions of their more traditional formulations. This improvement, considering the current economic climate, the improvements of the therapeutic benefit (e.g. reduced toxicity) without a real pharmaco-economic demonstration of medical benefit is insufficient to ensure the product utilization.<sup>1</sup> Moreover, the choice of an appropriate nanocarrier is not obvious. It must be taken into account that an ideal DDS should possess several characteristics to positively affect the biodistribution and targeting, the possibility to screen the nanocarriers and the need to avoid body clearance. It is still not clear to what extent this is possible without

## 5. Conclusions

substantially increase the complexity of the nanocarrier and without influencing commercial scale-up.<sup>2</sup>

The research conducted during these three years was oriented in this direction. The DDSs developed are all derived from natural materials and, despite the difficulties found to modify natural polymers compared to the synthetic ones, the former result to be biocompatible, biodegradable and economically more appealing than the latter. In addition, it was shown that the possibility to selectively add desired characteristics to the final nanovector can drastically change its fate. Taken altogether, the research works showed how adding functionality can lead to systems more appealing from a pharmacological point of view but less appealing from a business point of view. In addition, it was shown how a target design make possible to obtain DDSs resulting powerful but, at the same time, less prone to the realization at the industrial scale-up. This issue, together with the necessity to develop suitable and standardized screening methodology for determining optimal DDSs' characteristics, is the focus to whom researcher must convey their efforts.

Although nanotechnology has the potential to revolutionize medicine,<sup>2</sup> only in the next years it will be understood if it will represent a revolution or just an important contribution. My personal hope is that this research

project has added a small but important contribution to answer this important question.

1. R. Kirsh, S. Hood, C. Brook, A. Gilmartin, P. Dell'orco and T. Meek, *International journal of pharmaceuticals*, 2013, **454**, 530-531.
2. D. Peer, J. M. Karp, S. Hong, O. C. Farokhzad, R. Margalit and R. Langer, *Nature nanotechnology*, 2007, **2**, 751-760.